A Hair Bundle Proteomics Approach to Discovering Actin Regulatory Proteins in Inner Ear Stereocilia

by

Anthony Wei Peng

B.S. Electrical and Computer Engineering
Cornell University, 1999

SUBMITTED TO THE HARVARD-MIT DIVISION OF HEALTH SCIENCES AND TECHNOLOGY IN PARTIAL FULFILLMENT OF THE REQUIREMENTS FOR THE DEGREE OF

DOCTOR OF PHILOSOPHY IN SPEECH AND HEARING BIOSCIENCES AND TECHNOLOGY
AT THE
MASSACHUSETTS INSTITUTE OF TECHNOLOGY
JUNE 2009

Signature of Author: _____
Harvard-MIT Division of Health Sciences and Technology
May 1, 2009

Certified by: _____
Stefan Heller, PhD
Associate Professor of Otolaryngology Head and Neck Surgery Stanford University
Thesis Supervisor

Accepted by: _____
Ram Sasisekharan, PhD
Director, Harvard-MIT Division of Health Sciences and Technology
Edward Hood Taplin Professor of Health Sciences & Technology and Biological Engineering.

This page is intentionally left blank.

A Hair Bundle Proteomics Approach to Discovering Actin Regulatory Proteins in Inner Ear Stereocilia

by

Anthony Wei Peng

B.S. Electrical and Computer Engineering, Cornell University, 1999

Submitted to the Harvard-MIT Division of Health Science and Technology on May 7, 2009 in partial fulfillment of the requirements for the degree of Doctor of Philosophy in Speech and Hearing Bioscience and Technology

Abstract

Because there is little knowledge in the areas of stereocilia development, maintenance, and function in the hearing system, I decided to pursue a proteomics-based approach to discover proteins that play a role in stereocilia function. I employed a modified "twist-off" technique to isolate hair bundle proteins, and I developed a method to purify proteins and to process them for analysis using multi-dimensional protein identification technology (MudPIT).

The MudPIT analysis yielded a substantial list of proteins. I verified the presence of 21 out of 34 (62%) existing proteins known to be present in stereocilia. This provided strong evidence that my proteomics approach was efficient in identifying hair bundle proteins. Next, I selected three proteins and localized them to murine cochlear stereocilia. StarD10, a putative phospholipid binding protein, was detectable along the shaft of stereocilia. Nebulin, a putative F-actin regulator, was located toward the base of stereocilia. Finally, twinfilin 2, a putative modulator of actin polymerization, was found at the tips of stereocilia.

In order to determine the function of twinfilin 2, I localized the protein predominately to the tips of shorter stereocilia where it is up-regulated during the final phase of elongation. When overexpressed, I found that twinfilin 2 causes a shortening of microvilli in LLC-PK1/CL4 cells and in native cochlear stereocilia.

The main result of this thesis was determining the sub-cellular localization of three interesting proteins and functionally characterizing one protein. My thesis also confirmed the proteomics screen I developed as an efficient method for identifying proteins in stereocilia.

Thesis Supervisor: Stefan Heller

Title: Associate Professor, Department of Otolaryngology - Head and Neck Surgery, Stanford University School of Medicine, Stanford, CA

This page is intentionally left blank.

Acknowledgements

I am very blessed to have many people in my life to support me through completing my thesis and to teach me different skills and techniques.

My mentor, Dr. Stefan Heller, has been instrumental in shaping my research plan and constantly providing me support. He always had faith in me, and he continued to push me and challenge me to do better. His never-ending ideas always pushed me forward when I doubted.
Dr. Tony Ricci has also provided me with microscopy knowledge and given me invaluable advice.
Drs. Eduardo Corrales and Kazuo Oshima patiently taught me how to dissect the inner ear.
Sabine Mann taught me how to work with Sf9 cells and helped with protein expression and antibody production.
Zhigang Xu provided insight on cloning and helped with experiments.
Patrick Hsu spearheaded the work with StarD10.
The Heller lab has provided me with years of feedback and comments.
My thesis committee (Dr. M. Charles Liberman, Dr. William Sewell, and Dr. Clifford Woolf) guided me along, put me back on the path when I started to stray, and provided helpful feedback.
Drs. Inna Belyantseva and Thomas Friedman welcomed me to visit their lab and perform some of my experiments with them.

My parents, Thomas, Sophia, and the Chang's have supported me through all my schooling and my research. Without their love and support I would not be where I am today.
Finally, my fiancé Amanda Graves for her support and love. I'm truly lucky to have her, and I am lucky to join her wonderful family who has also supported me to the end.

This page is intentionally left blank.

Table of contents

This page is intentionally left blank.

Chapter 1: Introduction

1.1 Hearing Overview

Sounds are an integral part of our lives. It is a means for us to communicate easily, enjoy music, localize objects, and warn us of dangers in our environment. According to the National Institute on Deafness and Other Communication Disorders (NIDCD), 28 million Americans are affected by some form of hearing impairment. Approximately 2 to 3 out of 1000 newborn babies are deaf or hard of hearing. Additionally, the number of hearing impaired adults is increasing as people are living longer and as people trend toward listening to loud music; the amount of noise-induced hearing loss has been increasing significantly in the past decade (Daniel, 2007; Thorne et al., 2008). With this prevalence of hearing loss and its ever growing population of afflicted people, more needs to be understood about the auditory system to better treat patients with deafness and hearing loss.

Sound enters through the outer ear and travels through the external auditory meatus, impinging on the tympanic membrane. The sound energy from the acoustical wave in the ear canal is translated into mechanical motion of the middle ear ossicles with the tympanic membrane acting as a transducer. The stapes, the last of the middle ear ossicles, acts like a piston that exerts a pumping action at the oval window on the fluid-

filled scala vestibuli of the cochlea, creating a mechanical wave that travels along the cochlea and causes the basilar membrane of the Organ of Corti to oscillate (figure 1.1). Next, the motion is detected by specialized sensory hair cells, which are the mechano-sensitive transducers of the hearing and vestibular systems. The cochlear hair cells comprise of one row of inner hair cells (IHC) and three rows of outer hair cells (OHC). The apical surface of each hair cell displays a hair bundle composed of numerous specialized microvilli, termed stereocilia, and a single kinocilium (figure 1.2). The kinocilium disappears in the adult cochlea, but persists in the other inner ear organs (Kaltenbach et al., 1994). The mechano-electrical transduction (MET) apparatus housed in stereocilia converts the mechanical wave energy into changes of the hair cell's plasma membrane potential. The hair cell then chemically communicates with auditory nerve fibers, which carry the information to the central auditory pathway. In the central auditory pathway, sound is analyzed and this information is passed along to higher processing structures of the cerebrum.

The auditory pathway is quite amazing in its sensitivity and dynamic range. At threshold, our auditory system is able to reliably detect movements in the air molecules due to sound of an average of 10 picometers (Purves et al., 2001). Much of this sensitivity is due to the hair bundles, which can detect mechanical motions as small as 300 picometers, about the diameter of a gold atom (Purves et al., 2001). However, not only is the hearing system able to detect such low level sounds at threshold, it is also able to detect sounds twelve orders of magnitude greater in intensity (Berg, 2009). In order to understand how humans are able to have such low hearing thresholds, we must start by examining the sensitivity of the MET process.

1.2 Stereocilia structure importance for MET

Stereocilia transduce mechanical energy into electrical changes across the hair cell membrane. The basis of this process is thought to be a mechanically sensitive ion channel that detects tension in the tip-link, a molecular link that connects a shorter

stereocilium with its taller neighbor (figure 1.3). The structure and mechanical properties of the hair bundle are important to MET and contribute to MET sensitivity.

The characteristic staircase structure of the hair bundle contributes to the directional sensitivity. MET is sensitive only to one axis of movement of the hair bundle (Hudspeth, 1985). This is achieved by only detecting tensions across the tip-link. The differing heights of stereocilia allow for the tip-link to be angled (figure 1.3), and this angle helps to amplify the horizontal movement of the hair bundle.

The stiffness of the hair bundle and the coupling of the plasma membrane to the core of stereocilia also affect the sensitivity of MET. Since it is hypothesized that MET detects tension in the tip-links, this tension must be translated from the stereocilia core, where the movement occurs, to the membrane, where the tip-link is embedded. This connection can be either a direct molecular connection from the tip-link to the actin core, or an indirect connection that tensions the plasma membrane to the actin core. A decrease in coupling of the plasma membrane to the core is hypothesized for the change in MET sensitivity in the myosin VIIa mutant mouse (Kros et al., 2002; Self et al., 1998).

The flexing stiffness of the rootlet of stereocilia also affects the sensitivity of the system (Hudspeth, 1985). The more compliant the rootlet, the more the hair bundle moves for a given force, therefore allowing detection of smaller sound waves. Without a well-controlled structure of stereocilia, hair cells would not be able to function with the proper sensitivity, which could cause hearing loss.

1.3 Actin filament structure

To understand stereocilia structure, it is first important to understand the biology of actin filaments, which are the backbone of stereocilia. Actin filaments are made up of actin monomers. A two-stranded, right-handed helix arrangement of actin monomers

polymerizes into an actin filament with one turn of the helix every 37nm (Alberts et al., 2002). Actin filaments are polarized with a plus and minus end. When the filament is decorated with myosin sub-fragment 1, the plus end of the actin filament appears barbed and the pointed end appears pointed; hence the plus end is also referred to as the barbed end, and the minus end is also referred to as the pointed end (Alberts et al., 2002; Holmes et al., 1990; Moore et al., 1970). Structural differences between the barbed and pointed end of the actin monomer cause faster rates of association and dissociation from the barbed end. These rates, however, are altered in the presence of adenosine tri-phosphate (ATP) versus adenosine di-phosphate (ADP).

Actin monomers possess an internal binding site for ATP. An actin monomer has inherent enzymatic activity that catalyzes the hydrolysis of a bound ATP to form ADP. When actin is in monomer form, this hydrolysis reaction takes a long time, but when the actin monomer is added to a filament, the hydrolysis occurs very quickly (Alberts et al., 2002). ATP-bound actin monomers (ATP-actin) exhibit a lower dissociation constant (also called the critical concentration), meaning that ATP-actin prefers being bound to the actin filament. On the other hand, ADP bound monomers (ADP-actin) exhibit a higher critical concentration, therefore ADP-actin favors the unbound state (monomer form).

The relationship between the actin monomer concentration and the unique critical concentrations at the two ends of a filament determine which of three possible processes will occur: filament growth, filament shrinkage, or treadmilling. When the free actin monomer concentration is below both critical concentrations, the filament shrinks. Free actin monomer concentrations above both critical concentrations cause filament lengthening. Finally, when the free actin monomer concentration is between the critical concentration of the barbed and pointed ends, the phenomenon of actin treadmilling occurs. In the treadmilling process, ATP-actin is added to the barbed ends of actin filaments, and ADP-actin is removed from actin filament pointed ends resulting in no

real change in filament lengths, but actin is turned over in the filament (Alberts et al., 2002).

1.4 Stereocilia Structure

Stereocilia of the hair bundle are unique to hair cells, as no other cells have an organelle similar to it in structure (figure 1.2). The closest organelles to stereocilia are microvilli like those seen in the intestinal brush border, and stereocilia have likely evolved from these types of microvilli (DeRosier et al., 2000). The underlying backbone is similar between these two structures, but stereocilia differ from microvilli in their length, thickness, and organization, which is described in more detail below.

The filamentous actin core of stereocilia has many commonalities with microvilli (DeRosier et al., 2000). The actin core makes a rigid structure of a unipolar arrangement of actin filaments with their barbed ends located at the tips of stereocilia and pointed ends at the base. The actin filaments are cross-linked with bundling proteins, which generate a hexagonal packing lattice (Mooseker et al., 1984; Tilney et al., 1984). Actin filament barbed ends terminate in an electron-dense material in both the tips of microvilli and stereocilia (Mooseker et al., 1984; Tilney et al., 1983). At the stereocilia base, however, actin filaments form an electron dense rootlet, which is characteristic of hair cells. This rootlet extends below the apical surface of the hair cell into a meshwork of actin filaments forming the cuticular plate (Tilney et al., 1983).

Stereocilia are generally longer than brush border microvilli. Brush border microvilli are roughly 1-2μm in length (DeRosier et al., 2000), whereas mammalian stereocilia can range from a few μm in the cochlea to >40μm in the crista ampullaris. Stereocilia lengthening is unique; stereocilia start as short microvilli, then undergo a well controlled multi-step program of elongation during development before they stop growing and become part of the mature, highly-organized hair bundle. (DeRosier et al., 2000; Tilney et al., 1984).

A single mouse cochlear stereocilium is composed of about 1200 actin filaments (Mogensen et al., 2007). In contrast, microvilli are much thinner, consisting of approximately 20 actin filaments (DeRosier et al., 2000). During development, stereocilia do not attain their mature thickness of 220-530nm before they organize into the hair bundle (Mogensen et al., 2007). Instead, they first organize into their macro-hair bundle structure, with thickening occurring later.

The hair bundle is most unique in its organization. Brush border microvilli are fairly uniform on the apical side of the cell and cover most of the cells' apical surface. In contrast, hair bundles display a characteristic staircase structure exhibiting rows of nearly identical length stereocilia and a single kinocilium that indicates the polarity of the cell surface and only cover a portion of the apical surface (figure 1.2). The hair bundle's staircase structure is important to the cells' function, since it is within this structure that the mechanical sound energy is transduced into an electrical signal. With such a complex and precise structure, it is not surprising that stereocilia need a regulated pattern of development as well as maintenance of its structure.

1.5 Stereocilia Development

Development of the staircase structure of the hair bundle follows a well-orchestrated developmental pattern of growth. Although the final morphology of the hair bundle differs between species, stereocilia development in most species follows a similar path. I will focus on stereocilia development in the mammalian model, which can be divided into 4 phases: initial sprouting, initial staircase formation, ordered bundle formation, and final elongation and pruning (Kaltenbach et al., 1994). These phases are not necessarily distinct, as there can be some overlap between phases. Besides the development of individual hair bundles, there is also a gradient of stereocilia formation that takes place from base to apex in the cochlea that will not be discussed.

In the initial sprouting phase of hair bundle formation, microvilli form at the apical surface of hair cells. These microvilli are randomly spread throughout the surface of the cell. A single kinocilium also presents itself on the surface of the cell. This kinocilium is the only true cilium in hair cells, being the only structure that has tubulin microfilaments as its backbone (Sobkowicz et al., 1995). The kinocilium is first found in the center of the cell surface and the microvilli begin to form a dense tuft around it, giving the first indication of the future hair bundle. These microvilli can be distinguished from the surrounding supporting cell microvilli by their arrangement, density, and length (Kaltenbach et al., 1994; Mbiene et al., 1986; Mbiene et al., 1984; Tilney et al., 1992; Tilney et al., 1986). The kinocilium then migrates to the periphery of the cell, setting the excitatory direction of the hair cells as a result of the planar cell polarity signals present in the nascent sensory epithelium (Deans et al., 2007). The microvilli will grow longer, become thicker, and eventually grow to be stereocilia of the cell. However, initial microvilli are more numerous than the number of stereocilia present in the adult hair cells, as many of them will later be absorbed through a pruning stage.

The next stage of stereocilia development encompasses the initial staircase structure formation. During this phase, stereocilia undergo the first period of differential elongation. Stereocilia closest to the kinocilium begin to elongate first. The rate of elongation appears to be consistent across all rows of a given hair cell, and it is the staggered initiation of growth that develops the initial staircase pattern (Tilney et al., 1988). This staircase formation is not uniform, since tall stereocilia on the lateral edges of the differentiating hair bundle are not of equal length to those in the tallest stereocilia in the middle, giving a crescent like gradient in heights of the tallest stereocilia (Kaltenbach et al., 1994).

In the ordered bundle formation phase, the bundle becomes more structured and consistent. During this phase of growth, stereocilia equal out their lengths in each row, giving a more organized appearance (Kaltenbach et al., 1994). Stereocilia also thicken

during this time, adding to the appearance that the mature bundle will have (Kaltenbach et al., 1994; Tilney et al., 1992).

The final stage of growth consists of final elongation and pruning of extra stereocilia. During this stage, stereocilia undergo a second burst of growth to reach their mature lengths, while at the same time continuing to thicken as well (Kaltenbach et al., 1994). During this stage all the extra short stereocilia/microvilli on the surface of the cells that are not a part of the final hair bundle structure are reabsorbed back into the cell, leaving just those elongated stereocilia that make the mature hair bundle. As described later in this thesis (Chapter 5), the final growth stage happens between P5 and P13 in mice, a period when the tallest row of cochlear stereocilia doubles in length in the apex of the cochlea and the elongation of the shorter stereocilia appears to be stunted.

1.6 Actin Dynamics of Stereocilia

The backbone of stereocilia is composed of several cytoskeletal proteins, all of which contribute to the structure of stereocilia. Actin, being the most abundant, forms the core of filamentous actin made up of β- and γ-actin monomers. Stereocilia actin filaments are cross-linked (i.e. bundled) by the proteins fimbrin and espin (Tilney et al., 1989; Zheng et al., 2000). Some of the actin filaments extend into the cuticular plate, which is an actin-rich structure containing spectrin cross-links just beneath stereocilia in the apical part of the hair cell (Drenckhahn et al., 1991). Many of the actin filaments terminate juxtaposed to the plasma membrane at the base of the stereocilia shaft, where stereocilia taper. The protein radixin has been immunolocalized at these termination points, and it has been hypothesized that radixin anchors the actin filaments to the plasma membrane (Pataky et al., 2004).

Within the collection of proteins associated with the actin core of stereocilia, only fimbrin and espin are known to directly affect the dynamics of actin filaments. These two actin filament bundlers affect dynamics by decreasing the depolymerization rate of ADP-actin

from the pointed ends, which decreases the likelihood that a monomer is released from the actin filament because two separate reactions need to occur: 1. Dissociation of the actin monomer from the actin filament, and 2. Dissociation of the actin monomer from the filament bundler. The net result of the presence of fimbrin and espin is the elongation of the actin filament as polymerization continues at the barbed ends. This effect has been elegantly demonstrated in the epithelial cell line LLC-PK1/CL4 (CL4) and also in native hair cells, where overexpression of espin leads to a substantial increase in microvilli and stereocilia length (Loomis et al., 2003; Rzadzinska et al., 2005) (figure 1.4).

The rate of treadmilling in stereocilia appears to be proportional to the length of stereocilia (Rzadzinska et al., 2004). Longer stereocilia exhibit a faster rate of treadmilling than shorter stereocilia; therefore, the treadmilling rate may help to determine the length of stereocilia. Two proteins have been shown to be important for stereocilia lengthening: myosin XVa and whirlin. Myosin XVa is thought to be involved in the variable rate of treadmilling, since the quantity of myosin XVa at the tips of stereocilia also appears to be proportional to the length of stereocilia (Rzadzinska et al., 2004). The lack of functional myosin XVa in knockout mice results in abnormally short stereocilia, which may be due to a deficiency in actin treadmilling. Whirlin has been shown to interact with myosin XVa (Belyantseva et al., 2005; Delprat et al., 2005; Kikkawa et al., 2005). Since whirlin mutants have the same abnormally short stereocilia as the myosin XVa deficient mutants, it has been proposed that myosin XVa carries whirlin to the tips of stereocilia where whirlin is involved in modulating the rate of treadmilling. Although both myosin XVa and whirlin are necessary for the development of properly ordered hair bundles, neither of these proteins have been shown to directly interact with actin filaments to change their dynamics. Therefore, the observed hair bundle deficiencies are very likely a secondary consequence of the loss of myosin XVa and whirlin. Proteins and mechanisms that directly change the dynamics of actin filaments in stereocilia remain to be described.

1.7 Introduction to this thesis

The molecular mechanisms of hearing and hair cell function are poorly understood. Traditionally genetic approaches have played a major role in determining proteins important for hair cell function. Some of these proteins, particularly the Usher's Syndrome (USH) proteins, have been localized to stereocilia. This has provided our first detailed insights into the molecular makeup of stereocilia. However, many of the proteins and molecular mechanisms responsible for the development, function, and maintenance of stereocilia remain unknown. Any novel insight will substantially advance fundamental knowledge of the processes underlying the hearing and vestibular senses. These results could also lead to more effective treatment plans and possible cures for hearing impairment and vestibular deficiencies.

The goal of this thesis was to identify proteins directly responsible for stereocilia development and maintenance of the unique stereocilia staircase. We know that stereocilia are made of an actin filament backbone, but how the lengths of the various rows of stereocilia are regulated is not well understood. Proteins like myosin XVa and whirlin have been shown to be required for the final elongation of stereocilia (Belyantseva et al., 2005), but these proteins do not directly regulate actin filament lengthening. Espin and fimbrin directly regulate actin filament lengthening by bundling the filament together and stabilizing the filaments to allow for a longer filament structure (Bretscher, 1981; Loomis et al., 2003; Sekerkova et al., 2006), however, other proteins that regulate actin filament dynamics have not been described.

Actin filament regulation and dynamics have been explained in many other systems, but none of the common actin-regulating proteins have been unequivocally identified in stereocilia (Slepecky et al., 1992). Since stereocilia are composed of actin filaments and because stereocilia development is highly regulated, I hypothesize that there are likely multiple actin regulatory proteins that play distinct roles in setting and maintaining filament lengths.

To discover new proteins in stereocilia, I first considered the pros and cons of conventional protein discovery methods, which are genetic, yeast 2-hybrid, antibody, proteomic, and gene chip screening. Genetic screening offers an elegant strategy to identify important proteins that, when lost or malfunctioning, cause hearing and/or vestibular phenotypes. This would likely not work for actin regulatory proteins because numerous regulatory proteins are common to many cells. The ubiquitous nature of actin regulatory proteins would likely lead to neonatal lethality, preventing the realization of a hearing phenotype. The yeast-2-hybrid method is well suited to find interaction partners of proteins, but in the case of finding binding partners of actin, this method will pull out many clones of actin itself as well as many common regulatory proteins present in all cell types. Thus, this method is not specific to stereocilia structure. Antibody screening has mainly been implemented by immunizing mice with inner ear proteins and using the monoclonal antibodies produced by hybridoma cells generated from the spleen of the immunized mice. The antibody screen is likely the best of these conventional methods because I can localize proteins to my sub-cellular localization of interest, but this method is time consuming, low-throughput, and with the difficulty of immuno-staining stereocilia bundles, challenging as well.

Proteomics and genomics/gene chips are two possible high-throughput methods to consider for determining new hair bundle proteins. The proteomic screening of a complex sample of proteins, termed shotgun proteomics, is a difficult task to perform with hair bundles due to the low amounts of protein, but as technology has advanced, this challenge can be overcome. Innovative new sample separation methods and improved mass spectrometers now allow the detection of proteins that are present in low femtomole amounts (Wolters et al., 2001). A similar progression of technological evolution has recently happened with gene chip technology. Gene chips were also first plagued by the necessity of a large amount of cells or tissue, but as technology developed and sensitivity increased, discoveries continued to flourish (Schena et al., 1995). Gene chips have been instrumental in several discoveries in the hearing field (Abe et al., 2003; Sage et al., 2005), and it is conceivable that emerging proteomic

approaches will impact the hearing field in similar or even more prominent fashion (Ahmed et al., 2006; McGee et al., 2006; Thalmann et al., 2006). The proteomic approach has two main advantages over the gene chip approach. Proteomic expression profiling directly samples the proteins themselves and does not infer protein expression from mRNA expression, as mRNA transcripts can be unstable or remain dormant and untranslated. The second major advantage of proteomics is the ability to study proteins only in a particular sub-cellular location. Therefore, sample fractionation is a powerful proteomic tool to focus on proteins located in a functionally relevant sub-cellular region; mRNA expression analysis with gene chips does not offer this advantage. Overall, shotgun proteomic analysis offers an unprecedented new analytical tool to specifically identify hair bundle proteins.

In order to determine proteins specifically localized to stereocilia, I present a proteomics approach as an alternative to the conventional methods of discovering stereocilia proteins. I validate this approach as a general protein discovery method for stereocilia, since I do not specifically bias my technique toward certain types of proteins. I expect the majority of proteins found in my screen to be cytoskeletal proteins, because stereocilia are made predominately of an actin backbone, and for the interest of this thesis, I choose two cytoskeletal proteins and one lipid related protein for further experiments. One protein that was identified in the screen will be explored for its function in cochlear stereocilia.

Figure 1.1 (a) Shown is a schematic drawing of a cochlear cross-section. The rectangle delineates the area shown in (b) illustrating a section of the scala media with surrounding structures such as the organ of Corti and the stria vascularis. IHC = inner hair cell, OHC = outer hair cell. Images are courtesy of Stefan Heller.

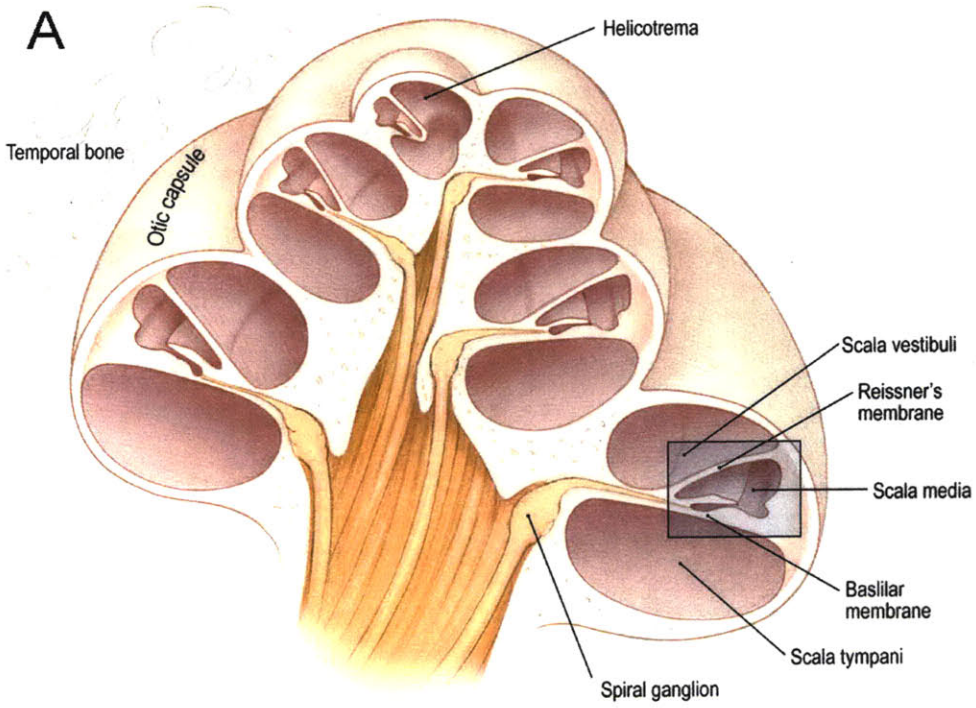

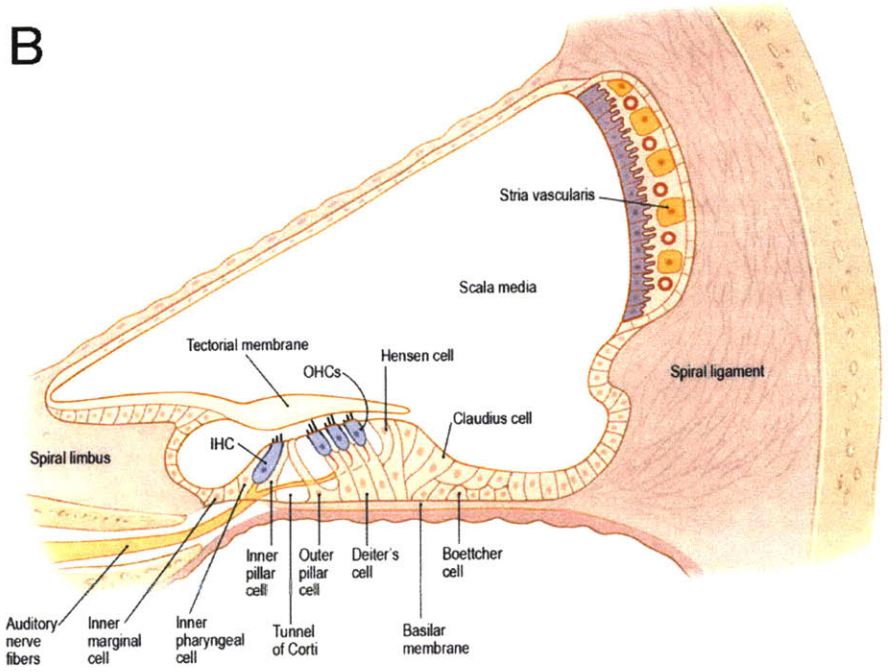

This page is intentionally left blank.

Figure 1.2 Stereocilia of (a) inner hair cells and (b) outer hair cells from a P9 mouse with the F-actin backbone labeled with phalloidin. (c) Schematic of the apical surface of an inner hair cell with the kinocilium labeled in green and stereocilia in white. Scale bar = 5μm,

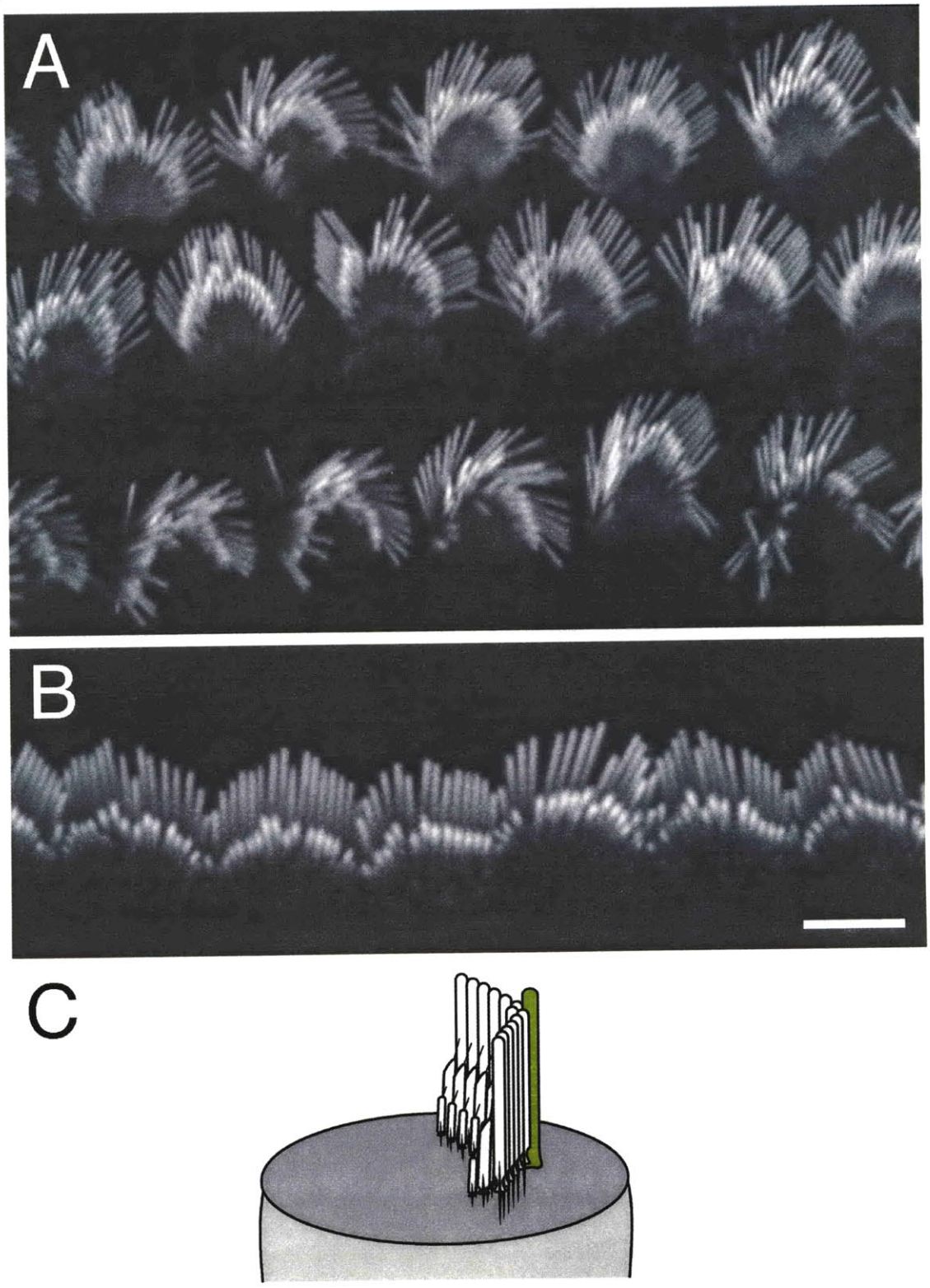

This page is intentionally left blank.

Figure 1.3 Schematic of the MET apparatus. A tip-link composed of cadherin 23 and protocadherin 15 connects the tall and middle row of stereocilia. The MET channel detects the tension in the tip link. Enlarged schematic image is courtesy of Stefan Heller.

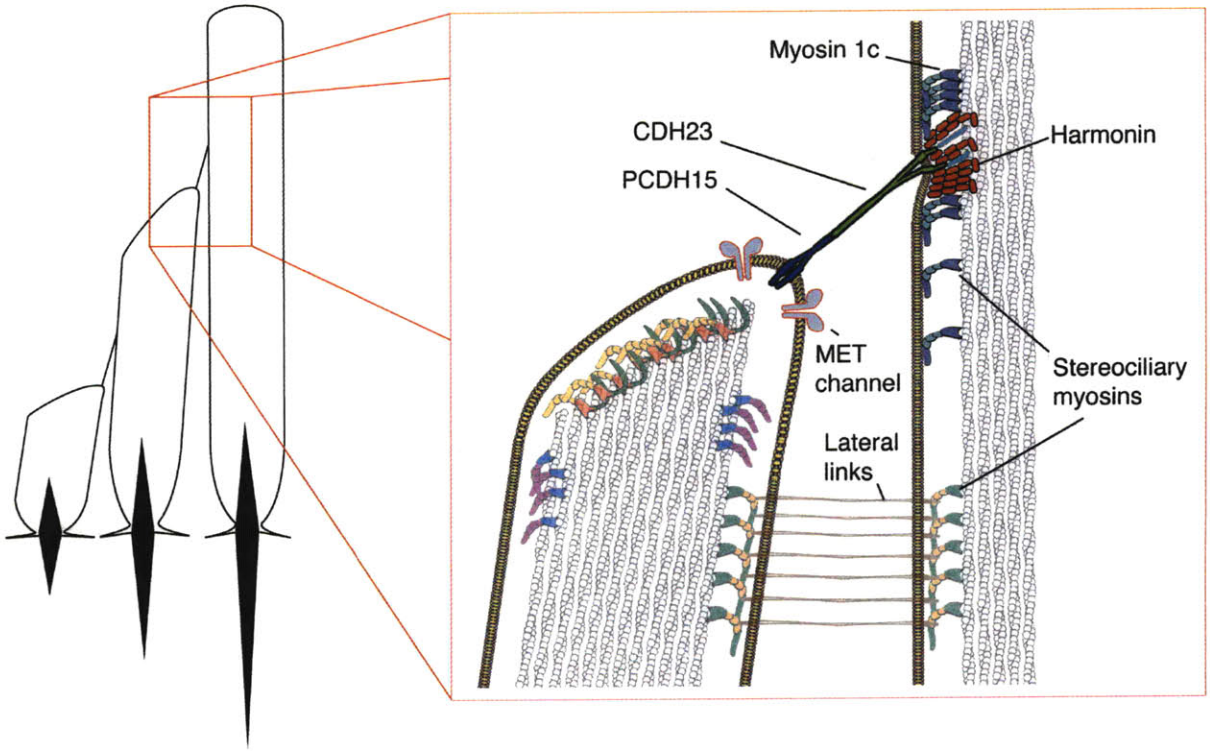

This page is intentionally left blank.

Figure 1.4 Microvilli of LLC-PK1/CL4 cells are prolonged when overexpressed with espin (green) resulting in longer microvilli than their neighbors as seen by F-actin staining (red). Scale bar = 5μm.

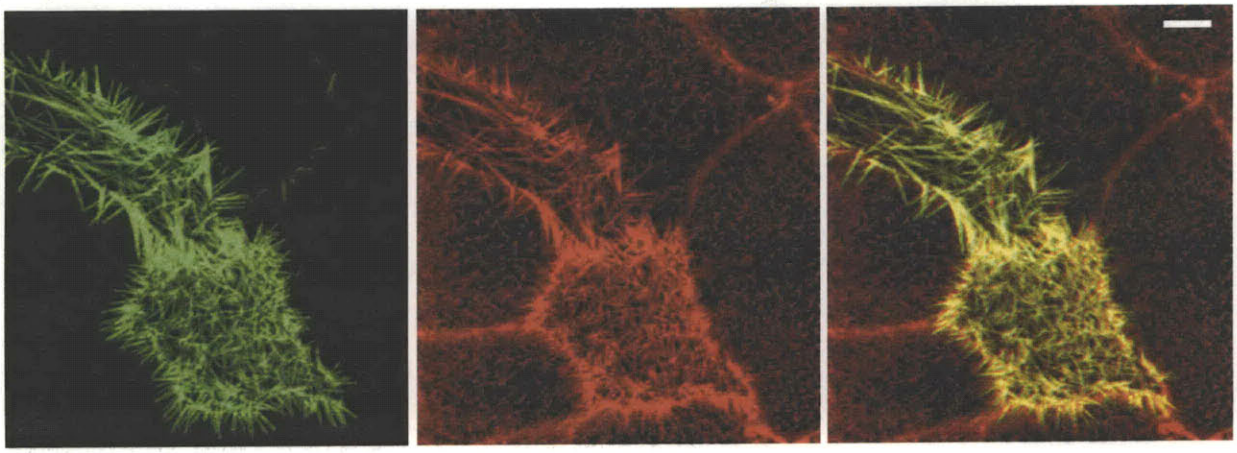

This page is intentionally left blank.

Chapter 2: Development of the Proteomics Screen

2.1 Introduction to Proteomics

Proteomics is the general name given to the large-scale study of proteins. Proteomics ranges from identification of proteins in complex mixtures to analysis of post-translational modifications of proteins. It encompasses both identification and quantification of proteins in cells and tissues. Mass spectrometry has revolutionized proteomics because of the ability to analyze proteins with a much smaller sample quantity and the ability to analyze mixtures of proteins in a high throughput manner. I will concentrate here on the identification of proteins in complex mixtures, since that is the goal of this thesis.

Traditionally, two-dimensional gel electrophoresis (2DGE) using immobilized pH gradients has been the most widely utilized tool for studying the proteome (Gorg et al., 2004; Hanash, 2000); however, there are a few drawbacks. In terms of protein coverage, the major drawback of 2DGE is the under-representation of membrane and low abundance proteins (Washburn et al., 2001). Both of which are likely to encompass proteins of interest to me, because I strive to get a comprehensive view of proteins in stereocilia. A second major drawback of 2DGE is the awkward and manual process of excising gel spots for protein identification. This is a crucial step in my study as I am

looking to identify all proteins that exist in my sample; therefore, I want a streamlined method. Unquestionably, 2DGE remains unsurpassed in its ability to simultaneously resolve and quantify proteins in complex mixtures. However, my application uses a small sample size and has a primary goal of identifying as many proteins as possible, therefore 2DGE was not the best choice.

To overcome many of the disadvantages of 2DGE, multi-dimensional protein identification technology (MudPIT) has been recently developed (Washburn et al., 2001; Wolters et al., 2001). In MudPIT, proteins are fragmented by tryptic digestion, and the resultant peptides are separated by two-dimensional liquid chromatography (LC) followed by online tandem mass spectrometry (MS/MS). Compared to conventional 2DGE, this technique has been shown to have a greater dynamic range of detection, coverage of both low abundance and membrane proteins, and a lower sample quantity requirement, which is due to minimal loss of material as a result of the analysis being fully automated (Roe et al., 2006; Washburn et al., 2001; Wolters et al., 2001). Since MudPIT is fully automated and overcomes many of the shortfalls of 2DGE, it has evolved as the method of choice for protein identification in complex mixtures of proteins.

Mass spectrometry based proteomics would not be possible without knowledge of the genome's DNA sequence. It relies on the knowledge of protein sequences (known and predicted) in order to identify and characterize the samples. Proteins are broken down into peptides and further broken into peptide fragments, which get analyzed, resulting in a mass spectrum for each peptide. These mass spectra are evaluated by an algorithm to determine the most probable peptide, and these peptides are then assigned to a protein. There are three major search algorithms for assigning a spectrum to a protein: Sequest, Mascot, and X!Tandem. Each algorithm can result in different sets of identified proteins and use of all three algorithms generally provides the greatest coverage of identified proteins (Sadygov et al., 2004). Using the program Scaffold (Proteome Software Inc, Portland, OR), the three database search results can be

combined and statistically validated to give both peptide confidence levels and protein identification confidence levels.

2.2 Development of the sample preparation method

In order to obtain the greatest coverage of proteins for the reasons discussed above, I decided to use a MudPIT-centered approach. I utilized all three search algorithms in conjunction with statistical validation through the Peptide Prophet algorithm provided by the software package Scaffold (Proteome Software Inc., Portland, OR) (Keller et al., 2002). Having decided on the method of analysis, I turned to sample preparation, which is often the most important step in a given proteomics experiment. The purity and cleanliness of the sample determines how accurate and relevant my results will be. My sample preparation method is three-fold: 1. Isolate hair bundles from the underlying cell bodies and solubilize the proteins, 2. Separate the proteins from the rest of the sample (DNA, RNA, lipids) and remove all compounds that are incompatible with the MudPIT analysis, and 3. Process the isolated proteins for a mass spectrometry-based screen. I ran several pilot studies to test how each of these steps could be accomplished and determined which method is optimal for my research goal.

2.2.1 Bundle isolation and protein solubilization

In order to analyze bundle proteins, I needed to isolate the hair bundles from their cell bodies. To do this, I needed to choose a model system that allows me to easily separate large amounts of hair bundles away from the rest of the cells. To separate stereocilia hair bundles from the rest of the cell, I tested two techniques: the "bundle blot" (Shepherd et al., 1989) and the "twist-off" (Gillespie et al., 1991). Both these techniques require a fairly flat epithelium, so I chose to use utricles, a vestibular organ that is flat and contains many hair cells. I selected the chicken as my model system instead of the more widely used mouse animal model, because chickens have a seven times larger sensory epithelium and six times more hair bundles in the utricle than the mouse and they are more cost-effective (Desai et al., 2005; Goodyear et al., 1999; Li et

al., 2008). I used embryonic day 18 (E18) chicks, a point where hair cell stereocilia are fully formed and the MET apparatus is assembled in the basilar papilla (Si et al., 2003); furthermore, evidence shows that chick vestibular hair cells develop on a similar or earlier time course based on mature marker expression (Li et al., 2004). From this evidence, I assume that E18 vestibular chicken hair bundles are morphologically and functionally like mature bundles, therefore express the proteins necessary for determining the final hair bundle morphology. The use of chickens in MS based proteomics only recently became possible after the genome was sequenced (Hillier et al., 2004), which is why I use the chicken as the source of my bundles and not other organisms that may possess even larger sources of bundles, such as the bullfrog or various fish.

The "twist-off" technique and the "bundle blot" technique immobilize hair bundles differently, but both methods use a shearing force to separate the hair bundles from the hair cell bodies. The "twist-off" technique consists of embedding hair bundles in an agarose gel to grab them, whereas the "bundle-blot" technique makes use of the adhesive quality of nitrocellulose to hold the hair bundles. The "twist-off" name comes from the twisting motion that ensues in order to shear the bundles off the hair cells. For the "bundle-blot" technique, the apical surface of the utricle was pushed against the nitrocellulose, then the utricle was pulled away leaving just hair bundles remaining on the nitrocellulose.

I found that the "Twist-off" technique yielded more hair bundles and was more consistently reproducible than the "Bundle blot" technique; therefore, I proceeded exclusively with this technique. To optimize the technique for the chicken utricle, I had to make some modifications to the originally proposed technique, which was designed for the bullfrog sacculus. I called my protocol the "rip-off" technique (summarized in figure 2.3a), because the utricles are ripped away from the hair bundles rather than twisted away. In the protocol, about 10-20 utricles are first dissected out of the chicken inner ear and placed inside a Teflon washer with the hair bundles exposed upward. The

washer is used to hold the small amount of molten agarose gel that is streamed over the top of the utricle with a 1mL pipette. I used an ultra-low gelling temperature agarose (Sigma Aldrich, A2576) in order to have the agarose as close to 39°C as possible when pipetted over the utricles in order to decrease the stress on the tissue. I used the agarose at a concentration of 4%, not the published 3%, because this was the optimum gel concentration that provided strong embedment of hair bundles in the gel for the chicken utricle. After the agarose was added, I placed the specimen at 4°C for 10 minutes to allow the gel to solidify.

Once the gel had solidified, I flipped the gel block over to expose the bottoms (maculae) of the utricles. I "ripped-off" each utricle separately to cause a shearing force across the hair bundles. Ripping was much more efficient for chicken utricle hair bundles than the originally proposed twist-off technique. I cleaned up the edges and any visible remaining tissue and cut out the agarose blocks containing bundles from each utricle. These gel plugs were now ready for protein solubilization.

I tested four different reagents in attempt to solubilize the proteins from the agarose: sodium dodecyl sulfate (SDS), urea, TritonX-100, and PPS silent surfactant (Protein Discovery, Knoxville, TN). PPS would maximize protein recovery by minimizing protein handling and processing steps, since simply adding acid to the solution can break down the detergent. Urea solubilized the protein, but also solubilized the agarose gel, resulting in added agarose contaminants in my sample. Triton X-100 was unable to disrupt the hair bundles from the agarose gel as assayed by F-actin staining of the gel plug after incubation with a Triton X-100 solution. SDS was the only detergent that disrupted the bundles from the agarose gel into solution without dissolving the gel, which is why I chose to proceed using SDS solubilization.

To solubilize the gel blocks, they were placed in a solution containing 2% SDS, 147mM Tris, and 0.51mM EDTA pH=8.5. The SDS solution also provided the advantage that it denatures all proteins, therefore, protecting my sample against proteases and ensuring

long-term stability. The SDS solution solubilized all proteins, lipids, and nucleic acids, while leaving the agarose gel intact. This allowed me to separate the solution from the gel by simple aspiration and to store the samples at -80°C until all dissections were completed.

To test the efficacy of hair bundle isolation and to visualize the hair bundles inside the agarose gel, I stained the gel blocks. I fixed the gel in 4% paraformaldehyde for 15 minutes and stained it with TritC-conjugated phalloidin, which labels the abundant F-actin in the hair bundle. With my technique, I obtained 812 ± 41 (mean±SEM; n = 7) distinct hair bundles in a given excised gel block, which corresponds to about 812 bundles recovered per utricular sensory epithelium. The isolated hair bundles have a similar morphology to hair bundles not subjected to my "rip-off" technique (figure 2.1a, 2.1b). Through improvement in my dissection technique and optimization of the agarose gel concentration, I greatly decreased the amount of cell body contamination (figure 2.1c). Cell body contamination is only seen to consist of 15 ± 0.72 (mean±SEM ; n = 7) cell bodies per gel block. This shows that I am achieving 98% efficiency in isolating pure hair bundles from the cell bodies.

2.2.2 Protein separation and detergent removal

The MudPIT analysis requires that most types of detergents be removed from the solution prior to loading the column. Many detergents, including SDS, interfere with binding, elution, and ionization of peptides on the columns during MudPIT analysis (Chen et al., 2007). Furthermore, tryptic digest will not work well, if at all, in SDS-containing samples. I tested two methods of protein separation and SDS removal.

The first technique uses the Proteospin Column (Norgen Biotek Corp., St. Catharines, ON, Canada), which implements a solid phase extraction technique applied in a spin column format. However, there are two drawbacks of this technique, namely a column limitation of 25μg of protein and inherent protein selectivity. The column protein

limitation stems from the amount of resin available to bind to proteins. The selectivity results from the column chemistry, which binds proteins with different affinities based on the protein's isoelectric point. This binding selectivity affects what proteins bind to and elute from the column. The selectivity becomes particularly problematic when the column is overloaded, as proteins with higher binding affinities will compete away proteins with lower binding affinities (Alpert et al., 2004).

The second technique to remove the SDS was trichloroacetic acid (TCA) precipitation followed by washes with acetone. TCA selectively precipitates proteins by decreasing the pH of the solution and causing the proteins to denature into a "sticky state" and aggregate (Sivaraman et al., 1997). TCA precipitation also exhibits protein selectivity (Zellner et al., 2005). It is unknown what types of proteins TCA precipitation is biased towards, but it appears to be related to the structure of the protein. I used 23% TCA for my precipitation in a solution with 20mM dithiothreitol (DTT), which inhibits the formation of disulfide bonds, to prevent proteins from covalently binding with each other.

In collaboration with Dr. Andrew Guzzetta at the Stanford University Mass Spectrometry core facility, we compared the Proteospin column with TCA precipitation using a 4 hour reverse phase (RP) LC/MS/MS, which is a conventional analysis method using only a single dimension of chromatography resulting in a lower sensitivity than MudPIT. As an initial test, we used 14 whole chicken utricles as starting material that was lysed in the SDS solution. Liquid chromatography elution profiles indicate the abundance of peptides coming off the column. A given peptide should always elute off the column around the same time for a given set of parameters, therefore different elution profiles suggest different peptide mixtures. Each technique gave different chromatograms and led to different sets of identified proteins, showing that each method may be selectively retaining different sets of peptides (figure 2.2). I set the thresholds for protein identification in these pilot experiments to >95% protein identification confidence, using only peptides with >95% confidence. The TCA precipitation method resulted in 67

identified proteins (table 2.1), whereas the spin column method identified 65 proteins (table 2.2), with 28 proteins common to both datasets.

Since each method had its own selectivity, I decided to test both methods in a small-scale hair bundle isolation experiment using hair bundle "rip-offs" of 120 utricles for each method. This scenario reflects the smaller protein amounts that I anticipate when using only hair bundles. The TCA precipitation method yielded 34 identified proteins (table 2.3), 9 of which are proteins known to reside in the hair bundle (table 2.4). Seven of the identified proteins are contaminants from blood, egg white, or human skin. The remaining 23 proteins are likely a mix of hair bundle proteins and possibly other contaminants. Nonetheless, this dataset demonstrates the feasibility of the experimental method, since I was able to identify many known hair bundle proteins using bundles isolated from only 120 utricles in conjunction with the less sensitive 4 hour LC/MS/MS method, compared to a MudPIT analysis. Additionally, three of the identified known proteins had been previously reported as specifically targeted to the hair bundles and are generally not detectable in the hair cell body; these proteins were: PTPRQ, radixin, and PMCA2 (Dumont et al., 2001; Goodyear et al., 1992; Pataky et al., 2004). This result indicated that I was able to specifically identify stereocilia proteins and achieve an enrichment of hair bundle proteins, since none of these 3 proteins were identified with the whole utricle samples.

Unfortunately, the spin column method did not yield any results, and based on a number of additional tests, I concluded that a certain protein concentration threshold must be surpassed in order for proteins to bind to the column. In this case, this would require the introduction of a carrier protein into the sample. This carrier protein would add to my sample contamination and may end up masking hair bundle proteins.

Based on these pilot experiments, I decided to proceed with using the TCA precipitation. The small-scale bundle experiment also gave me confidence to proceed with my large-scale experiment.

2.2.3 Protein cleavage

With the detergent removed, the next step in my sample preparation was the cleavage of proteins into peptides using trypsin. Trypsin is a very specific protease that cleaves proteins on the carboxyl-terminal side of lysines and arginines, except when they are followed by a proline. Tryptic fragments that are unique to a given protein average 14.6 amino acids long, which is a good length for mass spectrometry identification (Shadforth et al., 2005). Complete cleavage of the protein at well-defined sites is important for accurate identification of peptides and substantially decreases database search time.

For highly efficient trypsin digestion, the substrate (sample protein) needs to be denatured to allow access to all cleavable sites. Once denatured, the protein is reduced with DTT and carboxymethylated with iodoacetic acid in order to break disulfide bonds and prevent them from reforming. Urea is the traditional protein solubilizer and denaturant used in mass spectrometry because of its compatibility with reverse-phase liquid chromatography, a component of MudPIT analysis. However, urea has the disadvantage of denaturing the trypsin as well, and a concentration of urea low enough for sufficient trypsin activity may not be sufficient to completely denature the protein sample (Chen et al., 2007). Recently, other surfactants have also become compatible with MudPIT analysis, and possibly providing better protein denaturation.

In collaboration with Andrew Guzzetta at the core facility, we tested one of these newly developed surfactants, RapiGest^{TM} SF (Waters Corp., Milford, MA), which has been shown to increase the number of proteins identified over using urea as the denaturant during trypsin digest (Chen et al., 2007; Klammer et al., 2006). We compared RapiGest SF and urea as denaturants. Using TCA precipitated, SDS solubilized whole utricle lysates, we found that the urea solubilized sample identified 76 proteins compared to only 15 proteins identified in the RapiGest SF solubilized sample. This result along with additional experiences of Andrew Guzzetta, led me to decide that urea is the most feasible denaturant for my protocol, as it allows more protein identifications.

The final protocol (figure 2.3b) consisted of re-suspending the TCA precipitated protein pellet in 8M urea. Denatured proteins were reduced with 10mM DTT for 4 hours at ambient temperature and carboxymethylated with 25mM iodoacetic acid for 30 minutes in the dark. The protein solution was then diluted to 1M urea, and 1μg modified trypsin (Promega, Madison, WI), which decreases the amount of self-cleavage, was added, and the sample proteins were digested for 18 hours at ambient temperature. The peptides were purified from the solution using a Pepclean C-18 spin column (Thermo Fisher Scientific, Rockford, IL).

2.2.4 Large-scale proteomics method

With my proteomics screen fully developed (figure 2.3), I was ready to proceed with the full-scale experiment. For the experiment, I planned to isolate bundles from 2000 utricles. Before running the sample, I used $1/20^{th}$ of this sample for a test run to ensure that the MudPIT columns and the mass spectrometer were working properly. With this number of utricles, I expected to detect many of the cytoskeletal proteins and their related effectors. When estimating detection limits, I needed to make some assumptions. Assuming 100 stereocilia per bundle, 800 bundles recovered per utricle by the "rip-off" procedure (figure 2.1c), and a MS detection limit of 1 femtomole, I estimated the ability to detect proteins expressed at the level of 4 protein molecules per stereocilium. However, I also needed to take into account losses associated with TCA precipitation and chromatography. If I assumed 90% protein recovery after TCA precipitation and 80% after chromatography, then there is a net of 72% protein recovery after both processes. This means I should detect proteins expressed at the level of 6 molecules per stereocilium, which should be more sensitive than necessary for finding actin regulators. This is a theoretical estimate; inherent selectivity in TCA precipitation and chromatography columns as well as peptide exposure for tryptic digest affects which proteins and the amount of peptides retained for analysis. Even if the requisite peptides are injected into the mass spectrometer, there is a sampling effect and all proteins above the level of detection may not get analyzed. Nevertheless, I was expecting to obtain a relatively comprehensive data set that contains not only highly

abundant proteins, but also moderately abundant proteins and even some low abundant stereocilia proteins.

2.3 Conclusions

I have developed an effective technique to analyze hair bundle proteins. Using pilot experiments, I was able to optimize the method for maximizing the number of identified proteins. My finalized technique worked on a small-scale experiment using hair bundles from 120 utricles and successfully identified stereocilia enriched proteins. When applied to 1900 utricles, I was able to identify many more proteins, a result that will be described in detail in the next chapter.

During the development of my proteomics method, Dr. Gillespie's Laboratory published a paper describing a similar proteomics experiment. Their bundle isolation is largely similar with the exception that they use E20 instead of E18 chickens, and that they only isolated bundles from about 120 utricles (Shin et al., 2007). The major difference between our techniques lies in the extraction of proteins from the isolated bundle. Shin et al. dried the agarose plugs and immediately reduced and carboxymethylated the proteins. At this point they trypsinized the protein in the presence of 10% acetonitrile, which is more likely to help boost trypsin activity than to denature proteins (Haas et al., 1995). This sample preparation technique does not directly address lysis of the cell membrane, and it also does not denature proteins prior to trypsinization, therefore, increasing the chances of missed cleavages, reducing sensitivity, and complicating data analysis. Even if the protein recovery efficiency was equal to my technique, because I have different tissue harvesting and sample preparation methods, I am likely to have a different selectivity; therefore, our datasets may complement each other.

This page is intentionally left blank.

Figure 2.1 - Native hair bundle morphology (a) stained with TRITC-phalloidin matches the morphology of isolated hair bundles (b) in agarose. (c) There are 812 ± 41 SEM (n = 7) isolated hair bundles as indicated by phalloidin staining (red) per utricle with only 15 ± 0.72 SEM (n = 7) cell body contaminants as indicated by TOTO-3 nuclear staining (white). Scale bar = (a) 5μm, (b) 5μm, (c) 100μm

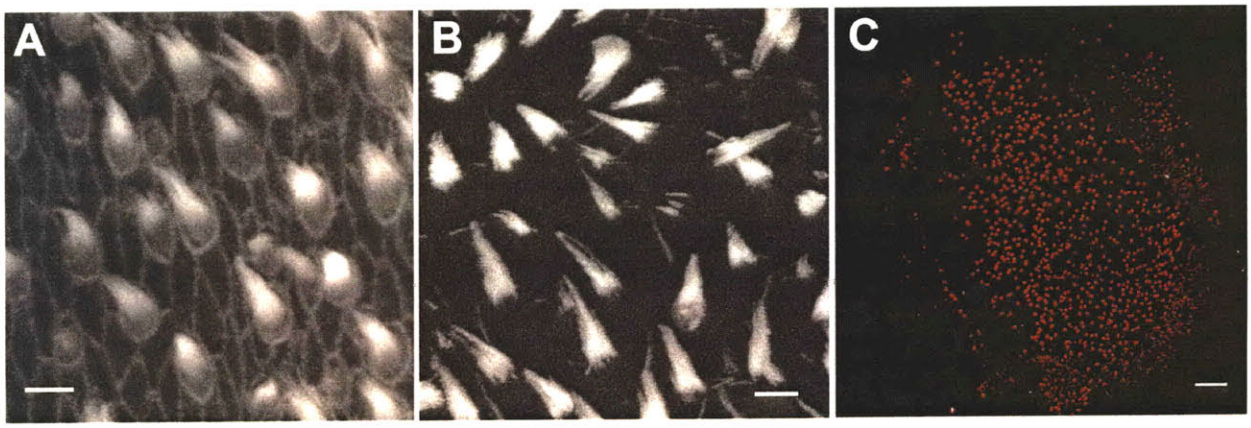

This page is intentionally left blank.

Figure 2.2 - Chromatograms from a 4-hour RP LC column of SDS solubilized whole utricles. The SDS was removed using the Proteospin column method (top) and the TCA precipitation method (bottom). Base peak abundance is plotted.

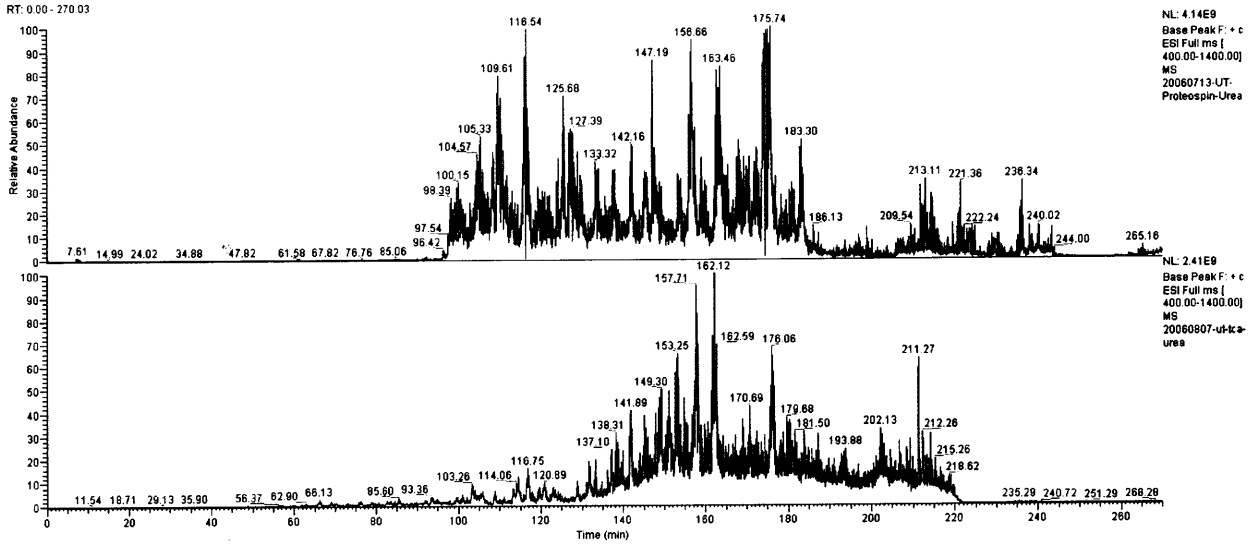

This page is intentionally left blank.

Figure 2.3 Summary of Proteomics Method with (a) the tissue isolation procedure and (b) the sample preparation and MudPIT analysis technique

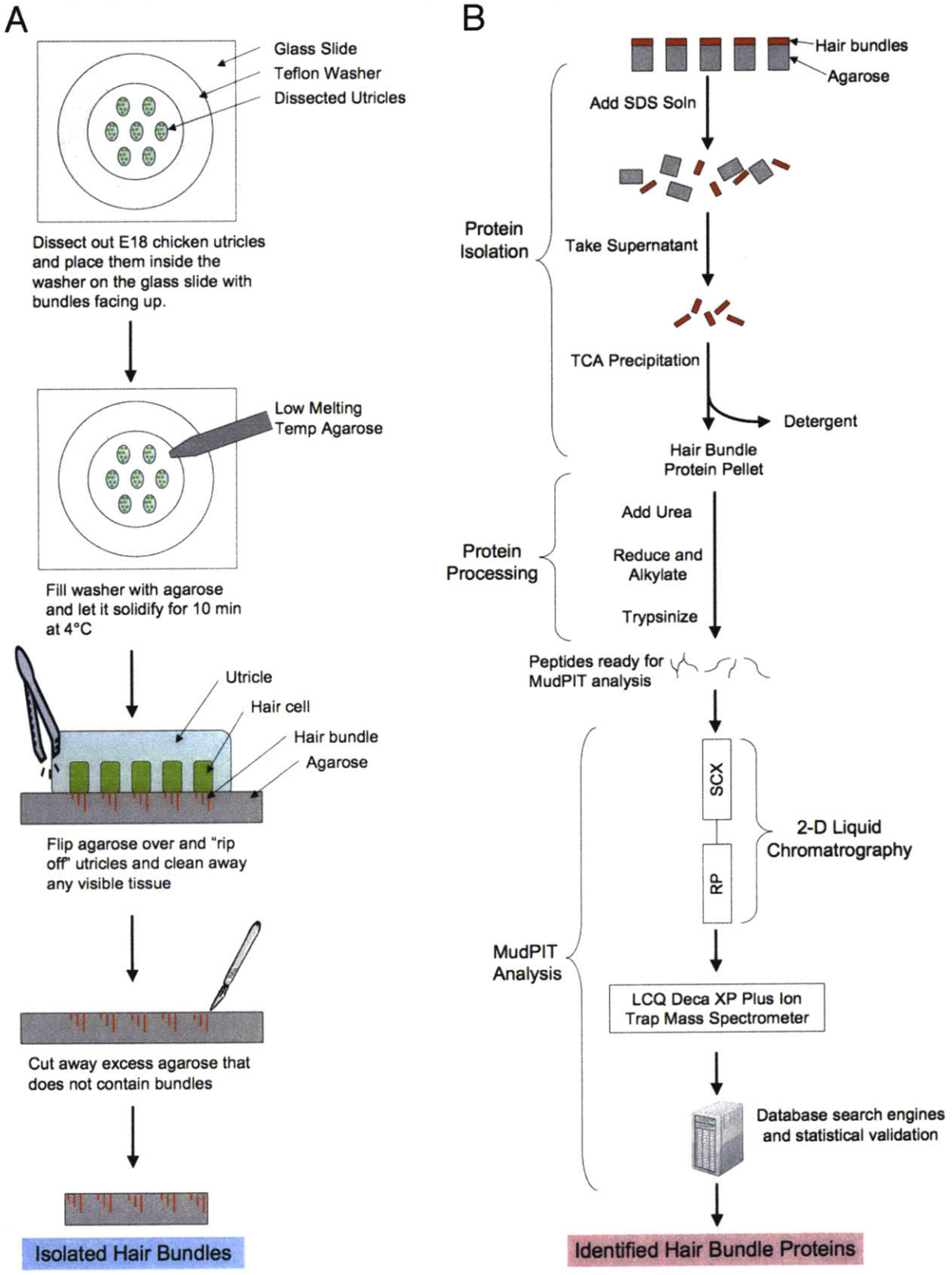

This page is intentionally left blank.

Table 2.1 Protein identification results from a proteomics experiment of 14 utricles using TCA precipitation followed by urea denaturation. Accession #'s are GI numbers from Genbank. IC = Identification confidence

Accession #	Protein Description	IC
1703121	Actin, cytoplasmic type 5	100%
2293562	Coch-5B2 [Gallus gallus]	100%
135474	Tubulin beta-7 chain (Tubulin beta 4')	100%
223280	tubulin alpha	100%
1628381	glyceraldehyde-3-phosphate dehydrogenase [Gallus gallus]	100%
122587	Hemoglobin subunit beta (Hemoglobin beta chain) (Beta-globin)	100%
1706653	Alpha-enolase (2-phospho-D-glycerate hydro-lyase) (Phosphopyruvate hydratase)	100%
3122072	Elongation factor 1-alpha 1 (EF-1-alpha-1) (Elongation factor Tu) (EF-Tu)	100%
82082513	ATP synthase beta chain, mitochondrial precursor	100%
211118	alpha-globin-D	100%
15546070	alpha 1 type IIA collagen precursor [Gallus gallus]	100%
50732571	PREDICTED: similar to RIKEN cDNA E030025L21 gene [Gallus gallus]	100%
122378	Hemoglobin alpha-A subunit (Hemoglobin alpha-A chain) (Alpha-A-globin)	100%
123575	47 kDa heat shock protein precursor (Collagen-binding protein 1)	100%
1351941	Annexin A5 (Annexin V) (Lipocortin V) (Endonexin II) (Calphobindin I) (CBP-I) (Placental anticoagulant protein I) (PAP-I) (PP4) (Thromboplastin inhibitor) (Vascular anticoagulant-alpha) (VAC-alpha) (Anchorin CII)	100%
52695585	Chain A, Triosephosphate Isomerase From Gallus Gallus, Loop 6 Mutant T175v	100%
211827	78-kD glucose-regulated protein precursor	100%
22651801	glucose regulated thiol oxidoreductase protein precursor [Gallus gallus]	100%
50732409	PREDICTED: similar to vimentin - chicken [Gallus gallus]	100%
17225596	ATP synthase alpha subunit [Gallus gallus]	100%
50758110	PREDICTED: similar to malate dehydrogenase, mitochondrial; malate dehydrogenase 2; Malate dehydrogenase 2 NAD (mitochondrial) [Gallus gallus]	100%
82197807	14-3-3 protein zeta	100%
50751518	PREDICTED: similar to peroxiredoxin 1 [Gallus gallus]	100%
123668	Heat shock protein HSP 90-alpha	100%
71895985	phosphoglycerate mutase 1 (brain) [Gallus gallus]	100%
125293	Creatine kinase B-type (Creatine kinase B chain) (B-CK)	100%
110279000	Histone H2B 1/2/3/4/6 (H2B I) (H2B II) (H2B III) (H2B IV) (H2B VI)	100%
1493827	histone H2A	100%
2996407	heat shock cognate 70 [Gallus gallus]	100%
12082647	lactate dehydrogenase B [Gallus gallus]	100%
119359	Endoplasmin precursor (Heat shock protein 90 kDa beta member 1) (Heat shock 108 kDa protein) (HSP108) (HSP 108) (Transferrin-binding protein)	100%
50729210	PREDICTED: similar to histone H1.02 - chicken [Gallus gallus]	100%
1582081	collapsin response mediator protein:ISOTYPE=CRMP-62	100%
50759528	PREDICTED: similar to neurofilament-L [Gallus gallus]	100%
46048903	voltage-dependent anion channel 2 [Gallus gallus]	100%
125608	Pyruvate kinase muscle isozyme	100%
3420726	Rab-GDP dissociation inhibitor [Gallus gallus]	100%

50758346	PREDICTED: similar to Clathrin heavy chain 1 (CLH-17) [Gallus gallus]	100%
115268	Collagen alpha-1(I) chain precursor	100%
22775582	ATP/ADP antiporter [Gallus gallus]	100%
57530768	protein disulfide isomerase family A, member 4 [Gallus gallus]	100%
1184958	elongation factor 2	100%
585535	Myelin P0 protein precursor (Myelin protein zero) (Myelin peripheral protein) (MPP)	100%
118088	Peptidyl-prolyl cis-trans isomerase B precursor (PPIase) (Rotamase) (Cyclophilin B) (S-cyclophilin) (SCYLP)	100%
12381875	ribosomal protein L22 [Gallus gallus]	100%
50750353	PREDICTED: similar to cytosolic NADP-dependent isocitrate dehydrogenase [Gallus gallus]	100%
61217546	Spliceosome RNA helicase BAT1 (DEAD box protein UAP56) (56 kDa U2AF65-associated protein)	100%
82197924	14-3-3 protein epsilon (14-3-3E)	100%
50750864	PREDICTED: similar to tubulin, alpha 2; tubulin alpha 2 [Gallus gallus]	100%
50745031	PREDICTED: similar to Protein disulfide isomerase A6 precursor (Protein disulfide isomerase P5) (Thioredoxin domain containing protein 7) [Gallus gallus]	100%
60302796	SH3 domain binding glutamic acid-rich protein like [Gallus gallus]	99%
44969651	calreticulin [Gallus gallus]	99%
50751232	PREDICTED: similar to alpha-1 type XI collagen [Gallus gallus]	99%
2827444	nucleoside diphosphate kinase [Gallus gallus]	99%
61097999	saccharopine dehydrogenase (putative) [Gallus gallus]	99%
28866788	Surf4 [Gallus gallus]	99%
71896205	hypothetical protein LOC431056 [Gallus gallus]	99%
50762238	PREDICTED: similar to valosin precursor [Gallus gallus]	99%
121988	Histone H2A variant	99%
33331366	phosphoglucomutase 1 [Gallus gallus]	99%
50736040	PREDICTED: similar to ATP binding cassette transporter A13 [Gallus gallus]	99%
1346814	Parvalbumin, thymic CPV3 (Parvalbumin 3)	98%
1149509	37kD Laminin receptor precursor /p40 ribosomal associated protein [Gallus gallus]	98%
50759011	PREDICTED: similar to Matrilin-4 precursor [Gallus gallus]	98%
45384528	ribosomal protein L13 [Gallus gallus]	98%
37723968	tenomodulin [Gallus gallus]	98%
47825387	phosphoribosylglycinamide formyltransferase, phosphoribosylglycinamide synthetase, phosphoribosylaminoimidazole synthetase [Gallus gallus]	98%

Table 2.2 Protein identification results from a proteomics experiment of 14 utricles using the Proteospin Column followed by urea denaturation. Accession #'s are GI numbers from Genbank. IC = Identification confidence

Accession #	Protein Description	IC
1703121	Actin, cytoplasmic type 5	100%
2293562	Coch-5B2 [Gallus gallus]	100%
135474	Tubulin beta-7 chain (Tubulin beta 4')	100%
223280	tubulin alpha	100%
1628381	glyceraldehyde-3-phosphate dehydrogenase [Gallus gallus]	100%
122587	Hemoglobin subunit beta (Hemoglobin beta chain) (Beta-globin)	100%
1706653	Alpha-enolase (2-phospho-D-glycerate hydro-lyase) (Phosphopyruvate hydratase)	100%
3122072	Elongation factor 1-alpha 1 (EF-1-alpha-1) (Elongation factor Tu) (EF-Tu)	100%
82082513	ATP synthase beta chain, mitochondrial precursor	100%
211118	alpha-globin-D	100%
15546070	alpha 1 type IIA collagen precursor [Gallus gallus]	100%
1346814	Parvalbumin, thymic CPV3 (Parvalbumin 3)	100%
50732571	PREDICTED: similar to RIKEN cDNA E030025L21 gene [Gallus gallus]	100%
122378	Hemoglobin alpha-A subunit (Hemoglobin alpha-A chain) (Alpha-A-globin)	100%
123575	47 kDa heat shock protein precursor (Collagen-binding protein 1)	100%
1351941	Annexin A5 (Annexin V) (Lipocortin V) (Endonexin II) (Calphobindin I) (CBP-I) (Placental anticoagulant protein I) (PAP-I) (PP4) (Thromboplastin inhibitor) (Vascular anticoagulant-alpha) (VAC-alpha) (Anchorin CII)	100%
129293	Ovalbumin (Plakalbumin) (Allergen Gal d 2) (Gal d II)	100%
52695585	Chain A, Triosephosphate Isomerase From Gallus Gallus, Loop 6 Mutant T175v	100%
211827	78-kD glucose-regulated protein precursor	100%
22651801	glucose regulated thiol oxidoreductase protein precursor [Gallus gallus]	100%
113575	Serum albumin precursor (Alpha-livetin) (Allergen Gal d 5)	100%
50732409	PREDICTED: similar to vimentin - chicken [Gallus gallus]	100%
17225596	ATP synthase alpha subunit [Gallus gallus]	100%
50758110	PREDICTED: similar to malate dehydrogenase, mitochondrial; malate dehydrogenase 2; Malate dehydrogenase 2 NAD (mitochondrial) [Gallus gallus]	100%
82197807	14-3-3 protein zeta	100%
211386	calmodulin	100%
50751518	PREDICTED: similar to peroxiredoxin 1 [Gallus gallus]	100%
1628382	alpha-globin [Gallus gallus]	100%
50728592	PREDICTED: similar to histone protein Hist2h3c1 [Gallus gallus]	100%
50756703	PREDICTED: similar to Phosphatidylethanolamine-binding protein (PEBP) (HCNPpp) (Basic cytosolic 21 kDa protein) [Gallus gallus]	100%
5921192	Collagen alpha-2(I) chain precursor	100%
113990	Apolipoprotein A-I precursor (Apo-AI) (ApoA-I)	100%
67476967	Endoplasmic reticulum protein ERp29	100%
50982399	annexin A6 [Gallus gallus]	100%
1730518	Phosphoglycerate kinase	100%
60302796	SH3 domain binding glutamic acid-rich protein like [Gallus gallus]	100%

50728840	PREDICTED: similar to cytoskeleton-associated protein 4; transmembrane protein (63kD), endoplasmic reticulum/Golgi intermediate compartment; type-II transmembrane protein p63 [Gallus gallus]	100%
128146	Neurofilament triplet M protein (160 kDa neurofilament protein) (Neurofilament medium polypeptide) (NF-M)	100%
113949	Annexin A2 (Annexin II) (Lipocortin II) (Calpactin I heavy chain) (Chromobindin-8) (p36) (Protein I) (Placental anticoagulant protein IV) (PAP-IV)	100%
226855	aldolase C	100%
222847	proteoglycan core protein [Gallus gallus]	100%
57530004	nucleobindin 2 [Gallus gallus]	100%
135767	Thioredoxin	100%
50729945	PREDICTED: similar to mitochondrial ATP synthase, O subunit [Gallus gallus]	100%
87244967	cell-cycle related and expression-elevated protein in tumor [Gallus gallus]	100%
71894959	microtubule-associated protein, RP/EB family, member 1 [Gallus gallus]	100%
212395	myosin alkali light chain	100%
18252632	zipcode-binding protein [Gallus gallus]	100%
50745403	PREDICTED: similar to protein disulfide-isomerase (EC 5.3.4.1) precursor - chicken [Gallus gallus]	100%
50752072	PREDICTED: similar to Vesicle-associated membrane protein 2 (VAMP-2) (Synaptobrevin 2) [Gallus gallus]	100%
71896903	heat shock 70kD protein binding protein [Gallus gallus]	100%
1350778	60S acidic ribosomal protein P0 (L10E)	100%
212873	vinculin	100%
123668	Heat shock protein HSP 90-alpha	99%
50757480	PREDICTED: similar to Tubulin beta-2 chain [Gallus gallus]	99%
71895985	phosphoglycerate mutase 1 (brain) [Gallus gallus]	99%
50757498	PREDICTED: similar to 60S ribosomal protein L12 [Gallus gallus]	99%
1149509	37kD Laminin receptor precursor /p40 ribosomal associated protein [Gallus gallus]	99%
50738496	PREDICTED: similar to Spectrin beta chain, brain 1 (Spectrin, non-erythroid beta chain 1) (Beta-II spectrin) (Fodrin beta chain) [Gallus gallus]	99%
3345475	keratin-19 [Gallus gallus]	99%
110227609	spectrin, alpha, non-erythrocytic 1 (alpha-fodrin) [Gallus gallus]	99%
50731093	PREDICTED: similar to acetyl-Coenzyme A acetyltransferase 1 precursor [Gallus gallus]	98%
127171	Myosin regulatory light chain 2, smooth muscle minor isoform (G1) (DTNB) (MLC-2) (Isoform L20-B1)	98%
11320877	aldehyde dehydrogenase-6 [Gallus gallus]	98%
71895845	non-POU domain containing, octamer-binding [Gallus gallus]	98%

Table 2.3 Protein identification results from a proteomics experiment of 120 bundles using TCA precipitation followed by urea denaturation. Accession #'s are GI numbers from Genbank. IC = Identification confidence. Proteins known to be in the hair bundle are shaded gray

Accession #	Protein Description	IC
1703121	Actin, cytoplasmic type 5	100%
2293562	Coch-5B2 [Gallus gallus]	100%
135474	Tubulin beta-7 chain (Tubulin beta 4')	100%
223280	tubulin alpha	100%
1628381	glyceraldehyde-3-phosphate dehydrogenase [Gallus gallus]	100%
122587	Hemoglobin subunit beta (Hemoglobin beta chain) (Beta-globin)	100%
1706653	Alpha-enolase (2-phospho-D-glycerate hydro-lyase) (Phosphopyruvate hydratase)	100%
3122072	Elongation factor 1-alpha 1 (EF-1-alpha-1) (Elongation factor Tu) (EF-Tu)	100%
122378	Hemoglobin alpha-A subunit (Hemoglobin alpha-A chain) (Alpha-A-globin)	100%
1351941	Annexin A5 (Annexin V) (Lipocortin V) (Endonexin II) (Calphobindin I) (CBP-I) (Placental anticoagulant protein I) (PAP-I) (PP4) (Thromboplastin inhibitor) (Vascular anticoagulant-alpha) (VAC-alpha) (Anchorin CII)	100%
52695585	Chain A, Triosephosphate Isomerase From Gallus Gallus, Loop 6 Mutant T175v	100%
211827	78-kD glucose-regulated protein precursor	100%
22651801	glucose regulated thiol oxidoreductase protein precursor [Gallus gallus]	100%
50732409	PREDICTED: similar to vimentin - chicken [Gallus gallus]	100%
17225596	ATP synthase alpha subunit [Gallus gallus]	100%
125293	Creatine kinase B-type (Creatine kinase B chain) (B-CK)	100%
2996407	heat shock cognate 70 [Gallus gallus]	100%
129293	Ovalbumin (Plakalbumin) (Allergen Gal d 2) (Gal d II)	100%
50757480	PREDICTED: similar to Tubulin beta-2 chain [Gallus gallus]	100%
50810565	PREDICTED: similar to type II alpha-keratin IIC [Gallus gallus]	100%
50728376	PREDICTED: similar to protein tyrosine phosphatase, receptor type, Q isoform 1 precursor; glomerular mesangial cell receptor protein-tyrosine phosphatase; glomerular mesangial cell receptor protein-tyrosine phosphatase precursor [Gallus gallus]	100%
115644	Calretinin (CR)	100%
295721	conalbumin [Gallus gallus]	100%
120165	Plastin-1 (Fimbrin)	100%
82082513	ATP synthase beta chain, mitochondrial precursor	99%
1346814	Parvalbumin, thymic CPV3 (Parvalbumin 3)	99%
50760887	PREDICTED: similar to keratin K12 [Gallus gallus]	99%
32363425	Radixin	99%
15281845	GTP binding protein Rab1a [Gallus gallus]	99%
71897051	cold inducible RNA binding protein [Gallus gallus]	99%
50732571	PREDICTED: similar to RIKEN cDNA E030025L21 gene [Gallus gallus]	98%
123575	47 kDa heat shock protein precursor (Collagen-binding protein 1)	98%
113990	Apolipoprotein A-I precursor (Apo-AI) (ApoA-I)	98%
50754256	PREDICTED: similar to plasma membrane calcium ATPase 2; ATPase isoform 2, Na+K+ transporting, beta polypeptide 2; ATPase isoform 2 Na+K+ transporting beta polypeptide 2 [Gallus gallus]	98%

Table 2.4 Stereocilia proteins identified in the small-scale hair bundle proteomics experiment in table 2.3. Stereocilia enriched proteins are highlighted in gray.

Known Hair Bundle Protein	Identification Confidence
β-Actin	100%
GAPDH	100%
Ptprq (hair cell antigen)	100%
Calretinin	100%
Fimbrin	100%
β-creatine kinase	100%
Radixin	99%
PV3	99%
PMCA2	98%

Chapter 3: Results of the Proteomics Screen

3.1 Overview of known hair bundle proteins

F-actin forms the rigid stereocilia backbone and is probably one of the most abundant stereocilia proteins. This backbone is thought to be linked directly or indirectly to the proteins involved in MET, the principal function of stereocilia. Ca^{2+} plays an important role in the functional aspect of MET; therefore, stereocilia contain many proteins to help with the buffering and removal of calcium. On top of these proteins, other proteins have been found through genetic screening, yeast 2-hybrid studies, antibody studies, and molecular cloning techniques.

I will discuss below the proteins that have been confirmed in stereocilia through immunostaining. Occurrence of these known proteins in my proteomic screen will act as positive controls to validate my technique, thereby, providing guideposts to aid in the interpretation of my MudPIT results.

3.1.1 Structural / Cytoskeletal Proteins

The backbone of stereocilia is composed of several cytoskeletal proteins, a few of which were mentioned in section 1.4. To recap, stereocilia are known to have β and γ actin monomers, which are crosslinked by fimbrin and espin (Tilney et al., 1989; Zheng et al.,

2000). Some of the F-actin is thought to terminate at the plasma membrane, where radixin anchors it, with the possible help of CLIC5 (Gagnon et al., 2006; Khan et al., 2007; Pataky et al., 2004). Additionally, two proteins localized to stereocilia, known to be important for regulating the length of stereocilia indirectly, are myosin XVa and whirlin (Belyantseva et al., 2005; Delprat et al., 2005; Kikkawa et al., 2005).

There are proteins that have been implicated in inter-stereocilia links. A characteristic of the hair bundle is that when a single stereocilium moves, the rest of the bundle moves with it, which illustrates these inter-stereocilia links are important for the structural integrity of the hair bundle, (Nayak et al., 2007). Stereocilin has been suggested to be a part of the horizontal top connecters of stereocilia, which help the bundle maintain its shape when moved (Verpy et al., 2008). Protocadherin 15 (Pcdh15) and cadherin 23 (Cdh23) both have been implicated as being components of the rigid tip-link that is responsible for conveying the force to gate the MET channel when stereocilia are deflected (Ahmed et al., 2006; Kazmierczak et al., 2007; Siemens et al., 2004). Protein tyrosine phosphatase receptor Q (Ptprq), otherwise known as the "hair cell antigen," is thought to be a component of the shaft connectors (Goodyear et al., 2003). Very large G-coupled receptor 1 (VLGR1), usherin, and vezatin are hypothesized to be a part of the ankle links of stereocilia (Adato et al., 2005a; McGee et al., 2006; Michalski et al., 2007)}. All of these proteins help to maintain the structure of the hair bundles and likely contribute to the mechanical properties of the hair bundle.

3.1.2 Ca^{2+} regulation proteins

Ca^{2+} plays a vital role as a signaling and modulating ion in stereocilia. Specific features of the MET channel and the properties of adaptation depend on the local Ca^{2+} concentration. Consequently, the control of local Ca^{2+} levels is very important in stereocilia, hence the presence of both Ca^{2+} buffers and Ca^{2+} pumps. Ca^{2+} buffering proteins calmodulin, calretinin, calbindin, and parvalbumin 3 (oncomodulin) have been localized to stereocilia (Hackney et al., 2005; Heller et al., 2002). These buffers work

along with plasma membrane Ca^{2+}-ATPase 2 (PMCA2), the main stereocilia Ca^{2+} pump, to keep the intracellular free calcium concentration low (Dumont et al., 2001).

3.1.3 pH regulation

PMCA2 pumps calcium out of stereocilia while transporting in H^+. Due to abundant activity of PMCA2, the amount of H^+ pumped into stereocilia is very high and would quickly change the pH of stereocilia. Na^+/H^+ exchangers (NHE) work to regulate the pH of stereocilia by transporting the H^+ out of stereocilia. NHE6 and NHE9, both able to act as K^+/H^+ exchangers, have been localized to stereocilia with NHE9 being the more prominent isoform (Hill et al., 2006).

3.1.4 Myosin Motors in stereocilia

In addition to myosin XVa, many other myosin motors have been localized to stereocilia. Myosin Ic has been put forward as being responsible for the slow and fast adaptation exhibited by hair cells (Holt et al., 2002; Stauffer et al., 2005). Myosin Ic has been localized to the tips of stereocilia by immunostaining (Gillespie et al., 1993), and it is hypothesized to be the motor required for tensioning the MET apparatus. Myosin VIIa is also found in stereocilia and malfunctions of this protein are responsible for USH1b. Based on mouse mutants, myosin VIIa appears to be required for the proper development of hair bundles as well as the proper functioning of MET (Gibson et al., 1995; Self et al., 1998). The evidence may indicate that myosin VIIa helps anchor stereocilia proteins to the actin core and keep the plasma membrane taut around the stereocilia core so that the elasticity of the membrane is kept to a minimum. Through immunohistochemical and biochemical studies, myosin VI is seen in stereocilia as well as in and near the cuticular plate (Hasson et al., 1997; Shin et al., 2007). Knockout models of myosin VI in mice show the importance of myosin VI in development, with mutants showing disorganized and fused stereocilia (Self et al., 1999). Myosin IIIa has recently been localized to stereocilia in a thimble like pattern at the tips of stereocilia (Schneider et al., 2006). It was known to be required for hearing, since mutations in the

motor domain lead to progressive, non-syndromic hearing loss DFNB30 (Walsh et al., 2002). Recent advances show that myosin IIIa is responsible for transporting espin 1 to the tips of stereocilia (Salles et al., 2009). Non-muscle myosin IIa (NMMHC-IIa) has also been localized to stereocilia, but its function has yet to be elucidated (Lalwani et al., 2008; Mhatre et al., 2004; Mhatre et al., 2006).

3.1.5 Energy metabolism proteins

An abundant amount of ATP is required to keep up with the metabolic processes in stereocilia from Ca^{2+} regulation to myosin motor movement. This high demand for ATP would require nearby ATP generation. Since stereocilia lack mitochondria, they turn to other methods for ATP generation. Stereocilia have been shown to have brain-type creatine kinase (B-CK), which helps to maintain stereocilia ATP levels by generating ATP from phosphocreatine (Shin et al., 2007). Glyceraldehyde-3-phosphate dehydrogenase (GAPDH) has also been localized to stereocilia likely participating in glycolysis to generate ATP (Shin et al., 2007).

3.1.6 Other scaffolding proteins

There have been a few other scaffolding proteins that are seen in stereocilia. The protein harmonin, an USH1c protein, has been shown to be an important scaffolding protein, interacting with all known USH1 proteins via its 3 PDZ domains (Adato et al., 2005b; Boeda et al., 2002; Reiners et al., 2005; Siemens et al., 2002). MAGI-1 a large scaffolding protein has been hypothesized to help organize proteins associated with the cadherin 23 side of the tip-link (Xu et al., 2008). Na^+/H^+ exchange regulatory factor 1 (NHERF-1) and NHERF-2, two PDZ scaffolding proteins, have been localized to stereocilia as well, and these proteins are likely helping to scaffold proteins to the Na^+/H^+ exchangers. Ca^{2+}-calmodulin serine kinase (CASK) and p55 have both been localized to stereocilia and can act as scaffolding proteins, which interact with whirlin and 4.1N, both which are also localized to stereocilia (Mburu et al., 2006).

3.2 Methods

The MudPIT analysis of my 1900 utricles was done in collaboration with Andrew Guzzetta. I implemented a modified version of the traditional MudPIT experiment by using a tetraphasic continuous column approach (Guzzetta et al., 2005). In this modified MudPIT analysis, the peptide mixture was separated by a triphasic MudPIT trap followed by a 15cm RP capillary column. In the triphasic MudPIT trap there was a RP section, followed by a SCX section, and finally another RP section. The first RP section served two purposes. First, it allowed us to load the column multiple times by allowing proteins to be retained in the column while the remaining fluid is washed through (McDonald et al., 2002). The second purpose was to desalt the sample. Desalting of the sample was necessary because if salts were present when loading onto the subsequent SCX portion, the salts would have competed for interaction sites on the column, which would have resulted in a loss of peptides. The SCX 2nd phase and the RP 3rd phase were used to separate the peptides in 2 dimensions based on the charge and hydrophobicity of the peptide, respectively. The final 15cm RP column was used to create a greater separation of the peptides, since better separation leads to more peptides being identified, due to fewer overlapping peaks on the chromatogram. For the MudPIT analysis, 8 salt steps off the SCX were used to bump off fractions onto the RP column, 0mM, 50mM, 100mM, 250mM, 500mM, 1000mM, 2500mM, and 5000mM ammonium acetate. Each salt step was run on a reverse phase column for 2 hours. The RP chromatograms for the salt steps are shown in figure 3.1.

The output of the 15cm column was coupled directly to a nano-electrospray ionizer, and these ions entered a LCQ Deca XP Plus ion trap mass spectrometer (Thermo Electron Corp, San Jose, CA). In the mass spectrometer, the peptides that enter are first analyzed to determine their mass to charge ratios and their abundance (1st MS). The three most abundant peptides were each subjected to collision-induced dissociation (CID), and the resulting peptide fragments were analyzed for their mass to charge ratio and abundance of each fragment (2nd MS), giving the output of the mass spectrometer.

This analysis lasted approximately 16 hours for a full MudPIT fractionation. Then, various search algorithms analyzed this data.

The search algorithms looked at the peptide fragment mass spectra to try to determine the amino acid sequence of that tryptic peptide. Depending on the location where the peptide breaks during CID, the algorithm can identify fragments that differ by a single amino acid. This is the ideal case which allows the algorithm to determine exactly which amino acid is missing, therefore helping to determine the amino acid sequence of the tryptic fragment. This procedure was repeated for all peptides that were separated in the course of the experiment. I used 3 different search algorithms, Sequest, Mascot, and X!Tandem, in order to benefit from the differences in selectivity that each algorithm offers (Sadygov et al., 2004). The tryptic fragment sequence was then searched against protein databases and matched to particular proteins, which led to the identification of a protein in the sample. Each algorithm assigned a score for each protein identification.

Traditionally, when only one algorithm is used for the protein identification, a threshold score is used as a cutoff for valid protein identifications. In order to combine the scores of multiple search algorithms and to increase the sensitivity of my analysis, Scaffold (Proteome Software, Portland, Oregon, USA) was used to validate protein identifications derived from MS/MS sequencing results. Scaffold verified peptide identifications assigned by Sequest and Mascot using the X!Tandem database searching program (Craig et al., 2003). Scaffold then probabilistically validated these peptide identifications using PeptideProphet (Keller et al., 2002) and derived corresponding protein probabilities using ProteinProphet (Nesvizhskii et al., 2003).

Using a protein probability greater than 99.9%, I identified 138 proteins, which were used for subsequent analysis. I discarded 14 proteins that were obvious contamination proteins, including egg white proteins, keratin, histones, and hemoglobin. The resultant 124 proteins were categorized according to their predicted molecular function or putative protein localization. The categories used were: Cytoskeletal, Energy Metabolism,

Soluble, Membrane, Ca^{2+} binding, Stress Response, Protein Synthesis Related, GTPase Regulation, Extracellular, Unknown, Nuclear, and Mitochondrial. Each protein was assigned a category by hand based on Gene Ontology (GO) annotations and the literature.

3.3 Analysis of identified proteins from the MudPIT and validation of approach

3.3.1. Results of proteomics screen

The MudPIT analysis proved to be successful. The results of 1900 utricle "rip-offs" yielded 138 proteins identified at a confidence level greater than 99.9%. Fourteen of these proteins were obvious contaminants, and were removed from my analysis, and the resulting list of proteins is shown in table 3.1. I categorized the proteins into their probable molecular function/localization (table 3.1). Using the spectral count (the number of mass spectra assigned to a given protein identification), I got a crude relational estimate of the abundance of the identified proteins (Liu et al., 2004). For instance, the most abundant protein by this method was actin, which had a spectral count of 298 (table 3.1). This result conforms to what is known about stereocilia in that they are made predominantly of actin.

Using the relative abundances as a measure of the amount of a protein, I found that the largest category was cytoskeletal proteins, which is the main category of proteins that I will later focus on (figure 3.2). The next largest category of proteins was energy metabolism-related proteins. This finding also confirmed the results reported by the Shin et al. (2007) MudPIT experiment. I also expected to find a number of extracellular proteins, since I was taking hair bundles along with any otolithic membrane remnants that stick to them. Proteins that were related to the stress response were likely a byproduct of my dissection method, since I streamed warm agarose over the hair bundles. Protein synthesis-related, nuclear, and mitochondrial proteins that were

identified were likely part of the small amount of cell body contamination seen in my sample since ribosomes, nuclei, and mitochondria have not been seen in stereocilia. However, these are putative protein functions and localizations; it is entirely possible that these proteins serve different functions in stereocilia, so they cannot be ruled out completely as contaminants. All of these presumptive contaminants make up 15% of proteins based on abundance and 25% of the proteins identified. These results indicate that the technique allows me to get a representation of hair bundle proteins, but I was not able to do so without any contaminating proteins.

3.3.2 Comparison to results from Dr. Gillespie's laboratory

As mentioned above, the Gillespie laboratory also pursued a similar method for discovering hair bundle proteins (Shin et al., 2007). They used a slightly different sample preparation method (see section 2.2.4), and ran multiple rounds of the mass spectrometry analysis with a modest amount of protein (hair bundles from about 100 utricles rather than a single run with large amounts of protein, which was done in my case). From my method, I expected to identify more proteins than the Gillespie laboratory because a larger protein sample size should increase sensitivity.

In order to directly compare the Gillespie Laboratory data to mine, I used the X!Tandem algorithm to search my data on the GPM website (www.thegpm.org), which was used for their data analysis. Of their 59 identified hair bundle proteins that are listed in their publication, only 9 of the proteins identified by Shin et. al. were not identified with my data using the GPM website (table 3.2). These 9 proteins contain obvious cell body contaminants and probable byproducts of the "twist-off" technique, namely: 47 kDa heat shock protein (HSP47_CHICK), Histone H2A, and Histone H4. Of the remaining 6 proteins, 4 of them were identified in Scaffold with >99% confidence and 14-3-3 protein theta (14-3-3T) was identified with 92% confidence, which leaves only Phosphoglucomutase 1 unidentified in my data. I was able to encompass their dataset and identify even more proteins with my analysis technique, than they were able to identify with their technique. This indicates that even with my sample preparation

method differing from their method (see section 2.3), I was able to overcome those differences and identify a larger set of proteins with a much larger sample size.

3.3.3 Identification of known stereocilia proteins

A good indication that the proteomics method is a valid technique for identifying hair bundle proteins, is to identify known hair bundle proteins in the dataset. Going through the literature, I found 34 proteins that have been localized to stereocilia via antibody staining (see section 3.1). Of these 34 proteins, I have identified 19 using Scaffold's analysis, and another 2 when using the GPM analysis, rounding out the identification to 62% of known stereocilia proteins (figure 3.3). This is a large feat considering that the 34 confirmed stereocilia proteins have taken researchers 20+ years to find, which confirms the power of the proteomics approach in determining the protein composition of a complex sample.

The known proteins that have been localized to stereocilia have come from various discovery methods. Considering the multiple techniques used, the known proteins of stereocilia could be considered a random sample of all the proteins in stereocilia. If this is the case, then my one time screen is able to identify roughly 62% of the proteins present in stereocilia. This does not mean that all the identified proteins in the screen (over 1000) are all present in stereocilia, as I have shown that there are probable contaminants present (see section 3.3.1) and many of these proteins exist at lower confidence values. Using only the Scaffold analysis identified proteins and their confidence values, 63 proteins would be false positives, leaving 930 identified proteins to be true identifications. If 930 proteins are true identifications with 25% considered contaminants, then a possible 697 stereocilia proteins were identified.

The known proteins that have been previously localized to stereocilia are found across all different species, so there could be some species differences in the exact proteins that are present in stereocilia. Therefore, some chicken stereocilia proteins could be different isoforms compared to those proteins identified in other species. An example of

this could be found in the proteins NHE6 and NHE9, which have been localized to stereocilia in the bullfrog and rat, respectively (Hill et al., 2006). It is possible that in chicken stereocilia, different isoforms are present, namely NHE5 and NHE7, which were identified in my screen at 92% and 99% confidence, respectively. Such a possibility could also increase the percentage of identified proteins that are truly in chicken stereocilia as well.

3.4 Conclusions

The large-scale experiment using hair bundles from 1900 utricles was successful. I identified 62% of known stereocilia proteins in my experiment, as well as many potential novel stereocilia proteins. This protein list can now be a reference list for people that are interested in specific groups of proteins in the hair bundle in order to facilitate the discovery of new stereocilia proteins as well as coming up with models of how stereocilia function.

My list of potential stereocilia proteins is in no way complete. Multiple large-scale experiments will likely need to take place to be able to identify all the proteins in stereocilia. Each time a complex sample is run through a given proteomics experiment, the number of proteins identified are increased (Liu et al., 2004). Furthermore, even though MudPIT analyses are better at identifying membrane proteins than traditional 2DGE, special techniques are likely necessary to yield a more complete dataset of membrane proteins (Fischer et al., 2006; Wu et al., 2003). More MudPIT experiments can only help to confirm confidence of identified proteins and to yield a more complete dataset.

For my thesis, I chose to pursue two cytoskeletal proteins and one putative phospholipid binding protein. The high abundance of cytoskeletal proteins in the hair bundle lends itself for identification by mass spectrometry methods. All the proteins that are currently known to directly affect actin dynamics were identified in the screen, namely espin and

fimbrin. Since all known proteins were identified, I hypothesize that the previously unknown proteins involved in regulating actin dynamics identified through my screen, are localized to the hair bundle as well.

This page is intentionally left blank.

Figure 3.1 Reverse-phase chromatograms for each salt step off the strong cation exchange column. Chromatograms show relative amounts of peptides off the LC column at the various time points. These chromatograms exhibit well separated peaks, which likely translates to many different identifiable peptides. The elution profile of each salt step is unique and indicates different peptides bumped off in each step.

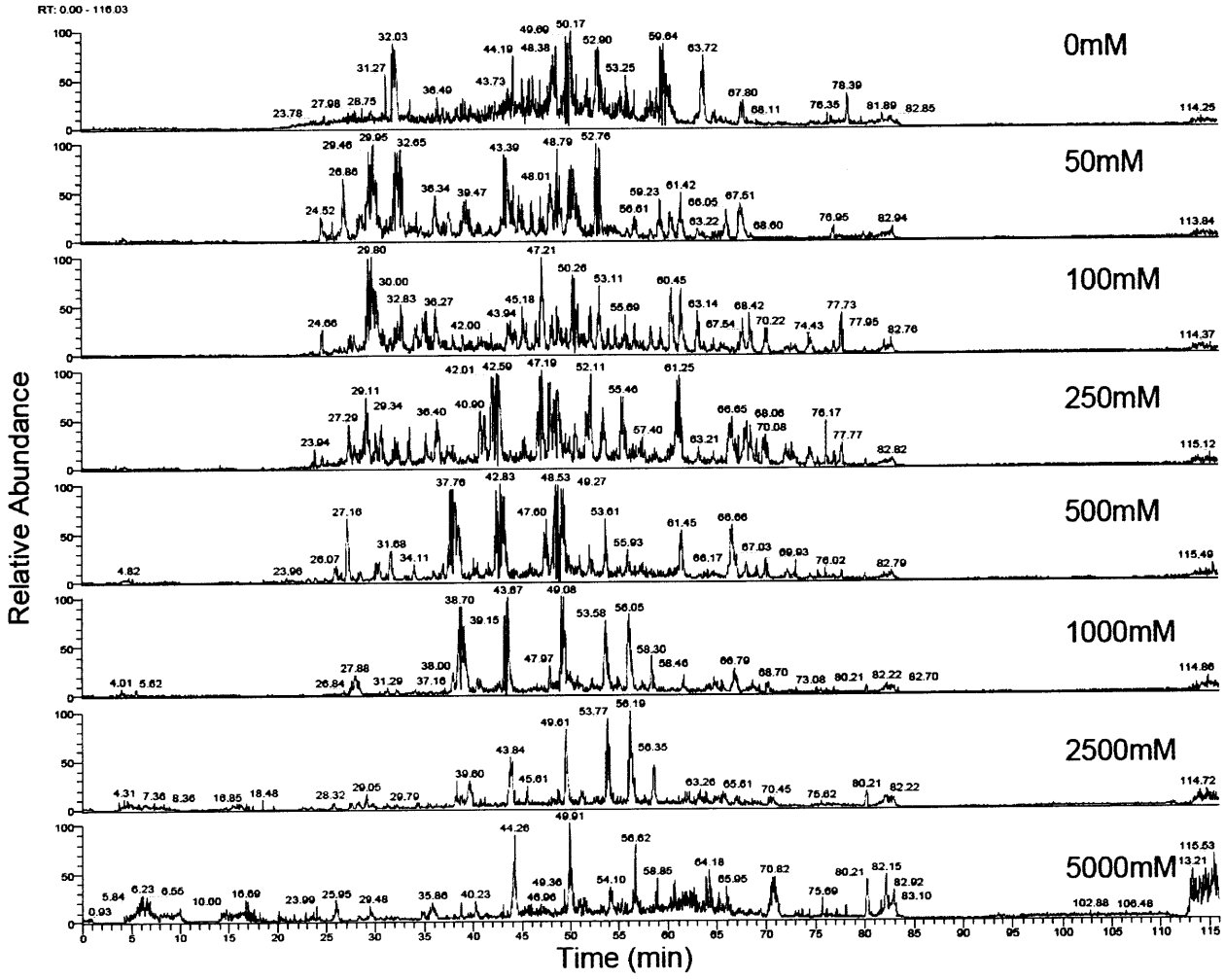

This page is intentionally left blank.

Figure 3.2 Distribution of the types of proteins found based on abundance. Spectral count of each protein is used as an abundance measure. Parentheses contain the number of proteins found in each category.

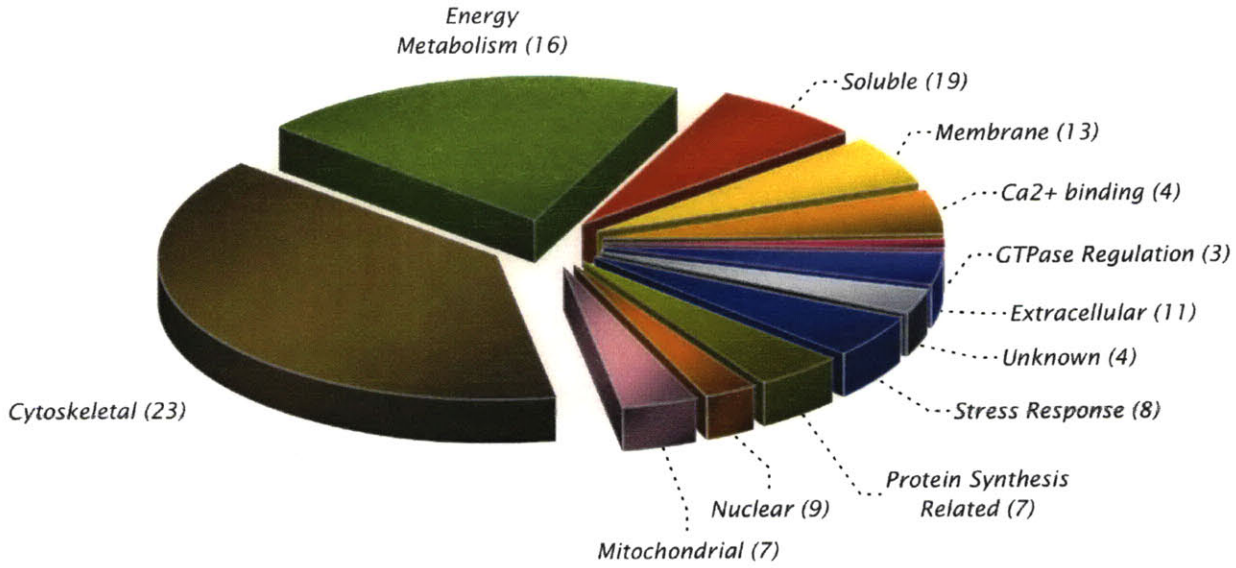

This page is intentionally left blank.

Figure 3.3 Diagram of known hair bundle proteins with their proposed localization and function. Different colors represent proteins that were identified by various search algorithms. Proteins are considered found if identified in Scaffold at >90% confidence and in GPM with a log(e) < -1.

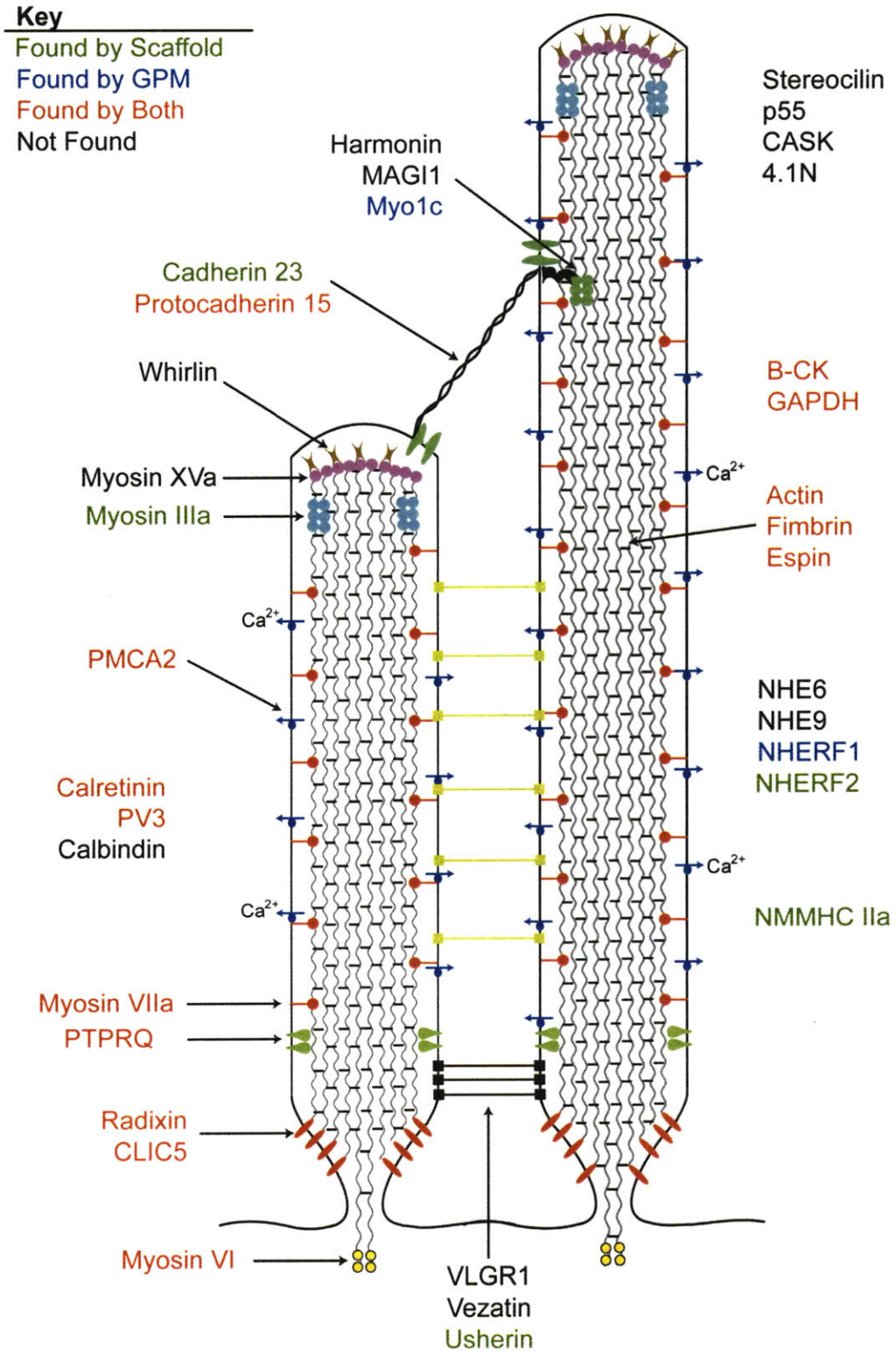

This page is intentionally left blank.

Table 3.1 Proteins identified at greater than 99.9% confidence as determined by Scaffold from the MudPIT analysis. Accession #'s are GI numbers from Genbank. Proteins known to be in the hair bundle are shaded gray. Newly identified proteins known to regulate actin filament dynamics are shaded yellow. SC= spectral count

Accession #	Protein name	SC	Molecular Function
46397330	Beta-actin	298	Cytoskeletal
125293	Creatine kinase B-type (B-CK)	64	Energy Metabolism
2506442	GAPDH	55	Energy Metabolism
135474	Tubulin beta-7 chain	48	Cytoskeletal
1706653	Alpha-enolase	45	Energy Metabolism
223280	Tubulin alpha	40	Cytoskeletal
50754256	Plasma membrane calcium ATPase 2 (PMCA2)	36	Ca2+ Binding
50728376	PTPRQ (Hair cell antigen)	24	Membrane
61657939	Myosin, heavy polypeptide 1	22	Soluble
1064974	Triosephosphate isomerase (TIM)	22	Energy Metabolism
120165	Plastin-1 (Fimbrin)	21	Cytoskeletal
1730518	Phosphoglycerate kinase	21	Energy Metabolism
3122072	Elongation factor 1-alpha 1	20	Protein Synthesis Related
32363425	Radixin	20	Cytoskeletal
45384370	Heat shock cognate 70	20	Stress Response
125608	Pyruvate kinase muscle isozyme	19	Energy Metabolism
115644	Calretinin (CR)	19	Ca2+ Binding
50732409	Vimentin	16	Cytoskeletal
1346814	Parvalbumin 3 (PV3)	16	Ca2+ Binding
82082513	ATP synthase beta chain	15	Mitochondrial
50751518	Peroxiredoxin 1	15	Mitochondrial
50755681	NHERF2	15	Cytoskeletal
45384364	GDP dissociation inhibitor 2	15	GTPase Regulation
63516	Unnamed protein product	14	Unknown
33340023	Collapsin response mediator protein-2A *	14	Cytoskeletal
4033392	78 kDa glucose-regulated protein (GRP 78)	13	Stress Response
75832162	Otoconin 90	13	Extracellular
22651801	Glucose regulated thiol oxidoreductase protein	13	Protein Synthesis Related
125149	Adenylate kinase isoenzyme 1	13	Energy Metabolism
56377792	Cellular retinoic acid binding protein I	13	Soluble
50759135	Espin	13	Cytoskeletal
50748374	Alpha cardiac actin	12	Cytoskeletal
50732571	RIKEN cDNA E030025L21 gene	12	Unknown
50746026	Zgc:66433	11	Unknown
57530666	ADP-ribosylation factor 1	11	GTPase Regulation
45382045	Myosin VI	10	Soluble
223033	Collagen alpha 1	10	Extracellular
6920068	L-lactate dehydrogenase B chain (LDH-B)	9	Energy Metabolism
1351941	Annexin A5	9	Membrane
17225596	ATP synthase alpha subunit	9	Mitochondrial

71897051	Cold inducible RNA binding protein	9	Stress Response
90990971	Valosin containing protein	8	Stress Response
57530768	Protein disulfide isomerase	8	Protein Synthesis Related
50766787	Tubulin beta-5 chain	8	Cytoskeletal
57530355	Malate dehydrogenase 1	7	Energy Metabolism
50756703	Phosphatidylethanolamine-binding protein (PEBP)	7	Membrane
50758346	Clathrin heavy chain 1 (CLH-17)	7	Membrane
123575	47 kDa heat shock protein precursor	7	Stress Response
50758110	Malate dehydrogenase 2	7	Energy Metabolism
226855	Aldolase C	7	Energy Metabolism
60302796	SH3 domain binding glutamic acid-rich protein like	7	Soluble
50756309	Polyubiquitin with 3 Ub domains	7	Stress Response
71896753	Heterogeneous nuclear ribonucleoprotein A2/B1	6	Nuclear
71895985	Phosphoglycerate mutase 1	6	Energy Metabolism
211528	Creatine Kinase	6	Energy Metabolism
50750495	L-NAME induced actin cytoskeletal protein	6	Soluble
50745292	Clic5-prov protein	6	Membrane
82197807	14-3-3 protein zeta	6	Soluble
57524920	Glucose phosphate isomerase	6	Energy metabolism
118463	Destrin (Actin-depolymerizing factor) (ADF)	6	Cytoskeletal
82233762	T-complex protein 1 subunit zeta (TCP-1-zeta)	6	Cytoskeletal
14579649	Heat shock protein 108	5	Stress Response
128146	Neurofilament triplet M protein (NF-M)	5	Cytoskeletal
75571441	Twinfilin-2	5	Cytoskeletal
50762370	Heterogeneous nuclear ribonucleoprotein K isoform a	5	Nuclear
45384260	Non-metastatic cells 2 (NM23B)	5	Mitochondrial
50750986	LIM only protein HLP	5	Nuclear
45384462	ATPase, H+ transporting	5	Mitochondrial
50749765	Glutathione-S-transferase omega 1	5	Soluble
2494246	Elongation factor 2 (EF-2)	5	Protein Synthesis Related
33521618	Heterogeneous nuclear ribonucleoprotein H1	5	Nuclear
45382235	Glutathione S-transferase A3	5	Soluble
45383015	Parkinson disease 7	5	Extracellular
50752612	Otolin-1	5	Extracellular
50738954	Ras-related protein	5	GTPase Regulation
45383077	Eukaryotic translation initiation factor 4A	5	Protein Synthesis Related
50750353	Cytosolic NADP-dependent isocitrate dehydrogenase	4	Energy Metabolism
50754851	StAR-related lipid transfer protein 10 (StARD10)	4	Membrane
1718088	Vacuolar ATP synthase subunit B	4	Membrane
50749462	Annexin VIII	4	Membrane
56605886	Lymphocyte cytosolic protein 1 (L-plastin)	4	Cytoskeletal

34921412	Gelsolin (Actin-depolymerizing factor) (ADF)	4	Cytoskeletal
50982399	Annexin A6	4	Membrane
212330	Myosin light chain 1f	4	Soluble
34922442	Otokeratin	4	Soluble
82197872	14-3-3 protein beta/alpha	4	Soluble
135446	Tubulin beta-1 chain	4	Cytoskeletal
71895253	DEAD/H (Asp-Glu-Ala-Asp/His) box polypeptide 3	4	Protein Synthesis Related
114378	Na+/K+ ATPase 2	3	Membrane
50745190	Cochlear otoferlin	3	Membrane
112971	Aspartate aminotransferase	3	Soluble
50760487	Forkhead box P4	3	Nuclear
126046	L-lactate dehydrogenase A chain (LDH-A)	3	Energy Metabolism
50732501	Alpha-2 type I collagen	3	Extracellular
50745403	Protein disulfide-isomerase precursor	3	Protein Synthesis Related
47420845	FUS/TLS	3	Nuclear
50794550	Nuclear poly(C)-binding protein	3	Nuclear
50758202	Pigment epithelium-derived factor	3	Soluble
17433708	Cofilin-2	3	Cytoskeletal
50755208	ALL1 fused gene from 5q31	3	Nuclear
50804055	Hypothetical protein KIAA0286	3	Unknown
50755288	Betaine homocysteine methyl transferase	3	Soluble
50754329	Transketolase	3	Soluble
4049439	Alpha tectorin	3	Extracellular
115268	Collagen alpha-1(I) chain	3	Extracellular
50781373	Apolipoprotein A-I	2	Extracellular
82197843	60 kDa heat shock protein (HSP-60)	2	Stress Response
50728414	Plasma membrane calcium ATPase 1 (PMCA1)	2	Ca2+ Binding
50760275	Splicing factor, arginine/serine-rich 3	2	Nuclear
50749344	Cadherin 23	2	Membrane
50730386	Hect domain and RLD 2	2	Soluble
50748800	NUANCE	2	Cytoskeletal
45383309	Alpha 1 type IIA collagen	2	Extracellular
50734052	Desmoplakin (DP)	2	Cytoskeletal
11320877	Aldehyde dehydrogenase-6	2	Mitochondrial
50764028	Aldose reductase	2	Soluble
60592998	3-oxoacid CoA transferase 1	2	Mitochondrial
7387581	Cochlin precursor (COCH-5B2)	2	Extracellular
45384320	Fatty acid binding protein 7	2	Soluble
1345652	Collagen alpha-3(VI) chain	1	Extracellular
50753294	Protein 4.1O	1	Cytoskeletal
45382679	Myosin, heavy polypeptide 10	1	Soluble
24212083	Protein piccolo (Aczonin)	1	Cytoskeletal
50748910	MAM domain containing protein 1	1	Membrane

* Interestingly CRMP-2 was originally identified by the current MIT President, Susan Hockfield (Minturn et al., 1995).

Table 3.2 Proteins identified by Shin et al, 2007 that were not identified in a GPM database search with the MudPIT data

Alpha-enolase (ENO1)
Ubiquitin (UBIQ_CHICK)
Calmodulin (CaM)
Phosphoglucomutase 1
47 kDa heat shock protein (HSP47_CHICK)
Histone H2A
Histone H4
Malic enzyme 1 NADP(+)-dependent cytosolic
14-3-3 protein theta (14-3-3T)

Chapter 4: Sub-cellular localization of three new stereocilia proteins identified in the proteomic screen

4.1 Introduction to the three newly identified proteins

The primary goal of the proteomics approach was to discover new proteins that are localized to hair cell stereocilia. My particular interest is in cytoskeletal regulatory proteins, but regardless, identification and localization of proteins to stereocilia are important because they validate the proteomics approach as a useful technique to identify all different types of stereocilia proteins. The proteomics screen would also identify proteins that are localized in the kinocilium of the hair bundle, because the kinocilium is part of the chicken vestibular hair bundle. Even though identification of kinocilia proteins was not the main objective of my approach, others that are interested in the molecular composition of this structure may find the results of the screen useful.

For further localization experiments, I chose to use the mouse cochlea model for several reasons. First, more antibodies are available that specifically label mouse protein isoforms, since mice are the more widely used animal model. Secondly, the mouse model provides more tools for future functional studies, therefore the initial localization of proteins to the mouse inner ear allows for an easy transition. Finally, I am ultimately

interested in understanding human hearing, and using a mammalian cochlear model brings me a step closer to a human correlate.

I have localized 3 new proteins to stereocilia that were previously unknown to be in stereocilia. Each of these proteins have been studied in other systems or contexts, but none of them have been previously linked to hair cells or to stereocilia. Those 3 proteins are StarD10, nebulin, and twinfilin 2, and each of them have potentially interesting functions that are outlined below.

StarD10 was identified in my MudPIT screen at a >99.9% confidence level. It is a protein that was originally identified as being overexpressed in breast cancer cells with a proposed function of transferring phospholipids (Olayioye et al., 2004; Olayioye et al., 2005). Outside of studies in breast cancer cells, only one other study exists on this protein regarding protein signaling (Olayioye et al., 2007). StarD10 is potentially interesting for stereocilia because phospho-inositide (4,5) biphosphate (PIP_2) has been shown to important for stereocilia function (Hirono et al., 2004), so StarD10 may be playing a role in regulating PIP_2 levels.

Nebulin was identified in the proteomics screen at a >99.0% confidence level. Nebulin is a giant protein that ranges between 600-900kD depending on the splice variant. Nebulin has been shown to be important for muscle sarcomere thin filament function (McElhinny et al., 2003). It has been proposed that nebulin may be acting as a ruler of thin filaments to set their length, with different splice variants being responsible for different thin filament lengths (Kazmierski et al., 2003; McElhinny et al., 2003). Alternatively, it has been recently suggested that nebulin may instead be responsible for stabilizing the thin filament, hence preventing filament depolymerization (Castillo et al., 2009). This protein could be interesting for stereocilia development or maintenance because it could be involved in acting as a ruler to determine stereocilia length, or help to stabilize the actin filaments in stereocilia. The lengths of tall and middle stereocilia are strictly regulated so that stereocilia of neighboring hair cells are of similar length.

Similarly, in a given cochlear place, the lengths of stereocilia are similar across age-matched animals.

Finally, I focused on twinfilin 2, which was identified at >99.9% confidence. Twinfilin 2 is made up of two actin depolymerizing factor homology (ADF-H) domains, which share high sequence homology with twinfilin 1 ADF-H domains. Using ESyPred3D, I predicted the structure of the twinfilin 2 ADF-H domains using the solved structures of the twinfilin 1 domains as a template (figure 4.1) (Lambert et al., 2002; Paavilainen et al., 2002; Paavilainen et al., 2007). The alignment of the twinfilin 2 predicted structure versus the twinfilin 1 solved structure has a root mean squared deviation of 0.12 and 0.34 angstroms for the amino-terminal and carboxyl-terminal ADF-H domains, respectively. This suggests that the functions and mechanisms of the more widely studied twinfilin 1 are likely similar to twinfilin 2, hence we can use knowledge of twinfilin 1 to hypothesize twinfilin 2 function as well. In *in vitro* studies, twinfilin 2 has been shown to sequester actin monomers and to cap barbed ends of actin filaments (Nevalainen et al., 2008). Twinfilin 2 could play a role in regulation of stereocilia lengths by directly interacting with the actin filaments and/or actin monomers.

With all these potential functions in stereocilia, the first step is to confirm the presence in stereocilia with immuno-fluorescence using antibodies that specifically recognize these proteins. To accomplish this I obtained antibodies from other laboratories as well as generating my own antibodies to visualize their locations in stereocilia.

4.2 Methods

4.2.1 Antibodies

I obtained some antibodies directed against nebulin and twinfilin 2 and generated my own antibodies to StarD10 and twinfilin 2 as well. Dr. Carol Gregorio (University of Arizona) graciously sent me affinity-purified rabbit antibodies directed against the

carboxyl-terminal nebulin repeats M160-M164 of the mouse protein and this antibody is used at a 1:100 dilution (Conover et al., 2009). Dr. Pekka Lappalainen (University of Helsinki) kindly sent me two different antibodies. The first antibody is a rabbit antibody-raised against mouse twinfilin 1, but also recognizes twinfilin 2 (Vartiainen et al., 2000; Vartiainen et al., 2003), used at 1:200 dilution. The second antibody is the former antibody that is depleted with twinfilin 2, so it preferentially identifies twinfilin 1 (Vartiainen et al., 2003), used at 1:200 dilution.

4.2.2 Sf9 cell protein expression and purification

Full length mouse StarD10 cDNA (NCBI accession NM_019990.4) with a carboxyl-terminal 6x-HIS tag was PCR amplified from a mouse cochlear cDNA library (Pompeia et al., 2004) using:

forward primer 5'-AAA TTT GGA TCC ACC ATG GAA AAG CCA GCT GCC TCA ACA-3'

reverse primer 5'- AAA TTT AAG CTT TTT ATT TTA CTA GTG ATG GTG ATG GTG ATG GGT GAG CGA GGT GTC ATC GTC-3'

The PCR product was cloned into pFastBac1 shuttle vector (Invitrogen, Carlsbad, CA) using BamHI and HindIII restriction sites. Similarly full-length mouse twinfilin 2 (NCBI accession NM_011876.3) with an amino-terminal 6x-HIS tag was PCR amplified from the mouse cDNA library using:

forward primer 5'- AAA TTT GGA TCC ACC ATG CAT CAC CAT CAC CAT CAC GCG CAC CAG ACC GGC ATC CAC -3'

reverse primer 5'- AAA TTT GTC GAC TTT ATT TCA CTA GCT GTC TTC CCC GTT CTC CCC-3'

The PCR product was cloned into pFastBac1 shuttle vector (Invitrogen, Carlsbad, CA) using BamHI and SalI restriction sites. Recombinant viruses expressing my proteins were generated using the Bac-to-Bac® baculovirus expression system (Invitrogen, Carlsbad, CA).

Sf9 cells were cultured in shaking conditions at 27°C in Grace's insect medium (Invitrogen, Carlsbad, CA) supplemented with 10% fetal bovine serum (FBS; Omega Scientific), 0.1% Pluronic F-68 (Gibco Invitrogen, Carlsbad, CA), and 50 μg/mL gentamycin (Gibco Invitrogen, Carlsbad, CA). Pluronic F-68 prevents the cells from sticking to each other. Shaking cultures were grown to a concentration of about 1.6 x 10^6 cells/mL and infected with a high titer virus and incubated for 3 days before harvesting recombinant protein.

For harvesting protein under native conditions, cells were collected by pelleting at 1000x*g* at 4°C for 5 minutes. Supernatant was removed and cells were washed with PBS and re-pelleted. Cells were then re-suspended in lysis buffer (0.5% TritonX-100, 50mM NaH_2PO_4, 300mM NaCl, 10mM imidazole, pH=8.0). Cells were lysed using nitrogen decompression with a cell disruption bomb (Parr Instrument Company, Moline, IL) and cell debris was pelleted at 14,000x*g* for 1 hour at 4°C. Supernatant containing soluble proteins was incubated with Talon metal affinity beads (Clontech Laboratories Inc., Mountain View, CA) for 2 hours rotating at 4°C. Beads were washed on a gravity flow column using wash buffer (50mM NaH_2PO_4, 300mM NaCl, 20mM imidazole, pH=8.0). Purified protein was eluted from the gravity flow column using elution buffer (50mM NaH_2PO_4, 300mM NaCl, 250mM imidazole, pH=8.0), which uses imidazole to compete protein away from the beads. Protein concentrations were estimated by comparing eluted protein band intensities to a dilution series of BSA band intensities using Coomassie stained-SDS-PAGE gels.

4.2.3 Antibody generation and affinity purification

Purified protein was sent to a commercial service provider (Covance Inc., Denver, PA) to be used to immunize rabbits with periodic boosts. StartD10 antibodies were generated using an expedited 77-day protocol, and twinfilin 2 antibodies were generated using a traditional 120-day protocol. Sera from rabbits showed immunoreactivity against my desired proteins in transfected HEK cells and on western blots (figure 4.2).

High-affinity antibodies were purified using gravity flow columns with the original antigen cross-linked to CNBr-activated sepharose beads (Amersham Biosciences, Pittsburg, PA). The final production bleed of antibody-containing serum was incubated for 2 hours at room temperature with the column material to allow antibody binding. The columns were then washed to remove non-specific antibodies. Antigen-specific antibodies were eluted by decreasing the pH from 7 to 2.4, and immediately neutralized. The affinity columns were then regenerated with washes of alternating pH for further antibody purifications.

4.2.4 HEK 293 cell transfection and immunostaining

Sera were tested on HEK 293 cells transfected with mammalian expression vectors encoding StarD10 and Twinfilin 2. StarD10 and twinfilin 2 cDNAs were cloned into a pcDNA3.1(+) mammalian expression vector (Invitrogen, Carlsbad, CA). HEK 293 cells, grown on coverslips, were transfected using Genejammer (Stratagene, La Jolla, CA) using the manufacturer's protocols. After 1 day incubation in a humidified 5% CO_2 37°C incubator, cells were fixed with 4% paraformaldehyde (PFA; 16% stock from Electron Microscopy Sciences, Hatfield, PA, diluted to 4% using PBS) for 30 minutes at room temperature. All steps were performed at room temperature unless otherwise indicated. Cells were permeabilized and blocked with PBT1 (0.1% Triton X-100, 1% BSA, 5% heat-inactivated goat serum in PBS, pH 7.3) for 10 minutes. Samples were incubated overnight at 4°C with StarD10 or twinfilin 2 purified antibody in PBT1. After primary antibody staining, the samples were washed twice with PBT1 for 5 minutes and twice with PBT2 (0.1% Triton X-100, 0.1% BSA in PBS) for 5 minutes, and incubated with 7.5 mg/ml FITC-conjugated goat anti-rabbit antibody (Jackson ImmunoResearch Inc., West Grove, PA) in PBT2 for 1 hour shaking, followed by two PBT2 washes and two PBS washes for 5 minutes each. Coverslips were then mounted in 50% glycerol/50% PBS on glass slides and imaged with either a confocal microscope (LSM Pascal, Zeiss, Germany) using a 63x 1.4NA oil immersion objective or with a CSU10 spinning disk

confocal (Yokogawa from 3I, Santa Monica, CA) with a QuantEM 512SC EMCCD (Photometrics, Tuscon, AZ) using a 100x 1.4NA oil immersion objective.

4.2.5 Whole-mount immuno-fluorescence

All animal procedures followed guidelines set forth by the National Institutes of Health and approved by Stanford's Administrative Panel on Laboratory Animal Care (APLAC). BALB/C mice were euthanized and decapitated to isolate the temporal bone. Cochleae were fixed for 1 hour in 4% PFA (16% stock from Electron Microscopy Sciences, Hatfield, PA, diluted to 4% using PBS) prior to being removed from the temporal bone, then tectorial membranes were removed. For nebulin staining, cochleae were dissected and fixed with -80°C methanol, 1% PFA for 10 minutes, or 4% PFA for 10 minutes. Cochleae were permeabilized and blocked with PBT1 for 10 minutes. All steps were performed at room temperature unless otherwise indicated. Samples were incubated overnight at 4°C with 1:75 purified anti-StarD10, 1:200 anti-nebulin M160-M164, or 1:200 anti-Twf1&2 in PBT1. After primary antibody staining, the samples were washed twice with PBT1 for 5 minutes and twice with PBT2 for 5 minutes, and incubated with 7.5 mg/ml FITC-conjugated goat anti-rabbit antibody (Jackson ImmunoResearch Inc., West Grove, PA) in PBT2 for 2 hours, followed by two PBT2 washes for 5 minutes. Samples were incubated with 0.4 μg/ml TRITC-conjugated phalloidin in PBS for 20 minutes followed by three 5-minutes washes with PBS, then mounted in DakoCytomation Fluorescent Mounting Medium (Dako, Carpinteria, CA). Primary antibody omission controls were done with the different fixation methods and none of them showed any significant fluorescence signal. Specimens were imaged with a confocal microscope (LSM Pascal/Exciter, Zeiss, Germany) using a 63x 1.4NA oil immersion objective or with a CSU10 spinning disk confocal (Yokogawa from 3I, Santa Monica, CA) with a QuantEM 512SC EMCCD (Photometrics, Tuscon, AZ) using a 100x 1.4NA oil immersion objective.

4.3 Sub-cellular localization of proteins in cochlear hair cells

4.3.1 StarD10

Whole-mount staining of mouse cochleae revealed StarD10 presence along the stereocilia bundle of both inner hair cells (IHC) and outer hair cells (OHC; figure 4.3). Expression of StarD10 was not apparent at postnatal day (P) 7, however, I did see the pronounced expression at P10 and beyond. The distribution of StarD10 in stereocilia appeared partially peripheral to the actin filament backbone, suggesting that the protein was not completely co-localized with the actin filament backbone, but rather also present in the region surrounding the actin core, which would be in agreement with an association of StarD10 with the stereocilia plasma membrane (figure 4.3c). Notably, the staining of StarD10 was not uniform from the bottom to the top of stereocilia, but rather exhibited an apparent lack or decrease of staining toward the bottom 1-2μm of stereocilia. This distribution pattern was reminiscent of the staining pattern seen of PIP_2 immunostaining in bullfrog saccular hair cells (Hirono et al., 2004), further suggesting a possible function of StarD10 in regulating lipid composition of stereocilia. The expression pattern of StarD10 appeared to be similar in both the IHC and the OHC stereocilia.

In addition to the stereocilia staining, StarD10 immunoreactivity was also apparent in hair cell bodies (figure 4.4). The staining that was present in hair cell bodies appeared to fill the whole cell body of both IHC and OHC.

4.3.2 Nebulin

To localize nebulin, I used an affinity-purified polyclonal antibody directed against the nebulin repeats M160-M164. I found that long PFA fixation protocols of 1 hour or longer mask the nebulin antigen. Ultra-cold methanol fixation is typically used to preserve epitopes for cytoskeletal proteins, and shorter PFA fixation protocols have been used for visualization of nebulin in myocytes (Hagedorn et al., 2006; McElhinny et al., 2005).

Using both 1% PFA fixation, short (10 min) 4% PFA fixation, and methanol fixation methods, nebulin staining of cochlear stereocilia was consistently observed (figure 4.5 and data not shown). Nebulin appeared to be localized in the stereocilia rootlet, present in the base of stereocilia and the cuticular plate in both IHC and OHC (figure 4.5). Looking at confocal sections where cuticular plate staining is not present with F-actin staining, individual puncta for each stereocilium are present, indicating the presence of nebulin in the base of stereocilia (figure 4.5c arrow). Moving towards the cuticular plate, three individual rows of puncta are visible, indicating that nebulin is located in all stereocilia rootlets (figure 4.5d arrowheads). Moving deeper into the cuticular plate, the short stereocilia row nebulin stain disappears first, followed by the second, then the third, further suggesting nebulin's location within the rootlet (figure 4.5e-i), since in OHC the short, middle, and tall stereocilia have short, intermediate, and long rootlets, respectively (Furness et al., 2008). The staining was present even when stereocilia have been sheared off the hair cell (figure 4.6). When stereocilia are sheared off, the rootlet that reaches from the stereocilium into the cuticular plate may remain embedded in the cuticular plate sticking out of the surface of the cell (Leibovici et al., 2005). Nebulin was detectable in stereocilia as early as P5 and persisted into older ages (up to P29 tested).

4.3.3 Twinfilin 2

Localization of twinfilin 2 was carried out using a polyclonal antibody raised against twinfilin 1, which also recognizes twinfilin 2 (twinfilin 1&2 antibody). This antibody showed a very interesting and consistent staining pattern. The tips of middle and short stereocilia were strongly labeled with faint to absent staining at the tips of tall stereocilia (figure 4.7). IHC short stereocilia are difficult to resolve with light microscopy, since they are thinner than middle and tall stereocilia. The diameter of short stereocilia is below the 200-nanometer resolution limit of light microscopy, making it difficult to see short stereocilia with the middle and tall stereocilia behind it. However, punctate staining just below the middle stereocilia tips suggests that the twinfilin 1&2 antibody also labels the tips of shorter stereocilia (figure 4.7 inset). The staining pattern was consistent across

IHC and OHC, suggesting a common function in both cell types. Based on this characteristic pattern, twinfilin 2 could play a role in regulating actin filament dynamics at the barbed ends, since the barbed ends are pointed towards the tips of stereocilia. In the tallest stereocilia there could be a different protein regulating this or twinfilin 2 could be present at lower levels, below the antibody detection limit.

When the twinfilin 1&2 antibody, which recognizes both twinfilin 1 and twinfilin 2, was depleted for immunoreactivity to twinfilin 2, it produced an antibody that was preferential towards twinfilin 1 (twinfilin 1 antibody). Stereocilia staining with the twinfilin 1 antibodies did not exhibit strong stereocilia tip staining, suggesting that twinfilin 2 is localized to stereocilia tips (figure 4.8), and this would be consistent with what the proteomics screen found, since it only identified twinfilin 2. The twinfilin 2 depleted antibodies used in the second staining experiment, acted as blocking controls, where the loss of specific staining at stereocilia tips was highly consistent with a specific immuno-reaction of the non-depleted antibodies with twinfilin 2 at the tips.

Twinfilin 1&2 also labels other parts of the organ of Corti. There was a prominent ring of staining around the apex of the hair cell in the region of the peri-cuticular necklace. This localization could associate twinfilin 1 and/or twinfilin 2 with the lateral edge of the cuticular plate or in the region of the junctions between hair cells and supporting cells (figures 4.7 and 4.9). Additionally, twinfilin 1&2 stained the inner and outer pillar cells (figure 4.9), and twinfilin 1 antibodies strongly labeled pillar cells, possibly indicating that only twinfilin 1 is present in pillar cells (asterisks, figure 4.9). Deiter's cells also are stained with both twinfilin 1 and twinfilin 1&2 antibodies (arrows, figure 4.9). Based on the pattern of both antibodies, the apical surface of the Deiter's cells appears to have twinfilin 2, whereas the phalange shaft contains twinfilin 1. The staining in other cells was not surprising, since both twinfilin 1 and twinfilin 2 can be found in tissues of many of the major organs in the body (Vartiainen et al., 2003). All of this suggests a specific role of twinfilin 2 in stereocilia, whereas both twinfilins may be playing a universal role in many of the supporting cells.

4.4 Conclusions

I have localized 3 proteins to stereocilia that were previously unknown to be in stereocilia. All three proteins were found in the proteomics screen at various confidence levels, but all of them have been localized to stereocilia of mouse cochlear hair cells. This confirms the power of the proteomics screen as a method for discovering proteins that are localized in stereocilia.

4.4.1 Antibody staining considerations

The localization of proteins in hair cell stereocilia can be tricky. There are a few considerations to keep in mind, and the proper controls are required in order to properly confirm protein presence in stereocilia. Stereocilia are generally sticky, and one has to be cautious when there appears to be punctate staining randomly distributed on stereocilia, which may be due to non-specific binding of the antibody to stereocilia. Proper blocking controls and affinity purification may help resolve this issue. Proper controls also need to exclude the possibility that the blocking buffer, often serum, is not generating the signal whereby serum proteins are binding to proteins in the specimen. This has been the case for staining with a Sigma gelsolin antibody (Clone GS-2C4), where the goat serum in the blocking buffer contains soluble gelsolin, or another protein that is detected by the gelsolin antibody. This serum protein was binding to actin filaments in the stereocilia, hence generating a false positive signal (figure 4.10). With the proper controls, one can often increase the confidence that an observed antibody stain is real. For my antibody staining, I have performed two control experiments, the first being the omission of primary antibody, and in the second control experiment I omit the heat-inactivated goat serum from my solutions.

A second consideration is that if an antibody does not label stereocilia, it also does not mean that the protein is not present. Antibody specificity and affinity affect the required density of antigen in order for a fluorescent signal to be detectable from the background; hence if an antibody does not label stereocilia, it could be that the antibody is not

specific enough or does not have a high enough affinity. Different fixation methods strongly affect the availability of antibody epitopes. For instance, chemical cross-linking fixation methods (paraformaldehyde and gluteraldehyde) can cause epitope masking due to over cross-linking. Traditionally, stereocilia staining protocols have included paraformaldehyde fixation (Belyantseva et al., 2005; Dumont et al., 2001; Hill et al., 2006; Khan et al., 2007; Kikkawa et al., 2005; Mburu et al., 2006), and recently some groups have turned to antigen retrieval methods to unmask antibody epitopes (Gagnon et al., 2006; Schneider et al., 2006; Shin et al., 2007). For formaldehyde fixation there are also considerations about the permeabilization method, since it can affect access and extraction of the protein as well as affecting localization of the proteins (Hagedorn et al., 2006; Melan et al., 1992). Other fixation methods may be more applicable to certain types of proteins. For example, methanol fixation is likely the preferred method for cytoskeletal proteins as it preserves antigenicity better than formaldehyde fixation; whereas, formaldehyde fixation is better at preserving structure. Part of the reason that methanol fixation has not been used extensively in stereocilia localization studies is likely it's incompatibility with phalloidin staining and its sub-optimal preservation of the stereocilia structure. Many researchers are concerned about generating crisp images of stereocilia, therefore structural preservation is of utmost importance. With different advantages and trade-offs for each fixation and permeabilization method, comparisons of multiple methods are generally required to fully test for localization of a protein in tissue. Without testing multiple fixation methods, the localization of nebulin to the stereocilia rootlet would have been missed.

These various considerations increase the number of protocols needed to test antibody staining of stereocilia, which generally results in a time consuming endeavor of troubleshooting using different reagents and fixation protocols. It is therefore beneficial to be confident that the protein of interest is in the hair bundle, and using the proteomics screen as a starting point can make one fairly certain of this.

Figure 4.1 Overlay of the predicted twinfilin 2 ADF-H domain structures with twinfilin 1 ADF-H domains using SwissPdb-Viewer. Twinfilin 1's structure is represented by the green ribbon and the predicted twinfilin 2 structure is represented by the red ribbon. (a) is the structure of the amino-terminal ADF-H domain, and (b) is the carboxyl-terminal ADF-H domain structure. The rms deviation calculated from the alpha carbons is 0.12 and 0.34 angstroms for (a) and (b) respectively.

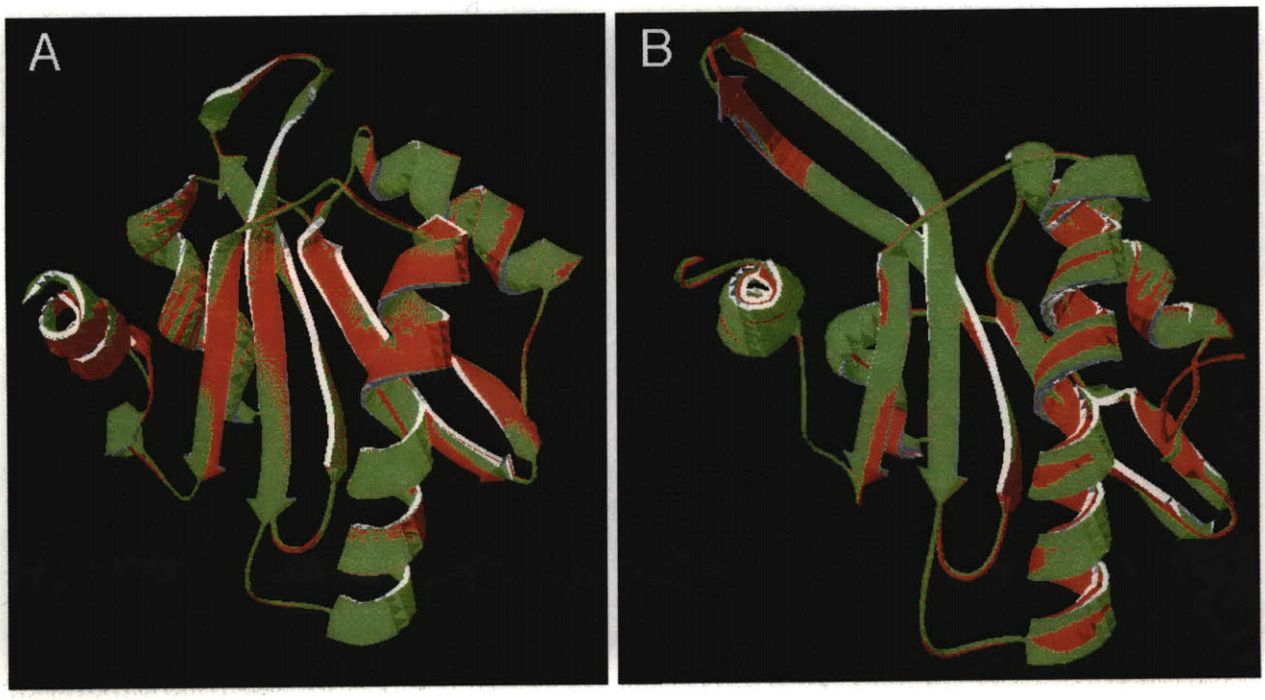

This page is intentionally left blank.

Figure 4.2 Antibody specificity verification on HEK cells. (a) Twf2 IRES mCherry vector transfected HEK cells are indicated in red and cells were stained with CA23 twinfilin antibody shown in green. (b) HEK cells were transfected with a myc tagged StarD10. Cells were labeled with StarD10 anti-sera in red and anti-myc antibody show in green. Transmitted light images show the presence of untransfected cells that are not stained by the antibodies. (c) Western blots of untransfected (lanes 3&4) and myc tagged twinfilin 2 (lanes 1&2) probed with CA23 Twf2 anti-sera show bands of the correct molecular weight for myc tagged twinfilin 2 (arrow; ~40kD). Inherent twinfilin 2 of HEK cells also appears to be labeled with the CA23 Twf2 antibody as seen by the arrowhead. (d&e) Western blots of unpurified StarD10 anti-sera (d) and purified anti-sera (e) label correctly sized bands (arrow; ~34kD). Lanes 1&2 are empty vector transfected HEK cells, and lanes 3&4 are myc tagged StarD10 transfected cells. Arrowhead in (d) indicates possible inherent human StarD10 present in HEK cells that the antibody also recognizes as these bands disappear when the antibody is purified (e). Scale bar = 5μm.

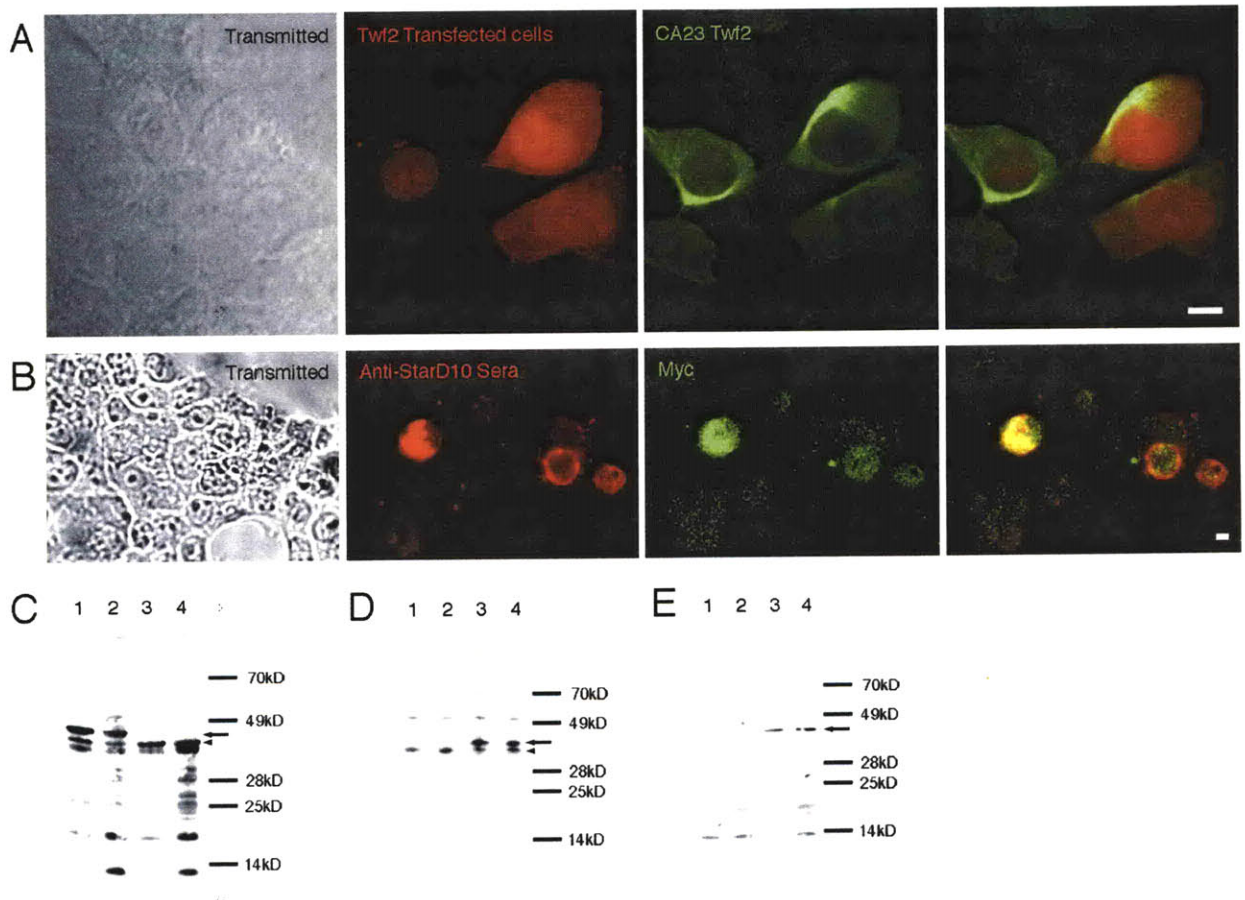

This page is intentionally left blank.

Figure 4.3 StarD10 immunostaining (green) is present in P13 cochlear stereocilia of (a) inner and (b) outer hair cells. Stereocilia F-actin is labeled with TritC-phalloidin (red). (c) Zoomed image of a single IHC stereocilium showing StarD10 localization predominately around the actin core. Scale bar = (a,b) 5μm (c) 1μm

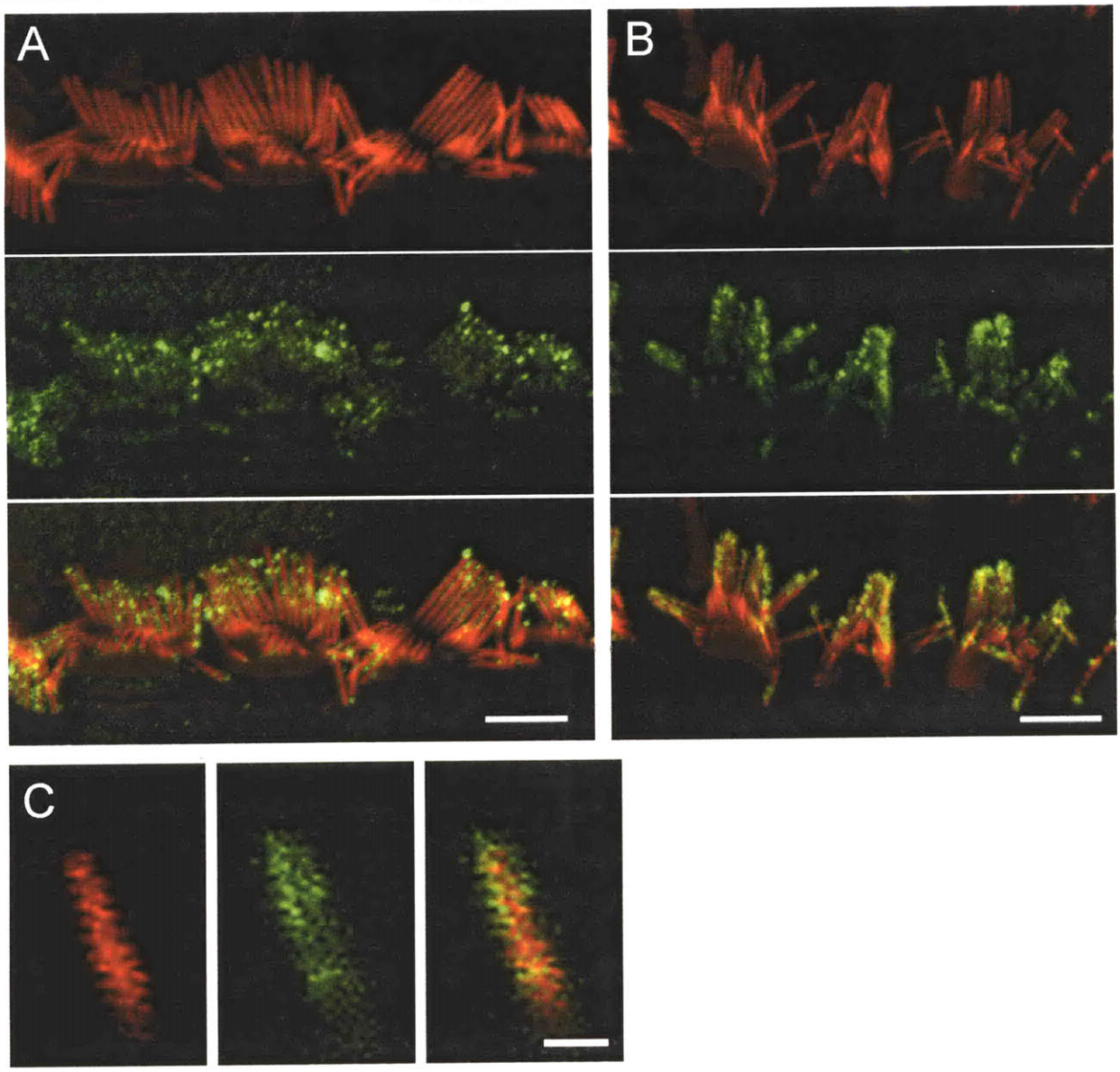

This page is intentionally left blank.

Figure 4.4 StarD10 staining is present in the cell bodies of P33 hair cells. Transmitted light image (left) shows the overview of the inner hair cell with * marking nuclei. Purified StarD10 (green) labels stereocilia as well as the cell body. Transmitted light image is of a single plane, fluorescent images are a projection of a confocal stack. Scale bar = 5μm

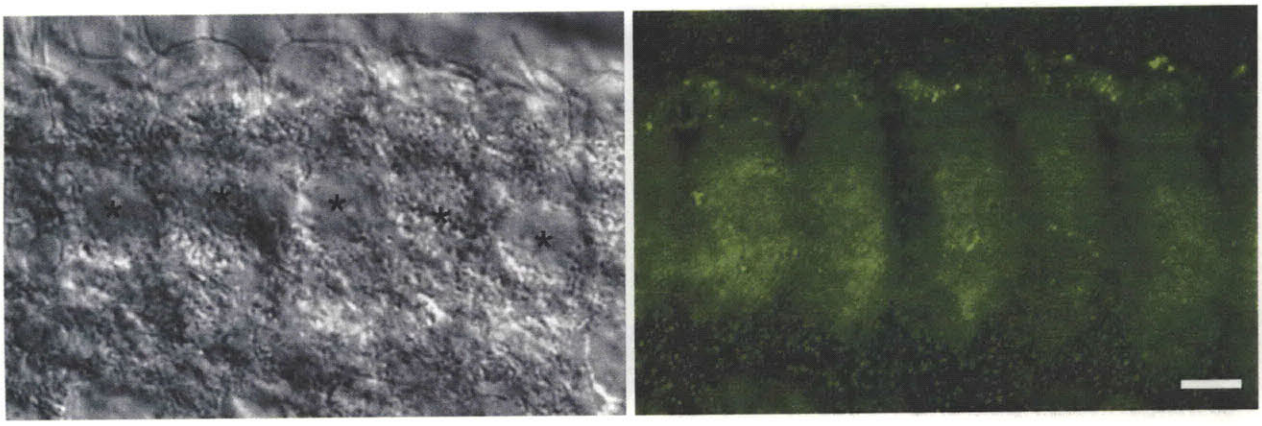

This page is intentionally left blank.

Figure 4.5 Nebulin immunostaining (green) is present in P29 cochlear stereocilia of both IHC (a,b) and OHC (c,d,f-i). F-actin is labeled with TritC-phalloidin (red). Nebulin is localized to IHC stereocilia base (a) and cuticular plate (b), likely in the rootlet structure. Extra staining on the surface of the cell is likely non-specific. Arrowheads show the well-patterned rows of the rootlet in the cuticular plate corresponding to where stereocilia originate from in the cuticular plate in (a). In OHC, a confocal plane (c) where no cuticular plate labeling is present with the F-actin staining, nebulin staining is present indicating the presence in the base of stereocilia (arrow). (d) Looking at one plane below (c) nebulin staining is present with distinct punta labeling the base of each stereocilium (arrowheads). (f-i) are confocal cross sections of the OHC rootlet, with a schematic shown in (e). Less rows of puncta (arrowheads) are present in planes deeper into the cuticular plate. Scale bar = 5μm

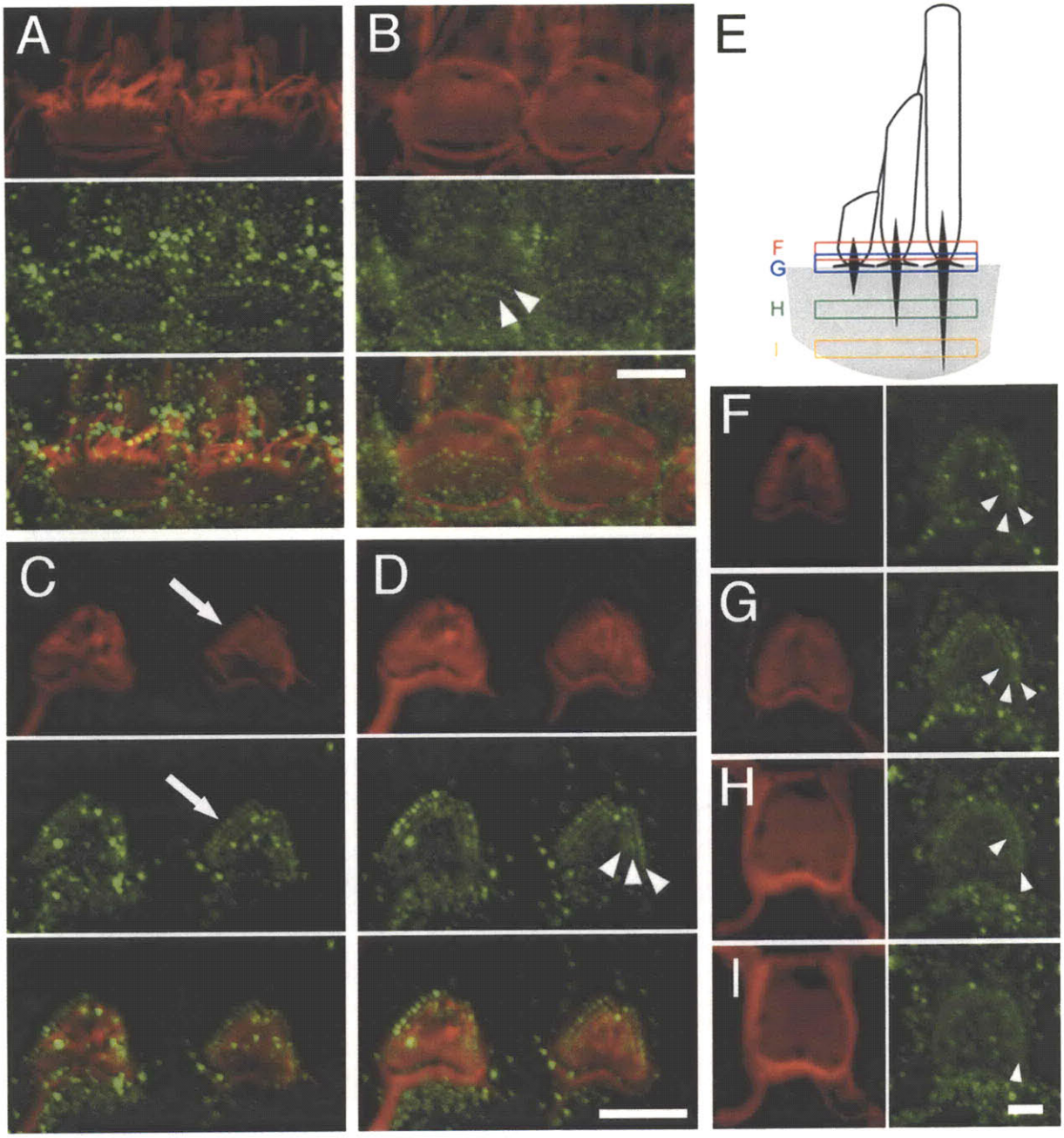

This page is intentionally left blank.

Figure 4.6 Nebulin labeling persists in P5 outer hair cells when the stereocilia are sheared off during the dissection process (arrows). Stereocilia F-actin is labeled with TritC-phalloidin (red). Scale bar = 5μm

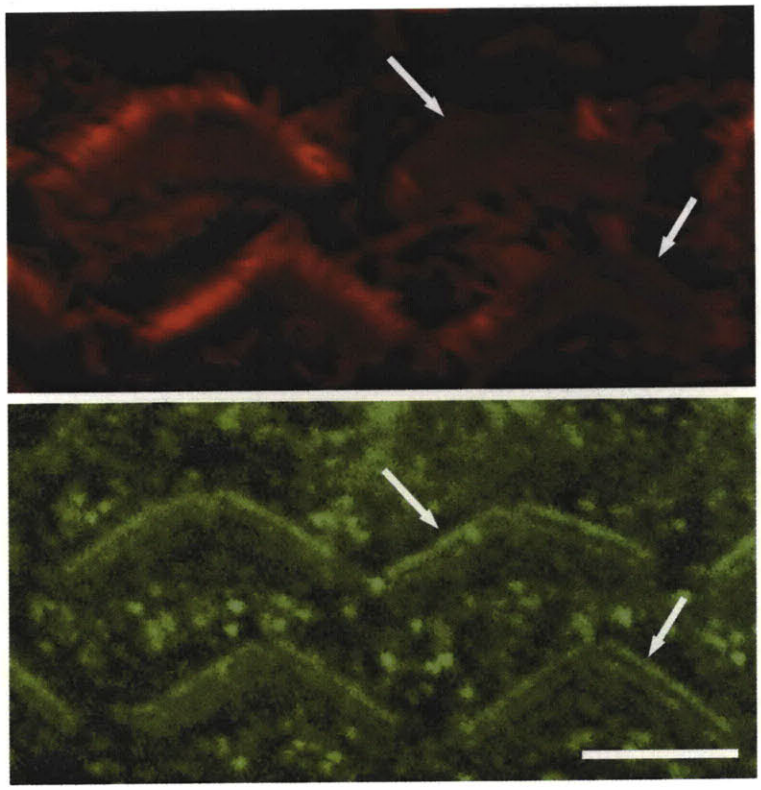

This page is intentionally left blank.

Figure 4.7 Localization using a twinfilin 1&2 antibody (green) on P56 mouse cochlea showing tip staining of the middle and short rows of stereocilia in (a) inner hair cells and (b) outer hair cells as well as the pericuticular necklace region of inner hair cells (arrowheads). Staining at the tips of short rows of stereocilia (arrows) can be seen in the inset (*). Stereocilia F-actin is labeled with TritC-phalloidin (red). Scale bar = 5μm

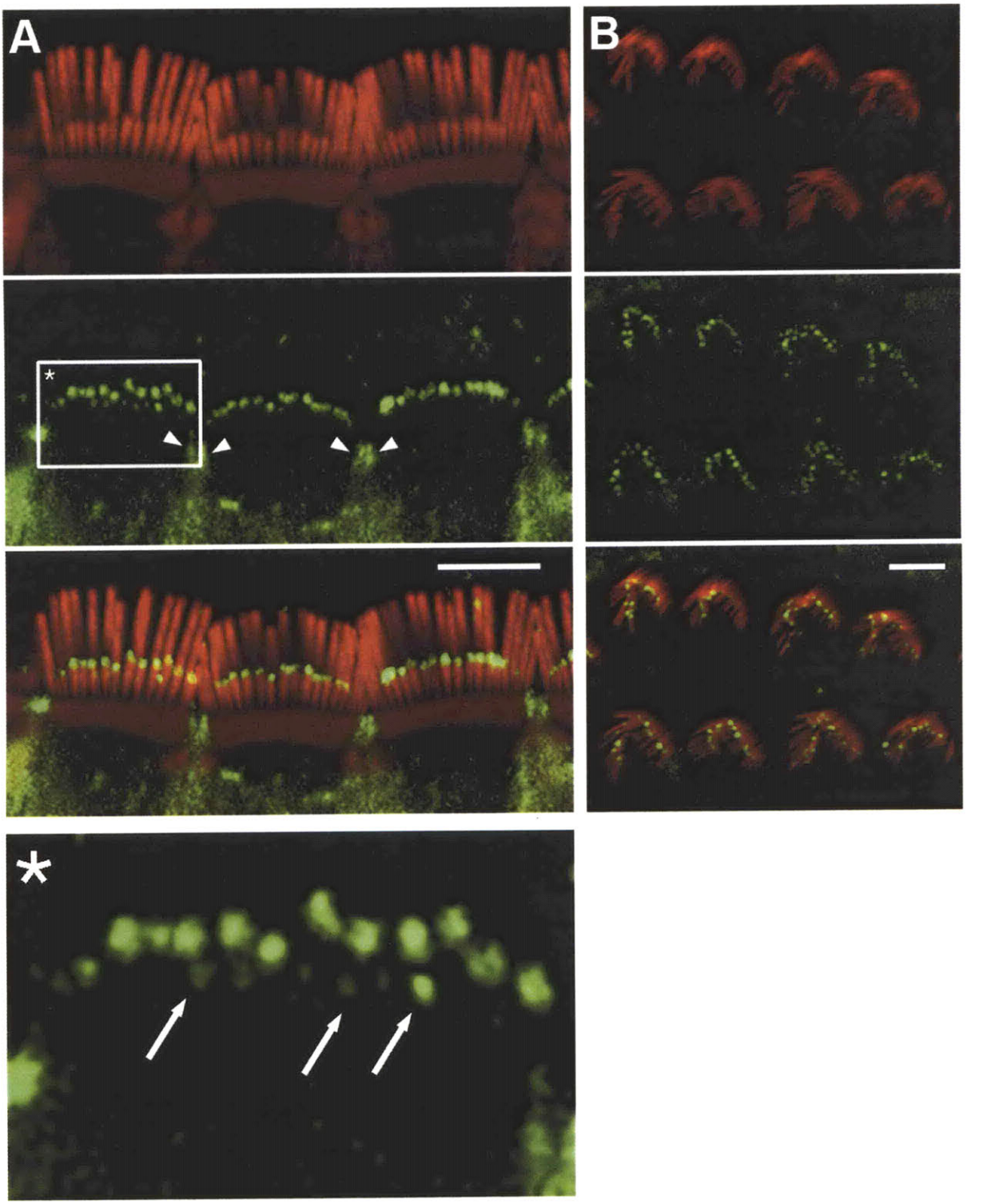

This page is intentionally left blank.

Figure 4.8 Twinfilin 1 staining (green) of cochlear stereocilia is absent in both (a) P28 inner hair cells and (b) P50 outer hair cells. Staining is strongly present in Deiter cell phalangeal processes (arrows). Stereocilia F-actin is labeled with TritC-phalloidin (red). Scale bar = 5μm

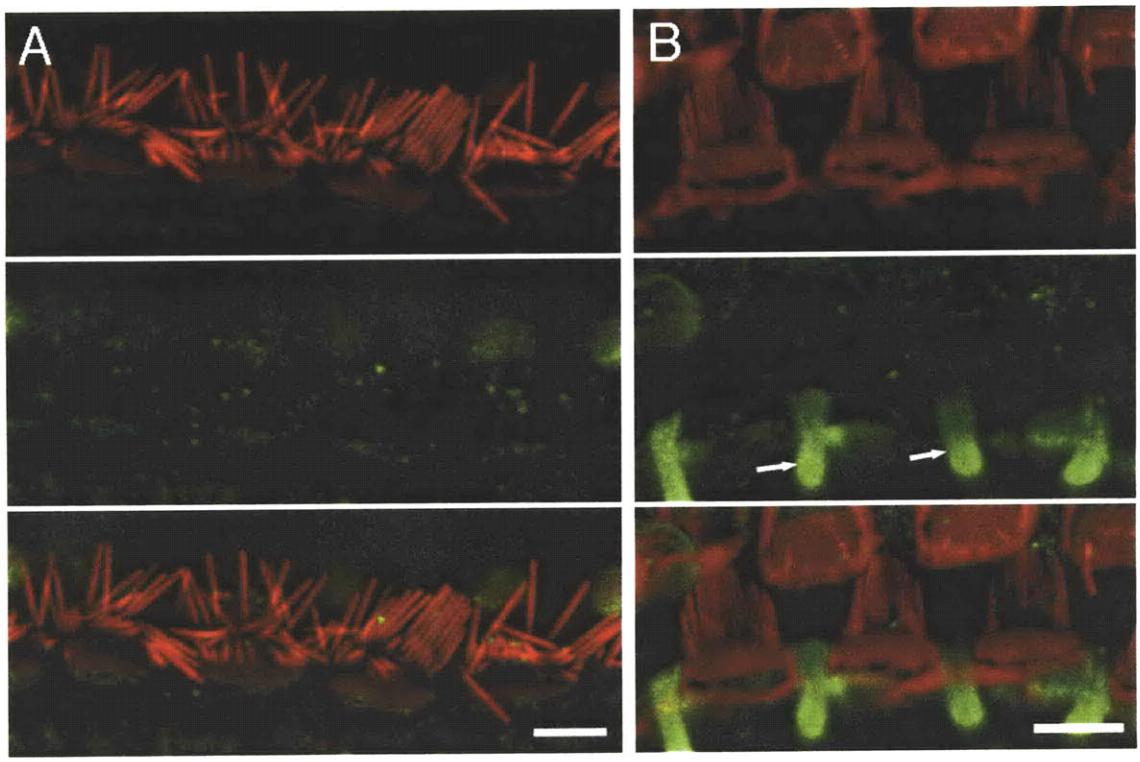

This page is intentionally left blank.

Figure 4.9 Twinfilin 1&2 (a) and twinfilin 1 (b) staining (green) showing staining in other areas of the cochlea besides the hair cell stereocilia. Pericuticular necklace staining is mainly seen with the twinfilin 1&2 antibody (arrowheads) and pillar cell staining seen more prominently with the twinfilin 1 antibody (*). Deiter cells phalangeal processes also appear to stain with twinifin 1&2 and the twinfilin 1 antibodies, suggesting that twinfilin 1 is the protein present here (arrows). Stereocilia F-actin is labeled with TritC-phalloidin (red). Scale bar = 5μm

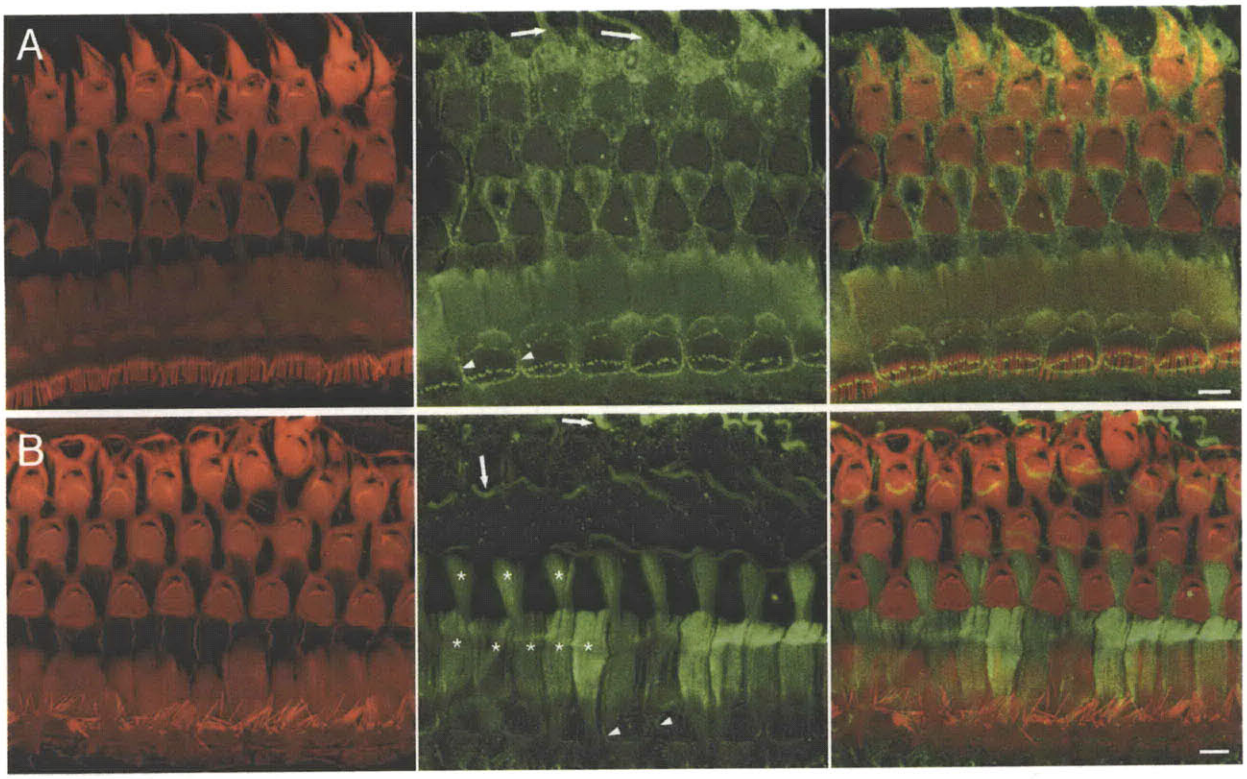

This page is intentionally left blank.

Figure 4.10 Proper antibody controls are required to elucidate false positive signals. (a) Gelsolin immunostaining appears to be present in stereocilia of the E18 chicken utricle when the antibody is blocked with goat serum, but (b) the labeling disappears when the antibody is blocked with just bovine serum albumin. F-actin is labeled with phalloidin in red and gelsolin is labeled in green. Scale bar = 10μm

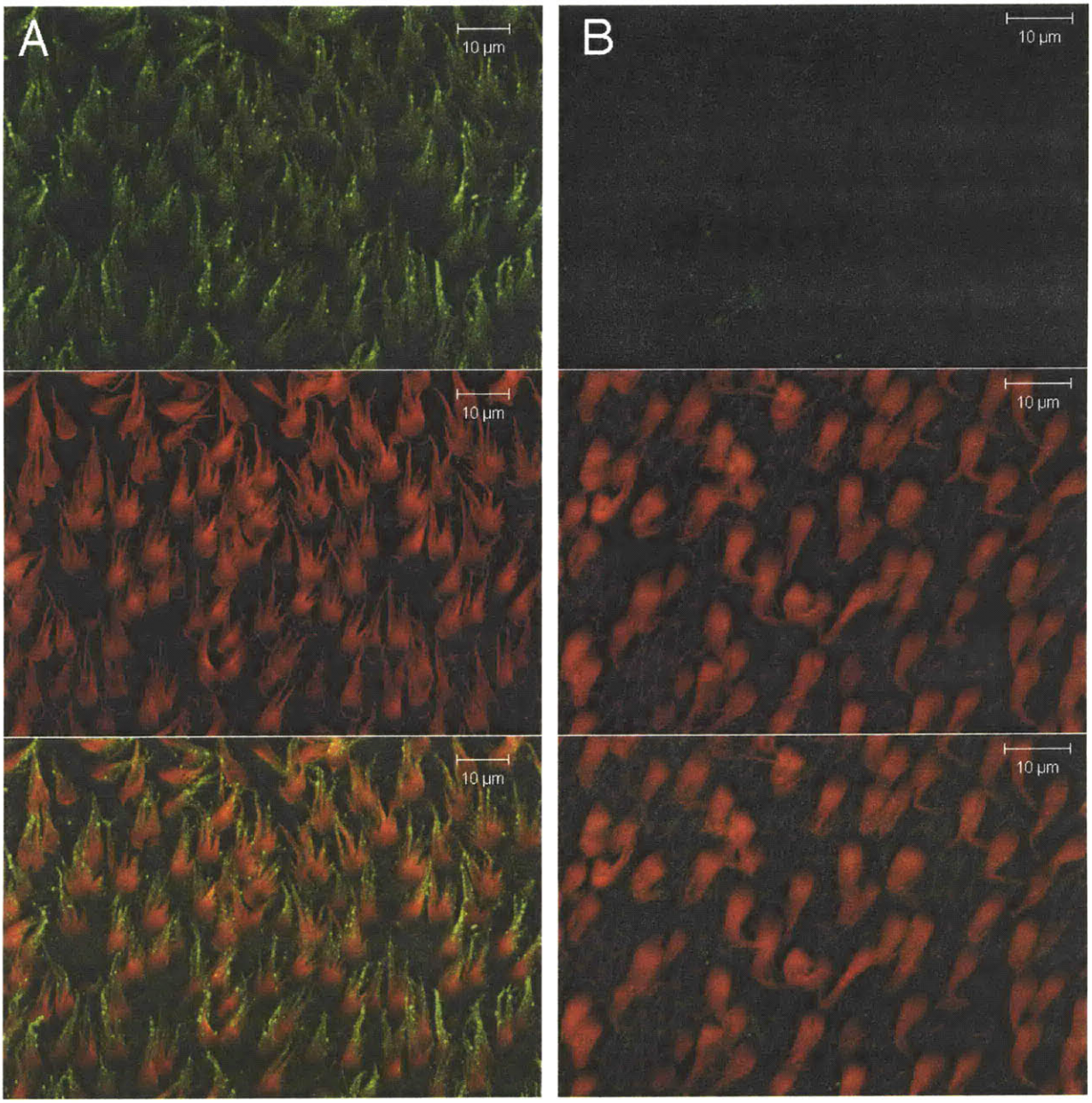

This page is intentionally left blank.

Chapter 5: Twinfilin 2, an actin filament regulatory protein in cochlear stereocilia

The following sections 5.1-5.4 are taken from a paper I am submitting:

5.1 Abstract

Cochlear auditory hair cells provide us with the sense of hearing through their ability to convert mechanical sound stimuli into electrical signals. This conversion happens in the hair bundle, an exquisitely mechano-sensitive organelle that protrudes from the cell's apical surface. In mammals, cochlear hair bundles are composed of 70-100 actin-filled stereocilia, which are organized in three rows in staircase fashion. At its core, each stereocilium is supported by actin filaments oriented with their barbed ends toward the tips of stereocilia. This filamentous actin core is treadmilling at a highly-regulated pace where the addition of actin monomers at stereocilia tips is counterbalanced by depolymerization at the pointed ends. The regulators of actin treadmilling in hair cells are unknown. Here we show that the barbed end capping protein twinfilin 2 is present at the tips of middle and short row mouse stereocilia precisely when the tall row of stereocilia elongates between postnatal days 7 and 13. We quantified stereocilia length changes, and we found the middle row of stereocilia shortened to acquire their final length between postnatal days 11 and 15, just when the expression level of twinfilin 2

reached mature levels. When we expressed twinfilin 2 in LLC/PK1-CL4 (CL4) cells, we observed a profound reduction of espin-induced microvilli length, pointing to a potent function of twinfilin 2 in reducing the steady state treadmilling of actin filaments. Misexpression of twinfilin 2 in cochlear inner hair cells before the protein is naturally expressed resulted in a significant reduction of stereocilia length. Our results demonstrate that twinfilin 2 plays an important role in the regulation of steady state treadmilling, which is an essential requirement for proper function of the mechano-electrical transduction apparatus in mature hair bundles.

5.2 Introduction

The filamentous actin in sensory hair cell stereocilia treadmills constantly, albeit the speed appears to vary between young, juvenile, and adult stereocilia. Any modulation of treadmilling affects stereocilia length, and hence also likely stereocilia function. Experiments using actin-GFP to label the incorporation and speed of actin polymerization in cultured rat inner hair cells revealed a rapid (2-3 μm/hour) polymerization rate in young stereocilia, corresponding to postnatal days 3-5 (Schneider et al., 2002). In mature stereocilia, at about postnatal day 15, the actin polymerization slowed down to about 2.5 μm/day, which is presumably the adult steady-state treadmilling rate. It is plausible that actin polymerization and depolymerization is tightly regulated at both ends. Beside actin crosslinking proteins, such as fimbrin and espin, which could be important in regulating actin dynamics at the pointed ends of filaments, no other candidate proteins have been proposed with a direct role in regulating actin dynamics in stereocilia.

5.3 Results and Discussion

To identify novel stereocilia proteins, we performed a mass spectrometry based proteomics analysis, and we identified two tryptic twinfilin 2 fragments with >99% confidence (figure 5.1A, B). Twinfilin 2 consists of two actin-depolymerizing factor homology domains that are connected by a short linker region. In biochemical assays,

twinfilin 2 displays a strong ability to cap actin filament barbed ends as well as the ability to sequester actin monomers (Nevalainen et al., 2008; Vartiainen et al., 2003). We hypothesized that twinfilin 2 could play a role in regulating stereocilia length because both its barbed end capping and actin monomer sequestering abilities would limit the lengths of actin filaments. We further hypothesized that localization of the protein toward stereocilia tips would be in agreement with a predominant function in barbed end capping, whereas twinfilin 2 localization along stereocilia shafts and toward the pointed ends would be consistent with a prevalent role in monomer sequestering. When we localized the protein in adult cochlear hair cells, we found strong immunolabeling of twinfilin 2 at the tips of the middle and short rows of stereocilia (figure 4.7A, B). The protein was also present faintly at the tips of tall stereocilia, but the labeling was too faint for reliable imaging. This localization is consistent with a role of twinfilin 2 in capping the barbed ends of stereocilia actin filaments in the middle and short rows of stereocilia, which points to a potential differential regulations of actin dynamics differently in the shorter two rows of stereocilia than in the tall row, where twinfilin 2 is present at very low levels, if at all. The localization pattern is also consistent between both inner and outer hair cells indicating a common mechanism of barbed end capping and length control between these hair cell types.

To determine a potential correlation between stereocilia growth and twinfilin 2 expression, we initially considered possible roles for twinfilin 2 in hair bundle development and neonatal hair bundle maturation and maintenance. At postnatal day 0, twinfilin 2 was not detectable in stereocilia, which led us to assume that twinfilin 2 is not present during initial hair bundle formation, growth, and consequently, not involved in staircase formation. Twinfilin 2 expression was first detectable, faintly, at the tips of middle row stereocilia at postnatal day 5 (data not shown). At postnatal day 7, the protein was detectable more robustly, and its expression gradually increased until postnatal day 13, when labeling intensities were comparable to the adult (figure 5.2A).

Postnatal hair bundle development consists of stereocilia thickening and a final elongation phase. To characterize stereocilia length changes in the mouse, we employed confocal microscopy and quantitative 3-dimensional image data analysis (Volocity, Improvision, Inc). We found that tall stereocilia exhibit a final burst of elongation from postnatal days 7–13, where their length increased from 3.31 μm ±0.11 (mean ±SD, n=3) to 5.37 μm ±0.14 (mean ±SD, n=3) (figure 5.2B). In contrast, middle row stereocilia do not show an elongation burst from postnatal day 5 until day 11 and maintain a length of approximately 2 μm (ANOVA P5-P11: p=0.57). Between postnatal day 11 and days 13–15, the middle row if stereocilia shortens about 10% at P13 and maintains this change at P15 (ANOVA P5-P15: p=0.004).

We conclude from these measurements, that between postnatal days 7 and 13, the middle row of stereocilia does not grow in length during a phase of rapid elongation of the tall row of stereocilia. Furthermore, as the tall stereocilia begin to level out, the short stereocilia shrink. The onset of expression of twinfilin 2 at postnatal day 5 is consistent with a role in impeding the growth of actin filaments in the middle row. The location of twinfilin 2 at stereocilia tips suggests that barbed end capping of the actin filaments is the mechanism by which this growth suppression is happening. When twinfilin 2 expression reaches adult levels at postnatal day 13, it appears to suppress the steady state treadmilling even further to a level that represents the mature stereocilia length, which is then maintained into adulthood. The tall row of stereocilia express very low amounts of twinfilin 2, if at all, and tall stereocilia consequently acquire a different steady state treadmilling equilibrium than the shorter two rows. It is conceivable that other regulators modulate the filamentous actin in tall stereocilia.

If twinfilin 2 is affecting the length of actin filaments, we would expect that it also does in CL4 cells, which can be used as an *in vitro* model system for parallel actin bundles like hair cell stereocilia (Loomis et al., 2003). These cells, when transfected with the stereocilia actin bundling protein espin, form prolonged microvilli of average lengths of 3.58μm ±0.31 (mean ±SEM, n=6 cells), which is on the order of tall stereocilia lengths

(figure 5.3A). When we expressed twinfilin 2 along with espin, the CL4 microvilli were significantly shorter (p=0.0080) and on the order of lengths of the middle row of stereocilia (2.56μm ± 0.07; mean ±SEM, n=6 cells; figure 5.3B).

The effect of twinfilin 2 expression in CL4 cells raised our curiosity to test its function in native hair cells. Because the protein is first detectable at postnatal day 5, we hypothesized that overexpression of twinfilin would affect stereocilia length and hair bundle morphology. To test this hypothesis, we co-expressed twinfilin 2 and enhanced green fluorescent protein (EGFP) in postnatal day 3-4 cochlear inner hair cells using gene gun transfection. After one day in vitro, we identified transfected cells by means of EGFP expression (figure 5.4A). We found that hair cells in which we overexpressed twinfilin 2 displayed significantly shorter stereocilia as their non-transfected neighbors (p=0.0327). The tall row stereocilia was stunted by 8% (2.19 μm ± 0.16 versus 2.01 μm ± 0.13, mean ±SEM, n=4; figure 5.4B). It is interesting that the tall stereocilia are affected by twinfilin 2 overexpression, which could be due to an immature gate keeping, specific transport mechanism in young hair cells, or simply due to the massive overexpression that puts twinfilin 2 all over the cell, including the tips of tall stereocilia. It is likely that the overexpression of twinfilin 2 causes twinfilin 2 to cap the barbed ends of actin filaments in tall stereocilia, preventing their further growth, resulting in the difference in transfected stereocilia heights versus untransfected heights.

The hair bundle is a precisely engineered structure where maintenance of stereocilia length is essential for proper function of the mechano-electrical transduction apparatus. Particularly the actin treadmilling in the shorter rows of stereocilia needs to be tightly controlled to avoid sporadic length changes, which would tighten or slacken the tip-link, and therefore arbitrarily shift the mechano-transducer's displacement-response curve. We show that twinfilin 2 is expressed at the correct time and place for fulfilling the role of a barbed end capping protein that shifts the treadmilling equilibrium in shorter stereocilia when compared with tall stereocilia, where actin polymerization and depolymerization is calibrated to an equilibrium that maintains longer filaments. Consequently, twinfilin 2 is

an important component of mature stereocilia, where we propose that the protein's function has to be tightly regulated so that actin treadmilling either stays out of the way of interfering with mechano-electrical transduction, or, more excitingly, that regulation of barbed end actin polymerization could be a modulator of the mechano-electrical transduction apparatus.

5.4 Methods

5.4.1 Antibodies and Clones

Antibodies recognizing only twinfilin 1 and recognizing both twinfilin 1 & 2 were graciously provided by Pekka Lappalainen. Twinfilin 2 was expressed using a pcDNA3.1-based vector harboring an IRES mCherry reporter. For gene gun experiments, twinfilin 2 was also cloned into a pTracer EF/V5/HIS (Invitrogen, Carlsbad, CA), which has a dual promoter EGFP reporter.

5.4.2 Mass Spectrometry

Chicken utricle hair bundles were isolated through a modified twist-off technique (Gillespie et al., 1991). Bundles were lysed with an SDS (2% SDS, 147mM Tris, and 0.51mM EDTA pH=8.5) solution and proteins were precipitated using 23% trichloroacetic acid. Protein was denatured with 10mM urea, carboxymethylated with 25mM iodoacetic acid, and trypsinized with 1μg modified trypsin (Promega, Madison, WI). The peptides were purified from the solution using a Pepclean C-18 spin column (Thermo Fisher Scientific, Rockford, IL). Resulting peptides were analyzed by modified version of the traditional MudPIT experiment by using a tetraphasic continuous column approach (Guzzetta et al., 2005). Scaffold (Proteome Software Inc) was used to statistically analyze database search results.

5.4.3 Whole Mount Surface Preparation Immunostaining

All animal procedures followed guidelines set forth by the National Institutes of Health. BALB/C mice were dissected at various ages according to the following protocol. Mice were euthanized and decapitated to isolate the temporal bone. Cochleae were fixed for 1 hour prior to completely removing from the temporal bone, then tectorial membranes were removed. Cochleae were permeabilized and blocked with PBT1 (0.1% Triton X-100, 1% BSA, 5% heat-inactivated goat serum in PBS, pH 7.3) for 10 minutes. All steps were performed at room temperature unless otherwise indicated. Samples were incubated overnight at 4°C with 1:200 anti-Twf1&2 in PBT1. After primary antibody staining, the samples were washed twice with PBT1 for 5 minutes and twice with PBT2 (0.1% Triton X-100, 0.1% BSA in PBS) for 5 minutes, and incubated with 7.5 mg/mL FITC-conjugated goat anti-rabbit antibody (Jackson ImmunoResearch Inc., West Grove, PA) in PBT2 for 2 hours, followed by PBT2 twice for 5 minutes. Samples were incubated with 0.4 μg/ml TRITC-conjugated phalloidin in PBS for 20 minutes followed by three 5-minutes washes with PBS, then mounted in DakoCytomation Fluorescent Mounting Medium (Dako, Carpinteria, CA) and imaged with a confocal microscope (LSM Pascal, Zeiss, Germany) using a 63x 1.4NA oil immersion lens.

5.4.4 Length Measurements

Some specimens used for length measurements were dissected as above, but were only permeabilized with PBT2, followed with incubation with phalloidin as stated above. Measurements were made using Volocity (Improvision Inc., Waltham, MA) with using Z-stacks taken with 0.4μm steps. All length measurements were made in the apical 900μm of the cochlea. Measurements for each animal were averaged and 3 animals were used for each age (n=3). ANOVA and paired Student T-Tests were performed using Excel. Graphs were made using Prism (GraphPad, Software, La Jolla, CA).

5.4.5 CL4 Cells

LLC-PK1/CL4 cells were obtained from ATCC (CL-101). Cells were cultured in a humidified chamber at 37°C and 5% CO_2 in M199 supplemented with 8% FBS (Omega Scientific, Tarzana, CA) and 1% Penicillin/streptomycin (Gibco, Carlsbad, CA). Cells were transfected using the Amaxa Nucleofector using solution L and program T-020 according to manufacturer's instructions. Transfected cells were grown for 3-5 days on coverslips and subsequently fixed in 4% paraformaldehyde for 25 minutes and visualized with 100x 1.4NA objective using a spinning disk confocal microscope. Length measurements of CL4 microvilli were done using Volocity (Improvision Inc, Waltham, MA). Sixteen microvilli were measured for each transfected cell and sixteen microvilli were measured for the neighboring untransfected cells. The averages for each transfected and neighboring untransfected cells were used for a paired T-test using the Prism (GraphPad, Software, La Jolla, CA).

5.4.6 Hair cell transfections

Organ of Corti cultures were prepared by dissecting out P3-P4 organs of Corti in Leibowitz cell culture medium (Invitrogen, Carlsbad, CA). The apical and middle turns of the OC were separated from the basal turn and cut into four pieces. Each cochlear piece was attached to a glass-bottom Petri dish (MatTek, Ashland, MA) coated with CellTak (Collaborative Biomedical Products, Bedford, MA) and maintained at 37°C and 5% CO2 in DMEM supplemented with 7% FBS for 1 day. Cultures were then transfected using a Helios gene gun (Bio-Rad). Gold particles of 1.0 μm diameter (Bio-Rad) were coated with plasmid DNA at a ratio of 2 μg of plasmid DNA to 1 mg of gold particles and precipitated onto the inner wall of Tefzel tubing, which was cut into individual cartridges containing ≈1 μg of plasmid DNA. Cartridges containing the pTracer EF/V5/HIS vector with Twf2 insert and control cartridges containing the pTracer EF/V5/HIS vector alone were prepared separately. Samples were bombarded with the gold particles from one cartridge per culture by using 120 psi of helium. After an additional 1-2 days in culture, samples were fixed in 4% paraformaldehyde, stained with

rhodamine–phalloidin, and observed by using a Zeiss LSM510 confocal microscope equipped with a 100x 1.4NA objective.

5.5 Additional experiments

5.5.1 Twinfilin 2 is expressed in all short stereocilia in *shaker 2* and *whirler* mice

Twinfilin 2 has been localized to cochlear stereocilia that are only about 2μm long in the mouse. This observation raised our interest in determining twinfilin 2's localization in a mouse model, which only has 2μm or shorter stereocilia. Here, we would expect to see twinfilin 2 in all of these stereocilia if it is indeed involved in maintaining short stereocilia by suppressing F-actin growth. Both the *shaker 2* and *whirler* mice exhibit these characteristically short stereocilia in the cochlea (Mogensen et al., 2007; Mustapha et al., 2007). Indeed twinfilin 2 is present at the tips of all stereocilia in both shaker 2 and whirler mice (figure 5.5). These two mouse models lack the proteins myosin XVa and whirlin, proteins that have been shown to be required for stereocilia elongation. The mechanism of this elongation is likely indirect because neither protein has any known actin-modulating function. The presence of twinfilin 2 at the tips of all stereocilia could suggest that the lack of these proteins allows twinfilin 2 to bind to the tips of all stereocilia, hence stunting their growth. This action of twinfilin 2 in *shaker 2* and *whirler* mice therefore could be responsible for the reduced length of stereocilia in these mouse mutants. Furthermore, I hypothesize that if twinfilin 2 localizes to the tips of stereocilia by an interaction with filament barbed ends, then I would expect that whirlin and myosin XVa could be involved in transporting an unidentified protein up to the tips of stereocilia that competes with twinfilin 2's binding site.

5.5.2 Additional Methods

Dissection and immuno-fluorescence staining of mutant mice followed the same procedure as above.

Shaker 2 and *whirler* mice were genotyped as follows. Mouse genomic DNA was isolated using the DNeasy Blood and Tissue Kit (Qiagen, Valencia, CA) according to manufacturer's instructions. For *shaker 2* genotyping, PCR was performed on genomic DNA using:

forward primer 5'-TTCCAGCATCACCTTTACCCCGTG-3'

reverse primer 5'-TTCCTGTCACCAAGCCTCACATCC-3'

PCR product was digested with Tse I restriction enzyme for 2 hours at 65°C. For analysis, Tse I digest product was electrophoresed on a 2.0% agarose gel. *Shaker 2* alleles exhibit 528bp and 196bp fragments, whereas wild-type (WT) alleles exhibit 416bp, 196bp, and 112bp fragments.

For *whirler* genotyping, PCR was performed with 2 primer sets:

1. To detect the mutant *whirler* allele

forward primer 5'-GGGGAATCAGACTCGTGCACTGCT-3'

reverse primer 5'-GGTGCACCTCCACCAGAACAAAGTG-3'

2. To detect the WT allele

forward primer 5'-TGGATGCTTCCTCAAGGACACCAGA-3'

reverse primer 5'-TATCCCCAGACTGAGAGCCCCAGAA-3'

PCR product was electrophoresed on a 2.0% agarose gel. *Whirler* alleles show a 330bp product whereas the WT allele shows a 571bp product.

Figure 5.1 (a) Protein sequence of twinfilin 2 with the identified peptides highlighted. Green highlight indicates an amino acid that was identified being carboxymethylated. (b) Mass spectra of identified peptide fragments for twinfilin 2 shown in (a).

A

M T H Q T G I H A T	T E L R D F F A K A	R N G S V R L I K V	I I E E E Q L V L G	A H K E L A R R W D
V D Y D A F V L P L	L D E Q Q P C Y V L	Y R L D S Q N A Q G	Y E W L F I S W S P	D N S P V R L K M L
Y A A T R A T V K K	E F G G G H I K D E	M F G T V K E D V S	L S G Y Q K **H V S S**	**C S A P A P L T A A**
E Q E L Q Q I R I N	E V K T E I S V E S	K H Q T L Q G L A F	P L Q L D A Q Q A I	Q T L K Q K K I N Y
I Q L K L D L E R E	T I D L V H T S P T	D I S D L P K R I P	Q D S A R Y H F F L	Y K H S H E G D Y L
E S V V F I Y S M P	G Y K C S I K E R M	L Y S S C K S R L L	D T V E Q E F C L E	I A K **K I E I D D G**
A E L T A E F L Y D	**E V H P K** Q H A F K	Q A F A K P K G P V	G K R G Q K R L I K	G P G E N G E D S

B

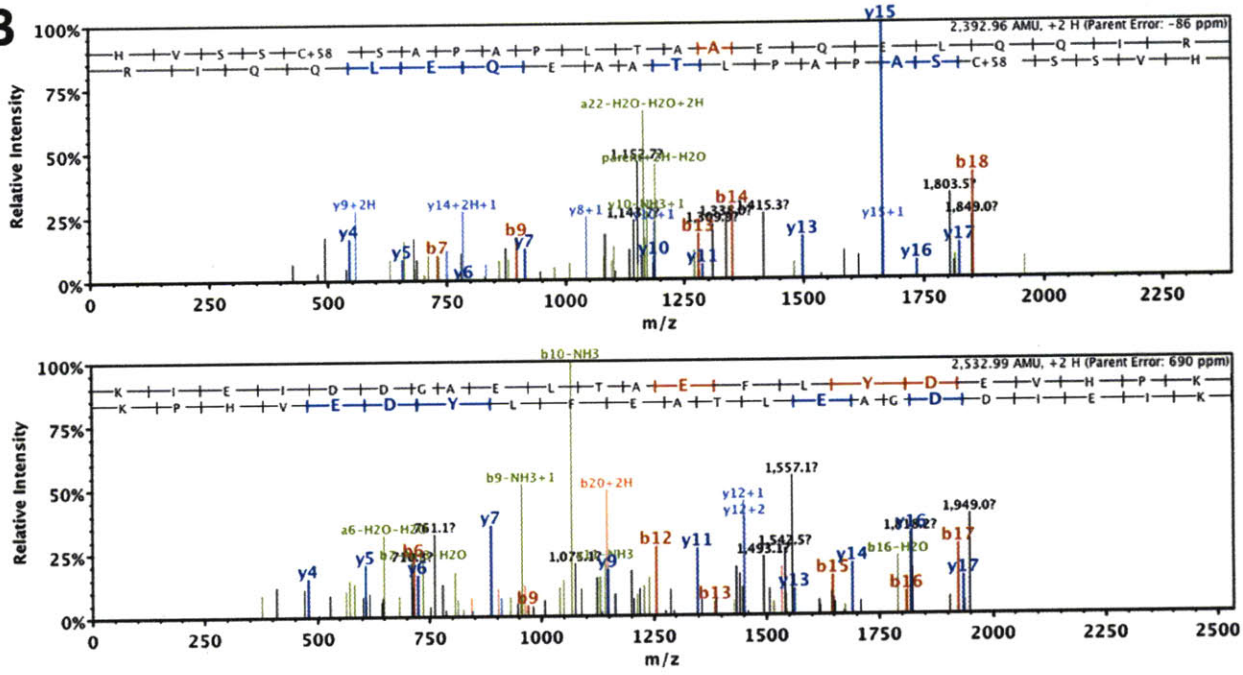

This page is intentionally left blank.

Figure 5.2 (a) Developmental expression of twinfilin 2 (green) showing increasing labeling intensity with age. Stereocilia F-actin is labeled with TritC-phalloidin (red). (b) Graph shows measured mouse stereocilia lengths for tall (red line) and middle (blue line) rows of stereocilia during development (mean ± SD, n=3). Stereocilia lengths were measured using Volocity (Improvision, Inc). All stereocilia were measured from images that were taken within 900μm from the apex of the cochlea. Stereocilia were only measured if the length of the stereocilium laid within about 4-5 Z-sections, since the resolution in Z is less than in the X-Y plane. All measurements for a given animal were averaged. This analysis was performed in 3 different mice and the animal averages were averaged for an overall average with a standard deviation, which is plotted in the graph. Scale bar = 2μm

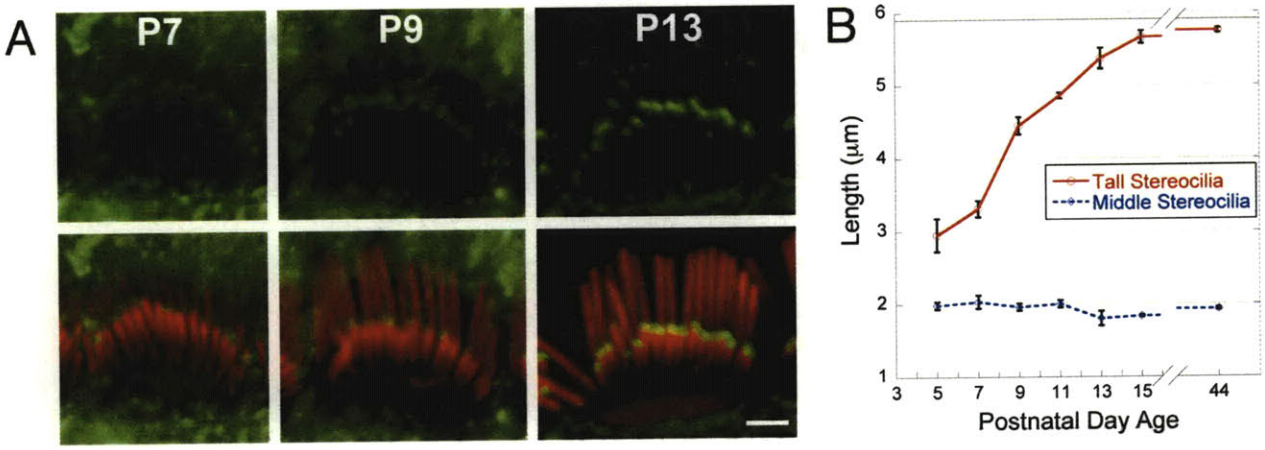

This page is intentionally left blank.

Figure 5.3 (a) LLC-PK1/CL4 cells stably expressing GFP-espin (green) are tranfected with a vector containing twinfilin 2 IRES mCherry. Red indicates a transfected cell. (b) Higher resolution image of the area indicated in the white box in (a) with the dotted line indicating the border between the transfected and untrasfected cells. (c) Microvilli lengths on a transfected cell were measured and compared with a neighboring untransfected cell (mean ± SEM, n=6). Paired t-test indicates a significant change in microvilli lengths upon transfection of twinfilin 2. Sixteen microvilli lengths were measured in Volocity (Improvision Inc.) for each transfected cell and the neighboring untransfected controls. The average length of the transfected cell was compared to the average length of the untransfected neighbors in a two-tailed paired T-test. Scale bar = 5μm

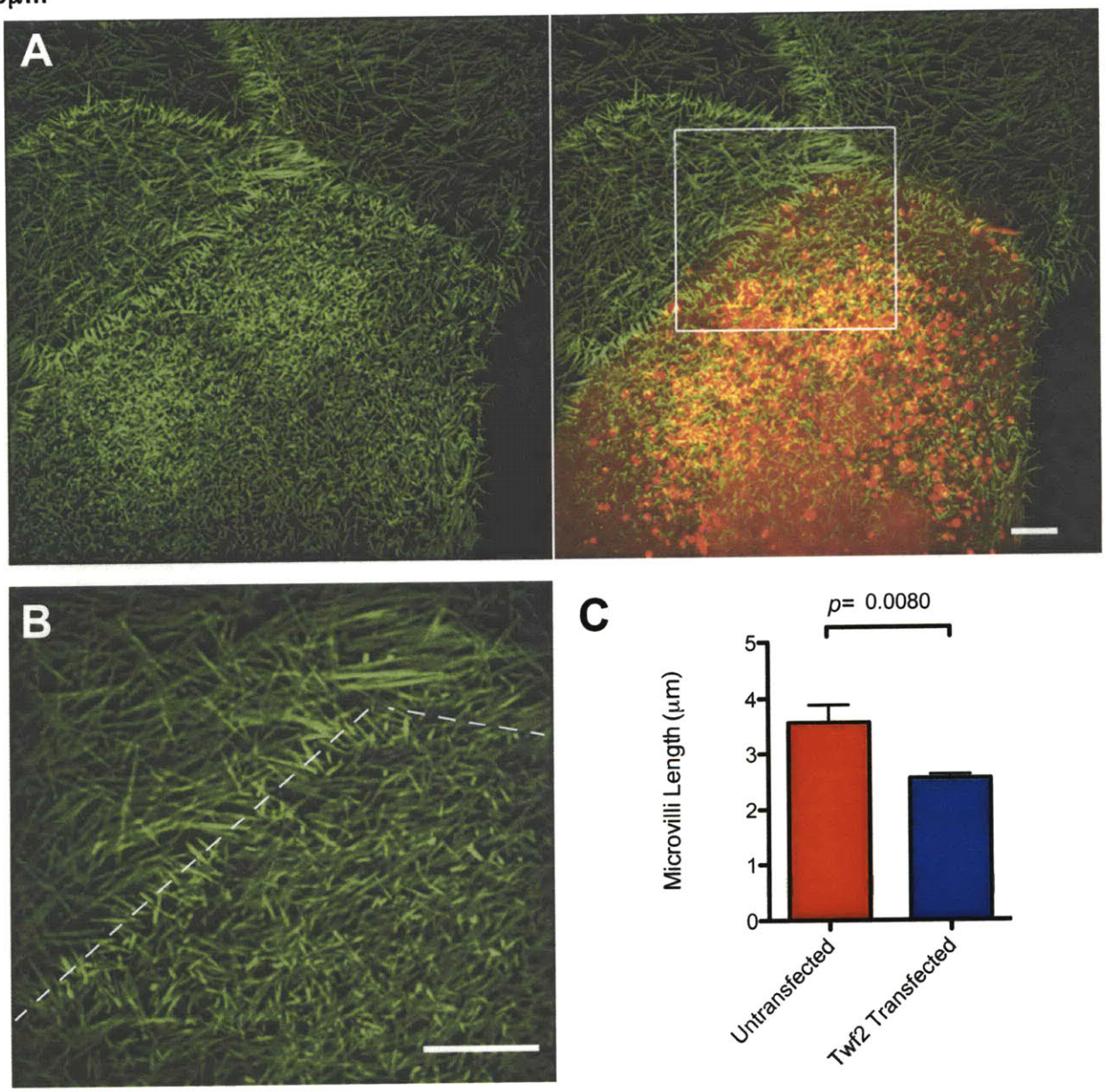

This page is intentionally left blank.

Figure 5.4 *In vivo* hair cell transfections of twinfilin 2. Hair cells were transfected with twinfilin 2 with a dual promoter expression of EGFP (green). Stereocilia F-actin is stained with phalloidin (red). Cochleae were dissected at P3-P4, transfected after 1 day in vitro (DIV) and images are taken at 2-3 DIV. (b) Individual filament measurements for each image are averaged for the untransfected and transfected cell. Image averages are plotted and used for the statistical analysis with a one-tailed paired T-test, n=4. Scale bar = 5μm

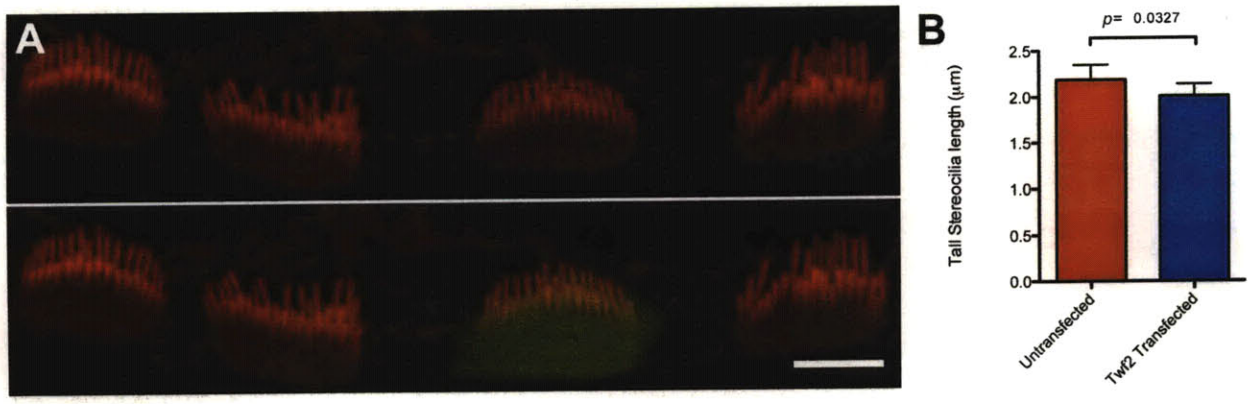

This page is intentionally left blank.

Figure 5.5 Twinfilin 2 (green) is localized to tips of all stereocilia in (a) P13 *Shaker 2* and (b) P12 *whirler* mice. Stereocilia F-actin is labeled with TritC-phalloidin (red). Scale bars = 5μm

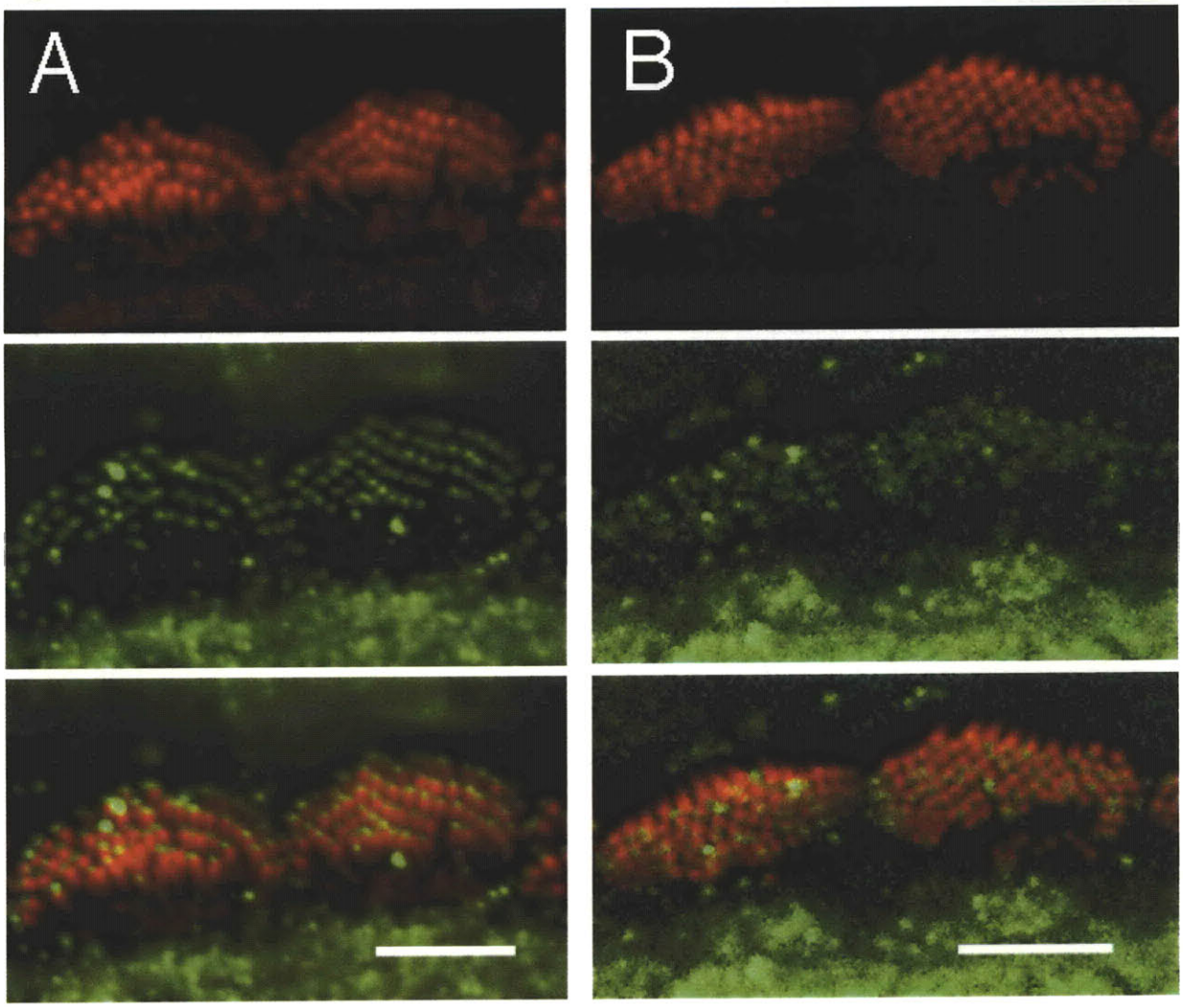

This page is intentionally left blank.

Chapter 6: Concluding remarks

6.1 Discussion

6.1.1 Proteomics of hair bundles

The protein list found in this proteomic screen has not likely identified all the proteins in stereocilia. In order to further identify even more proteins, more MudPIT analyses would be necessary. Due to the many types of proteins present in stereocilia, however, a more directed approach to identify certain types or groups of proteins may be more applicable. For example, membrane proteins would be very interesting to try to find because the MET channel has not yet been identified. Identifying all the membrane proteins may lead to identification of a candidate for the MET channel. Another possibility is to use the proteomics technique to investigate protein complexes. For example, it is possible to immuno-precipitate a known protein from the stereocilia and to analyze the interacting proteins (the protein complex) by mass spectrometry techniques.

In addition to pursuing the identification of more stereocilia proteins, the current list of putative hair bundle proteins is already quite extensive. Further analysis using protein localization techniques can confirm more proteins to stereocilia. Researchers interested in various aspects of stereocilia can use this database as a starting point in looking into

different aspects of stereocilia function. For instance, there are many tubulin related proteins within the database and these could be used to study kinocilium function and processes. Additionally, analysis of signaling pathways within stereocilia can also be done to determine which signaling pathways may be playing a prominent role in hair bundle function and maintenance.

In this thesis, I studied the actions of one actin regulatory protein found in the proteomic screen. There are still four other known direct actin filament regulators that have not been found in stereocilia as highlighted in table 3.1. Each of these proteins and possibly more may play a role in how the stereocilia structure is maintained, as the structure is complex and likely requires multiple proteins to achieve and maintain filament lengths.

6.1.2 StarD10

StarD10's localization has been confirmed in stereocilia. The next step is to identify the function of the protein. StarD10's localization pattern suggests a possible regulation of the lipid composition of the stereocilia membrane.

The distribution of StarD10 in hair cells is similar to the distribution of PIP_2 in hair cells. PIP_2 has been localized to bullfrog stereocilia and appears to be present only in the top part of the bundle and is absent toward the base of stereocilia (Hirono et al., 2004). The StarD10 localization that I found in stereocilia is similar to the PIP_2 localization, suggesting a potential functional interaction between StarD10 and PIP_2. If StarD10 is able to regulate PIP_2 or other phosphoinositide phosphate lipids, this is could have a profound meaning to many cell types. PIP_2 plays a role in multiple signaling pathways and affects actin regulatory proteins like gelsolin, profilin, and twinfilin 2; therefore, properties of StarD10 and its regulation could affect many signal transduction pathways.

Determining the lipids that StarD10 interacts with and correlating that to which lipids are expressed in the stereocilia membrane would give insight to the function in stereocilia.

By using fluorescent proteins that bind to PIP_2 to monitor PIP_2 levels and location, I could determine how overexpression of StarD10 affects both PIP_2 localization and density (Stauffer et al., 1998). These experiments will be carried out in collaboration with other members of my advisor's laboratory.

6.1.3 Nebulin

Nebulin's localization suggests a possible role in rootlet regulation and structure. Based on the current knowledge of the function of nebulin, there are two likely scenarios occurring in the stereocilia rootlet. First, nebulin could be acting as a molecular ruler to determine the length of the rootlet. Stereocilia rootlets range from about 0.3μm to 1.3μm (Furness et al., 2008), and nebulin has been implicated to maintain lengths of thin filaments, which are up to 1.3μm long (Kruger et al., 1991). For this molecular ruler scenario to be true, nebulin would have to interact with barbed-end capping proteins and pointed-end capping proteins in order to set the length of the filament. Neither tropomodulin nor capping protein, proteins that have been found to regulate this process in the thin filaments, have been found to be associated with the stereocilia rootlet or hair cells; therefore, it is unlikely that nebulin is acting as a molecular ruler, unless these or other barbed and pointed end cappers are found to be associated with the rootlet and interact with nebulin. Additionally, the rootlet filaments would have to end at the top of the rootlet in order for this molecular ruler to be effective; it appears that at least some of the stereocilium shaft filaments continue into the rootlet, decreasing the likelihood of the molecular ruler scenario (Furness et al., 2008).

The second possible function of nebulin is to act as a stabilizer of the actin filaments in the rootlet. Recent research has implicated that nebulin acts to stabilize the thin filament and set a minimum length, but the actual length is regulated by another mechanism (Castillo et al., 2009). In hair cells, stereocilia taper at the rootlet making it a mechanically fragile area, and this is also the site of damage in chronic, but not acute overstimulation (Liberman, 1987; Liberman et al., 1987). Without reinforcement of the

rootlet, it is unlikely that the stereocilia are able to handle excessive forces even in the acute overstimulation case. Espin, a filament cross-linker, could help strengthen the rootlet as it does in the stereocilium shaft, but it is not present in the rootlet (Furness et al., 2008). Espin bundles actin filaments by binding together two actin filaments with a given separation distance. This also works to stabilize the filaments and decrease the depolymerization of filaments. It is possible that instead of espin working to stabilize actin filaments in the rootlet, nebulin and proteins like tropomyosin may take on this role instead, since tropomyosin has also been found to be in the stereocilia rootlet (Furness et al., 2008). However, neither protein is thought to bind two filaments to each other, therefore potentially allowing a closer packing arrangement of actin filaments, as seen in the rootlet.

6.1.4 Twinfilin 2

Twinfilin 2 was shown to localize to the tips of middle and short stereocilia in the cochlea. It is able to regulate the length of actin filaments in both CL4 cells and stereocilia. This result begs the question of how twinfilin 2 is achieving the regulation, since it has both the ability to cap actin filament barbed ends, as well as sequester actin monomers.

If twinfilin 2 caps filament barbed ends, then it would change the dynamics of actin filaments. Capping the barbed ends of actin filaments prevents the addition of actin monomers, thereby preventing growth and leading to a shorter filament. This model fits well with the localization pattern seen in stereocilia, since twinfilin 2 appears to be only present at the barbed ends of filaments.

Sequestration of actin monomers would have a similar effect on filament lengths. By sequestering the actin monomers, twinfilin 2 again would prevent the actin monomers from being added to the filament. In stereocilia, this may be happening at the local level with twinfilin 2 being concentrated to the tips of stereocilia and locally sequestering the actin monomers and preventing the addition onto actin filament barbed ends. However,

there is a second possible effect with the monomer sequestration function. Sequestration of monomers may also happen toward the pointed ends of filaments, which may also increase depolymerization at pointed ends by decreasing the concentration of free actin monomers. This would also cause shorter actin filaments, however, this is not likely happening in stereocilia because twinfilin 2 is not found near the pointed ends of actin filaments.

Since both functions of twinfilin 2 result in the same shortened actin filaments, I need to be able to separate the two functions of twinfilin 2 in order to determine the functionally relevant mechanism in stereocilia. Truncation of the twinfilin 2 protein, leaving only one ADF-H domain, effectively disrupts the protein's capping ability (Nevalainen et al., 2008; Paavilainen et al., 2007). Testing the truncated protein for an effect on stereocilia length would help to determine if a sequestering ability is sufficient for stereocilia length regulation. However this would not rule out a capping mechanism as being physiologically relevant.

Twinfilin 2's characteristic localization brings up the question as to how twinfilin 2 achieves the asymmetrical distribution. Is twinfilin 2 concentrated at the tips of stereocilia by a mere interaction with the actin filament barbed end? If this is the case, there must a blocking protein that is present at the tips of tall stereocilia that prevents the interaction with filament-barbed ends from occurring. In the *shaker 2* and *whirler* mice it would appear that the blocking protein is missing from the stereocilia, since twinfilin 2 is present at the tips of all stereocilia. This suggests that myosin XVa, whirlin, or another protein that binds whirlin prevents the interaction in the tallest stereocilia in the cochlea.

There is still the possibility that other proteins present only at the tips of middle and short stereocilia are responsible for concentrating twinfilin 2. Finding an interaction partner to twinfilin 2 that has a similar distribution could support this possibility. This interaction partner may also be misregulated in the *shaker 2* and *whirler* mutants,

without being a direct consequence of the absence of myosin XVa or whirlin, but rather a consequence of the lack of a staircase structure or the presence of extra rows of stereocilia, as seen in these mutants. Twinfilin 2's localization to all stereocilia would then be a consequence of the misregulation of the interaction partner in these mutant mice.

Twinfilin 2 is present in many different tissues. The functions in each of these tissues has yet to be determined, except for one study, which has found that a loss of twinfilin 2 in neurons causes decreased neurite growth and that an overexpression has the opposite effect (Yamada et al., 2007). This function is contrary to what I have found, which could mean that twinfilin 2 has various effects depending on the specific cell process. Neurite growth is achieved using highly branched actin filament structures in lamellapodia. The highly branched filament structures are regulated differently than the parallel actin filaments found in stereocilia. Consequently, it is difficult to compare stereocilia growth regulation with neurite growth regulation. Nevertheless, my findings may provide insight into how twinfilin 2 may play distinct roles in parallel, and possibly branched, actin filament regulation and may specifically help us to understand twinfilin 2's role in other parallel actin filament structures like microvilli or filopodia.

Recent research suggests that the MET channel is located at stereocilia tips of the shorter rows of stereocilia, and not in the tallest row (Beurg et al., 2009). This raises the question as to whether twinfilin 2, which is located at the same place as the MET channel, is involved in any of the functional aspects of MET. These new findings bring into question the adaptation model that has been previously accepted with myosin Ic-based motors climbing and sliding along the actin core near the upper tip-link insertion site. Adaptation is known to be regulated by Ca^{2+}. With no MET channels present where myosin Ic is located, then it is unlikely responsible for the adaptation mechanism. Since adaptation involves a decrease in the tension in the tip-link, another possibility is that the tip of the shorter stereocilium could grow in length to relieve the tension in the tip-link. Such a process could be mediated by twinfilin 2 whereby I hypothesize that

calcium entry through the MET channel, causes twinfilin 2 to uncap the filament barbed ends allowing filament polymerization and an increase in stereocilium length, thus relieving the tension. Such a model would require rigorous verification.

6.2 Summary

The main goal set out by this thesis was to establish a proteomics screening technique of hair bundles and to localize novel stereocilia proteins in the inner ear. To that end, I have developed and performed a mass spectrometry analysis of inner ear hair bundles, localized 3 proteins to stereocilia, and provided functional data on one of these proteins. The findings of this research can be summarized as:

1. I have developed an effective technique to identify hair bundle proteins using the MudPIT technique. The proteomics analysis of hair bundles has provided a dataset of putative proteins that can be used as a strong starting point for studying the molecular components of stereocilia and kinocilia. The screen was able to identify many of the currently known stereocilia proteins as well as a great number of other proteins, whose localization can be confirmed through immuno-staining experiments.
2. Three new stereocilia proteins from the proteomic analysis have been localized in stereocilia by immuno-staining. Each protein has a characteristic localization within cochlear stereocilia, and I hypothesized potential functions for each of the three proteins.
3. Twinfilin 2 is localized to the tips of short and middle rows of cochlear stereocilia. It is involved in regulating stereocilia lengths through regulation of actin filament lengths. The regulation appears to prevent the growth of the short and middle rows of stereocilia while the tall row continues to elongate.

This page is intentionally left blank.

References

Abe, S., Katagiri, T., Saito-Hisaminato, A., Usami, S., Inoue, Y., Tsunoda, T., Nakamura, Y. 2003. Identification of CRYM as a candidate responsible for nonsyndromic deafness, through cDNA microarray analysis of human cochlear and vestibular tissues. Am J Hum Genet 72, 73-82.

Adato, A., Lefevre, G., Delprat, B., Michel, V., Michalski, N., Chardenoux, S., Weil, D., El-Amraoui, A., Petit, C. 2005a. Usherin, the defective protein in Usher syndrome type IIA, is likely to be a component of interstereocilia ankle links in the inner ear sensory cells. Human Molecular Genetics 14, 3921-3932.

Adato, A., Michel, V., Kikkawa, Y., Reiners, J., Alagramam, K.N., Weil, D., Yonekawa, H., Wolfrum, U., El-Amraoui, A., Petit, C. 2005b. Interactions in the network of Usher syndrome type 1 proteins. Human Molecular Genetics 14, 347-356.

Ahmed, Z.M., Goodyear, R., Riazuddin, S., Lagziel, A., Legan, P.K., Behra, M., Burgess, S.M., Lilley, K.S., Wilcox, E.R., Riazuddin, S., Griffith, A.J., Frolenkov, G.I., Belyantseva, I.A., Richardson, G.P., Friedman, T.B. 2006. The tip-link antigen, a protein associated with the transduction complex of sensory hair cells, is protocadherin-15. J Neurosci 26, 7022-34.

Alberts, B., Johnson, A., Lewis, J., Raff, M., Roberts, K., Walter, P. 2002. Molecular Biology of the Cell. 4th ed. Garland Science, New York.

Alpert, A.J., Shukla, A.K. 2004. Displacement Chromatography Effects Can Cause Highly Selective Sampling of Peptides During Solid Phase Extraction Cleanup, ABRF.

Belyantseva, I.A., Boger, E.T., Naz, S., Frolenkov, G.I., Sellers, J.R., Ahmed, Z.M., Griffith, A.J., Friedman, T.B. 2005. Myosin-XVa is required for tip localization of whirlin and differential elongation of hair-cell stereocilia. Nature Cell Biology 7, 148-U60.

Berg, R.E. 2009. Sound [Online]. Available by Encyclopaedia Britannica Online <http://www.britannica.com/EBchecked/topic/555255/sound> (verified April 8, 2009).

Beurg, M., Fettiplace, R., Nam, J.H., Ricci, A.J. 2009. Localization of inner hair cell mechanotransducer channels using high-speed calcium imaging. Nat Neurosci.

Boeda, B., El-Amraoui, A., Bahloul, A., Goodyear, R., Daviet, L., Blanchard, S., Perfettini, I., Fath, K.R., Shorte, S., Reiners, J., Houdusse, A., Legrain, P., Wolfrum, U., Richardson, G., Petit, C. 2002. Myosin VIIa, harmonin and cadherin 23, three Usher I gene products that cooperate to shape the sensory hair cell bundle. Embo Journal 21, 6689-6699.

Bretscher, A. 1981. Fimbrin is a cytoskeletal protein that crosslinks F-actin in vitro. Proc Natl Acad Sci U S A 78, 6849-53.

Castillo, A., Nowak, R., Littlefield, K.P., Fowler, V.M., Littlefield, R.S. 2009. A nebulin ruler does not dictate thin filament lengths. Biophys J 96, 1856-65.

Chen, E.I., Cociorva, D., Norris, J.L., Yates, J.R., 3rd. 2007. Optimization of mass spectrometry-compatible surfactants for shotgun proteomics. J Proteome Res 6, 2529-38.

Conover, G.M., Henderson, S.N., Gregorio, C.C. 2009. A myopathy-linked desmin mutation perturbs striated muscle actin filament architecture. Mol Biol Cell 20, 834-45.

Craig, R., Beavis, R.C. 2003. A method for reducing the time required to match protein sequences with tandem mass spectra. Rapid Commun Mass Spectrom 17, 2310-6.

Daniel, E. 2007. Noise and hearing loss: a review. J Sch Health 77, 225-31.

Deans, M.R., Antic, D., Suyama, K., Scott, M.P., Axelrod, J.D., Goodrich, L.V. 2007. Asymmetric distribution of prickle-like 2 reveals an early underlying polarization of vestibular sensory epithelia in the inner ear. J Neurosci 27, 3139-47.

Delprat, B., Michel, V., Goodyear, R., Yamasaki, Y., Michalski, N., El-Amraoui, A., Perfettini, I., Legrain, P., Richardson, G., Hardelin, J.P., Petit, C. 2005. Myosin XVa and whirlin, two deafness gene products required for hair bundle growth, are located at the stereocilia tips and interact directly. Human Molecular Genetics 14, 401-410.

DeRosier, D.J., Tilney, L.G. 2000. F-actin bundles are derivatives of microvilli: What does this tell us about how bundles might form? J Cell Biol 148, 1-6.

Desai, S.S., Zeh, C., Lysakowski, A. 2005. Comparative morphology of rodent vestibular periphery. I. Saccular and utricular maculae. J Neurophysiol 93, 251-66.

Drenckhahn, D., Engel, K., Hofer, D., Merte, C., Tilney, L., Tilney, M. 1991. Three different actin filament assemblies occur in every hair cell: each contains a specific actin crosslinking protein. J Cell Biol 112, 641-51.

Dumont, R.A., Lins, U., Filoteo, A.G., Penniston, J.T., Kachar, B., Gillespie, P.G. 2001. Plasma membrane Ca2+-ATPase isoform 2a is the PMCA of hair bundles. J Neurosci 21, 5066-78.

Fischer, F., Wolters, D., Rogner, M., Poetsch, A. 2006. Toward the complete membrane proteome: high coverage of integral membrane proteins through transmembrane peptide detection. Mol Cell Proteomics 5, 444-53.

Furness, D.N., Mahendrasingam, S., Ohashi, M., Fettiplace, R., Hackney, C.M. 2008. The dimensions and composition of stereociliary rootlets in mammalian cochlear hair cells: comparison between high- and low-frequency cells and evidence for a connection to the lateral membrane. J Neurosci 28, 6342-53.

Gagnon, L.H., Longo-Guess, C.M., Berryman, M., Shin, J.B., Saylor, K.W., Yu, H., Gillespie, P.G., Johnson, K.R. 2006. The chloride intracellular channel protein CLIC5 is expressed at high levels in hair cell stereocilia and is essential for normal inner ear function. J Neurosci 26, 10188-98.

Gibson, F., Walsh, J., Mburu, P., Varela, A., Brown, K.A., Antonio, M., Beisel, K.W., Steel, K.P., Brown, S.D.M. 1995. A Type-Vii Myosin Encoded by the Mouse Deafness Gene Shaker-1. Nature 374, 62-64.

Gillespie, P.G., Hudspeth, A.J. 1991. High-Purity Isolation of Bullfrog Hair Bundles and Subcellular and Topological Localization of Constituent Proteins. Journal of Cell Biology 112, 625-640.

Gillespie, P.G., Wagner, M.C., Hudspeth, A.J. 1993. Identification of a 120 kd hair-bundle myosin located near stereociliary tips. Neuron 11, 581-94.

Goodyear, R., Richardson, G. 1992. Distribution of the 275 kD hair cell antigen and cell surface specialisations on auditory and vestibular hair bundles in the chicken inner ear. J Comp Neurol 325, 243-56.

Goodyear, R.J., Gates, R., Lukashkin, A.N., Richardson, G.P. 1999. Hair-cell numbers continue to increase in the utricular macula of the early posthatch chick. J Neurocytol 28, 851-61.

Goodyear, R.J., Legan, P.K., Wright, M.B., Marcotti, W., Oganesian, A., Coats, S.A., Booth, C.J., Kros, C.J., Seifert, R.A., Bowen-Pope, D.F., Richardson, G.P. 2003. A receptor-like inositol lipid phosphatase is required for the maturation of developing cochlear hair bundles. J Neurosci 23, 9208-19.

Gorg, A., Weiss, W., Dunn, M.J. 2004. Current two-dimensional electrophoresis technology for proteomics. Proteomics 4, 3665-3685.

Guzzetta, A.W., Chien, A.S. 2005. A double-vented tetraphasic continuous column approach to MuDPIT analysis on long capillary columns demonstrates superior proteomic coverage. J Proteome Res 4, 2412-9.

Haas, R., Rosenberry, T.L. 1995. Protein denaturation by addition and removal of acetonitrile: application to tryptic digestion of acetylcholinesterase. Anal Biochem 224, 425-7.

Hackney, C.M., Mahendrasingam, S., Penn, A., Fettiplace, R. 2005. The concentrations of calcium buffering proteins in mammalian cochlear hair cells. J Neurosci 25, 7867-75.

Hagedorn, M., Neuhaus, E.M., Soldati, T. 2006. Optimized fixation and immunofluorescence staining methods for Dictyostelium cells. Methods Mol Biol 346, 327-38.

Hanash, S.M. 2000. Biomedical applications of two-dimensional electrophoresis using immobilized pH gradients: Current status. Electrophoresis 21, 1202-1209.

Hasson, T., Gillespie, P.G., Garcia, J.A., MacDonald, R.B., Zhao, Y., Yee, A.G., Mooseker, M.S., Corey, D.P. 1997. Unconventional myosins in inner-ear sensory epithelia. J Cell Biol 137, 1287-307.

Heller, S., Bell, A.M., Denis, C.S., Choe, Y., Hudspeth, A.J. 2002. Parvalbumin 3 is an abundant Ca2+ buffer in hair cells. J Assoc Res Otolaryngol 3, 488-98.

Hill, J.K., Brett, C.L., Chyou, A., Kallay, L.M., Sakaguchi, M., Rao, R., Gillespie, P.G. 2006. Vestibular hair bundles control pH with (Na+, K+)/H+ exchangers NHE6 and NHE9. J Neurosci 26, 9944-55.

Hillier, L.W., Miller, W., Birney, E., Warren, W., Hardison, R.C., Ponting, C.P., Bork, P., Burt, D.W., Groenen, M.A., Delany, M.E., Dodgson, J.B., Chinwalla, A.T., Cliften, P.F., Clifton, S.W., Delehaunty, K.D., Fronick, C., Fulton, R.S., Graves, T.A., Kremitzki, C., Layman, D., Magrini, V., McPherson, J.D., Miner, T.L., Minx, P., Nash, W.E., Nhan, M.N., Nelson, J.O., Oddy, L.G., Pohl, C.S., Randall-Maher, J., Smith, S.M., Wallis, J.W., Yang, S.P., Romanov, M.N., Rondelli, C.M., Paton, B., Smith, J., Morrice, D., Daniels, L., Tempest, H.G., Robertson, L., Masabanda, J.S., Griffin, D.K., Vignal, A., Fillon, V., Jacobbson, L., Kerje, S., Andersson, L., Crooijmans, R.P., Aerts, J., van der Poel, J.J., Ellegren, H., Caldwell, R.B., Hubbard, S.J., Grafham, D.V., Kierzek, A.M., McLaren, S.R., Overton, I.M., Arakawa, H., Beattie, K.J., Bezzubov, Y., Boardman, P.E., Bonfield, J.K., Croning, M.D., Davies, R.M., Francis, M.D., Humphray, S.J., Scott, C.E., Taylor, R.G., Tickle, C., Brown, W.R., Rogers, J., Buerstedde, J.M., Wilson, S.A., Stubbs, L., Ovcharenko, I., Gordon, L., Lucas, S., Miller, M.M., Inoko, H., Shiina, T., Kaufman, J., Salomonsen, J., Skjoedt, K., Wong, G.K., Wang, J., Liu, B., Wang, J., Yu, J., Yang, H., Nefedov, M., Koriabine, M., Dejong, P.J., Goodstadt, L., Webber, C., Dickens, N.J., Letunic, I., Suyama, M., Torrents, D., von Mering, C., *et al.* 2004. Sequence and comparative analysis of the chicken genome provide unique perspectives on vertebrate evolution. Nature 432, 695-716.

Hirono, M., Denis, C.S., Richardson, G.P., Gillespie, P.G. 2004. Hair cells require phosphatidylinositol 4,5-bisphosphate for mechanical transduction and adaptation. Neuron 44, 309-20.

Holmes, K.C., Popp, D., Gebhard, W., Kabsch, W. 1990. Atomic model of the actin filament. Nature 347, 44-9.

Holt, J.R., Gillespie, S.K.H., Provance, D.W., Shah, K., Shokat, K.M., Corey, D.P., Mercer, J.A., Gillespie, P.G. 2002. A chemical-genetic strategy implicates myosin-1c in adaptation by hair cells. Cell 108, 371-381.

Hudspeth, A.J. 1985. The cellular basis of hearing: the biophysics of hair cells. Science 230, 745-52.

Kaltenbach, J.A., Falzarano, P.R., Simpson, T.H. 1994. Postnatal development of the hamster cochlea. II. Growth and differentiation of stereocilia bundles. J Comp Neurol 350, 187-98.

Kazmierczak, P., Sakaguchi, H., Tokita, J., Wilson-Kubalek, E.M., Milligan, R.A., Muller, U., Kachar, B. 2007. Cadherin 23 and protocadherin 15 interact to form tip-link filaments in sensory hair cells. Nature 449, 87-91.

Kazmierski, S.T., Antin, P.B., Witt, C.C., Huebner, N., McElhinny, A.S., Labeit, S., Gregorio, C.C. 2003. The complete mouse nebulin gene sequence and the identification of cardiac nebulin. J Mol Biol 328, 835-46.

Keller, A., Nesvizhskii, A.I., Kolker, E., Aebersold, R. 2002. Empirical statistical model to estimate the accuracy of peptide identifications made by MS/MS and database search. Anal Chem 74, 5383-92.

Khan, S.Y., Ahmed, Z.M., Shabbir, M.I., Kitajiri, S., Kalsoom, S., Tasneem, S., Shayiq, S., Ramesh, A., Srisailpathy, S., Khan, S.N., Smith, R.J., Riazuddin, S.,

Friedman, T.B. 2007. Mutations of the RDX gene cause nonsyndromic hearing loss at the DFNB24 locus. Hum Mutat 28, 417-23.

Kikkawa, Y., Mburu, P., Morse, S., Kominami, R., Townsend, S., Brown, S.D.M. 2005. Mutant analysis reveals whirlin as a dynamic organizer in the growing hair cell stereocilium. Human Molecular Genetics 14, 391-400.

Klammer, A.A., MacCoss, M.J. 2006. Effects of modified digestion schemes on the identification of proteins from complex mixtures. J Proteome Res 5, 695-700.

Kros, C.J., Marcotti, W., van Netten, S.M., Self, T.J., Libby, R.T., Brown, S.D., Richardson, G.P., Steel, K.P. 2002. Reduced climbing and increased slipping adaptation in cochlear hair cells of mice with Myo7a mutations. Nat Neurosci 5, 41-7.

Kruger, M., Wright, J., Wang, K. 1991. Nebulin as a length regulator of thin filaments of vertebrate skeletal muscles: correlation of thin filament length, nebulin size, and epitope profile. J Cell Biol 115, 97-107.

Lalwani, A.K., Atkin, G., Li, Y., Lee, J.Y., Hillman, D.E., Mhatre, A.N. 2008. Localization in stereocilia, plasma membrane, and mitochondria suggests diverse roles for NMHC-IIa within cochlear hair cells. Brain Res 1197, 13-22.

Lambert, C., Leonard, N., De Bolle, X., Depiereux, E. 2002. ESyPred3D: Prediction of proteins 3D structures. Bioinformatics 18, 1250-6.

Leibovici, M., Verpy, E., Goodyear, R.J., Zwaenepoel, I., Blanchard, S., Laine, S., Richardson, G.P., Petit, C. 2005. Initial characterization of kinocilin, a protein of the hair cell kinocilium. Hear Res 203, 144-53.

Li, A., Xue, J., Peterson, E.H. 2008. Architecture of the mouse utricle: macular organization and hair bundle heights. J Neurophysiol 99, 718-33.

Li, H., Liu, H., Balt, S., Mann, S., Corrales, C.E., Heller, S. 2004. Correlation of expression of the actin filament-bundling protein espin with stereociliary bundle formation in the developing inner ear. J Comp Neurol 468, 125-34.

Liberman, M.C. 1987. Chronic ultrastructural changes in acoustic trauma: serial-section reconstruction of stereocilia and cuticular plates. Hear Res 26, 65-88.

Liberman, M.C., Dodds, L.W. 1987. Acute ultrastructural changes in acoustic trauma: serial-section reconstruction of stereocilia and cuticular plates. Hear Res 26, 45-64.

Liu, H., Sadygov, R.G., Yates, J.R., 3rd. 2004. A model for random sampling and estimation of relative protein abundance in shotgun proteomics. Anal Chem 76, 4193-201.

Loomis, P.A., Zheng, L., Sekerkova, G., Changyaleket, B., Mugnaini, E., Bartles, J.R. 2003. Espin cross-links cause the elongation of microvillus-type parallel actin bundles in vivo. J Cell Biol 163, 1045-55.

Mbiene, J.P., Sans, A. 1986. Differentiation and maturation of the sensory hair bundles in the fetal and postnatal vestibular receptors of the mouse: a scanning electron microscopy study. J Comp Neurol 254, 271-8.

Mbiene, J.P., Favre, D., Sans, A. 1984. The pattern of ciliary development in fetal mouse vestibular receptors. A qualitative and quantitative SEM study. Anat Embryol (Berl) 170, 229-38.

Mburu, P., Kikkawa, Y., Townsend, S., Romero, R., Yonekawa, H., Brown, S.D.M. 2006. Whirlin complexes with p55 at the stereocilia tip during hair cell development. Proceedings of the National Academy of Sciences of the United States of America 103, 10973-10978.

McDonald, W.H., Ohi, R., Miyamoto, D.T., Mitchison, T.J., Yates, J.R. 2002. Comparison of three directly coupled HPLC MS/MS strategies for identification of proteins from complex mixtures: single-dimension LC-MS/MS, 2-phase MudPIT, and 3-phase MudPIT. Int. J. Mass Spectrom. 219, 245-251.

McElhinny, A.S., Kazmierski, S.T., Labeit, S., Gregorio, C.C. 2003. Nebulin: the nebulous, multifunctional giant of striated muscle. Trends Cardiovasc Med 13, 195-201.

McElhinny, A.S., Schwach, C., Valichnac, M., Mount-Patrick, S., Gregorio, C.C. 2005. Nebulin regulates the assembly and lengths of the thin filaments in striated muscle. J Cell Biol 170, 947-57.

McGee, J., Goodyear, R.J., McMillan, D.R., Stauffer, E.A., Holt, J.R., Locke, K.G., Birch, D.G., Legan, P.K., White, P.C., Walsh, E.J., Richardson, G.P. 2006. The very large G-protein-coupled receptor VLGR1: a component of the ankle link complex required for the normal development of auditory hair bundles. J Neurosci 26, 6543-53.

Melan, M.A., Sluder, G. 1992. Redistribution and differential extraction of soluble proteins in permeabilized cultured cells. Implications for immunofluorescence microscopy. J Cell Sci 101 (Pt 4), 731-43.

Mhatre, A.N., Li, J., Kim, Y., Coling, D.E., Lalwani, A.K. 2004. Cloning and developmental expression of nonmuscle myosin IIA (Myh9) in the mammalian inner ear. J Neurosci Res 76, 296-305.

Mhatre, A.N., Li, Y., Atkin, G., Maghnouj, A., Lalwani, A.K. 2006. Expression of Myh9 in the mammalian cochlea: localization within the stereocilia. J Neurosci Res 84, 809-18.

Michalski, N., Michel, V., Bahloul, A., Lefevre, G., Barral, J., Yagi, H., Chardenoux, S., Weil, D., Martin, P., Hardelin, J.P., Sato, M., Petit, C. 2007. Molecular

characterization of the ankle-link complex in cochlear hair cells and its role in the hair bundle functioning. J Neurosci 27, 6478-88.

Minturn, J.E., Fryer, H.J., Geschwind, D.H., Hockfield, S. 1995. TOAD-64, a gene expressed early in neuronal differentiation in the rat, is related to unc-33, a C. elegans gene involved in axon outgrowth. J Neurosci 15, 6757-66.

Mogensen, M.M., Rzadzinska, A., Steel, K.P. 2007. The deaf mouse mutant whirler suggests a role for whirlin in actin filament dynamics and stereocilia development. Cell Motil Cytoskeleton 64, 496-508.

Moore, P.B., Huxley, H.E., DeRosier, D.J. 1970. Three-dimensional reconstruction of F-actin, thin filaments and decorated thin filaments. J Mol Biol 50, 279-95.

Mooseker, M.S., Bonder, E.M., Conzelman, K.A., Fishkind, D.J., Howe, C.L., Keller, T.C., 3rd. 1984. Brush border cytoskeleton and integration of cellular functions. J Cell Biol 99, 104s-112s.

Mustapha, M., Beyer, L.A., Izumikawa, M., Swiderski, D.L., Dolan, D.F., Raphael, Y., Camper, S.A. 2007. Whirler mutant hair cells have less severe pathology than shaker 2 or double mutants. J Assoc Res Otolaryngol 8, 329-37.

Nayak, G.D., Ratnayaka, H.S., Goodyear, R.J., Richardson, G.P. 2007. Development of the hair bundle and mechanotransduction. Int J Dev Biol 51, 597-608.

Nesvizhskii, A.I., Keller, A., Kolker, E., Aebersold, R. 2003. A statistical model for identifying proteins by tandem mass spectrometry. Anal Chem 75, 4646-58.

Nevalainen, E.M., Skwarek-Maruszewska, A., Braun, A., Moser, M., Lappalainen, P. 2008. Two biochemically distinct and tissue-specific twinfilin isoforms are generated from mouse twinfilin-2 gene by alternative promoter usage. Biochem J.

Olayioye, M.A., Buchholz, M., Schmid, S., Schoffler, P., Hoffmann, P., Pomorski, T. 2007. Phosphorylation of StarD10 on serine 284 by casein kinase II modulates its lipid transfer activity. J Biol Chem 282, 22492-8.

Olayioye, M.A., Hoffmann, P., Pomorski, T., Armes, J., Simpson, R.J., Kemp, B.E., Lindeman, G.J., Visvader, J.E. 2004. The phosphoprotein StarD10 is overexpressed in breast cancer and cooperates with ErbB receptors in cellular transformation. Cancer Res 64, 3538-44.

Olayioye, M.A., Vehring, S., Muller, P., Herrmann, A., Schiller, J., Thiele, C., Lindeman, G.J., Visvader, J.E., Pomorski, T. 2005. StarD10, a START domain protein overexpressed in breast cancer, functions as a phospholipid transfer protein. J Biol Chem 280, 27436-42.

Paavilainen, V.O., Merckel, M.C., Falck, S., Ojala, P.J., Pohl, E., Wilmanns, M., Lappalainen, P. 2002. Structural conservation between the actin monomer-binding sites of twinfilin and actin-depolymerizing factor (ADF)/cofilin. J Biol Chem 277, 43089-95.

Paavilainen, V.O., Hellman, M., Helfer, E., Bovellan, M., Annila, A., Carlier, M.F., Permi, P., Lappalainen, P. 2007. Structural basis and evolutionary origin of actin filament capping by twinfilin. Proc Natl Acad Sci U S A 104, 3113-8.

Pataky, F., Pironkova, R., Hudspeth, A.J. 2004. Radixin is a constituent of stereocilia in hair cells. Proc Natl Acad Sci U S A 101, 2601-6.

Pompeia, C., Hurle, B., Belyantseva, I.A., Noben-Trauth, K., Beisel, K., Gao, J., Buchoff, P., Wistow, G., Kachar, B. 2004. Gene expression profile of the mouse organ of Corti at the onset of hearing. Genomics 83, 1000-11.

Purves, D., Augustine, G.J., Fitzpatrick, D., Lawrence, C.K., Lamantia, A.-S., McNamara, J.O., Williams, S.M. 2001. Neuroscience, Second ed. Sinauer Associeates Inc.

Reiners, J., van Wijk, E., Marker, T., Zimmermann, U., Jurgens, K., te Brinke, H., Overlack, N., Roepman, R., Knipper, M., Kremer, H., Wolfrum, U. 2005. Scaffold protein harmonin (USH1C) provides molecular links between Usher syndrome type 1 and type 2. Human Molecular Genetics 14, 3933-3943.

Roe, M.R., Griffin, T.J. 2006. Gel-free mass spectrometry-based high throughput proteomics: Tools for studying biological response of proteins and proteomes. Proteomics 6, 4678-87.

Rzadzinska, A., Schneider, M., Noben-Trauth, K., Bartles, J.R., Kachar, B. 2005. Balanced levels of Espin are critical for stereociliary growth and length maintenance. Cell Motil Cytoskeleton 62, 157-65.

Rzadzinska, A.K., Schneider, M.E., Davies, C., Riordan, G.P., Kachar, B. 2004. An actin molecular treadmill and myosins maintain stereocilia functional architecture and self-renewal. J Cell Biol 164, 887-97.

Sadygov, R.G., Cociorva, D., Yates, J.R., 3rd. 2004. Large-scale database searching using tandem mass spectra: looking up the answer in the back of the book. Nat Methods 1, 195-202.

Sage, C., Huang, M., Karimi, K., Gutierrez, G., Vollrath, M.A., Zhang, D.S., Garcia-Anoveros, J., Hinds, P.W., Corwin, J.T., Corey, D.P., Chen, Z.Y. 2005. Proliferation of functional hair cells in vivo in the absence of the retinoblastoma protein. Science 307, 1114-8.

Salles, F.T., Merritt, R.C., Jr., Manor, U., Dougherty, G.W., Sousa, A.D., Moore, J.E., Yengo, C.M., Dose, A.C., Kachar, B. 2009. Myosin IIIa boosts elongation of stereocilia by transporting espin 1 to the plus ends of actin filaments. Nat Cell Biol.

Schena, M., Shalon, D., Davis, R.W., Brown, P.O. 1995. Quantitative monitoring of gene expression patterns with a complementary DNA microarray. Science 270, 467-70.

Schneider, M.E., Belyantseva, I.A., Azevedo, R.B., Kachar, B. 2002. Rapid renewal of auditory hair bundles. Nature 418, 837-8.

Schneider, M.E., Dose, A.C., Salles, F.T., Chang, W., Erickson, F.L., Burnside, B., Kachar, B. 2006. A new compartment at stereocilia tips defined by spatial and temporal patterns of myosin IIIa expression. J Neurosci 26, 10243-52.

Sekerkova, G., Zheng, L., Loomis, P.A., Mugnaini, E., Bartles, J.R. 2006. Espins and the actin cytoskeleton of hair cell stereocilia and sensory cell microvilli. Cell Mol Life Sci 63, 2329-41.

Self, T., Mahony, M., Fleming, J., Walsh, J., Brown, S.D.M., Steel, K.P. 1998. Shaker-1 mutations reveal roles for myosin VIIA in both development and function of cochlear hair cells. Development 125, 557-566.

Self, T., Sobe, T., Copeland, N.G., Jenkins, N.A., Avraham, K.B., Steel, K.P. 1999. Role of myosin VI in the differentiation of cochlear hair cells. Dev Biol 214, 331-41.

Shadforth, I., Crowther, D., Bessant, C. 2005. Protein and peptide identification algorithms using MS for use in high-throughput, automated pipelines. Proteomics 5, 4082-95.

Shepherd, G.M., Barres, B.A., Corey, D.P. 1989. "Bundle blot" purification and initial protein characterization of hair cell stereocilia. Proc Natl Acad Sci U S A 86, 4973-7.

Shin, J.B., Streijger, F., Beynon, A., Peters, T., Gadzala, L., McMillen, D., Bystrom, C., Van der Zee, C.E., Wallimann, T., Gillespie, P.G. 2007. Hair bundles are specialized for ATP delivery via creatine kinase. Neuron 53, 371-86.

Si, F., Brodie, H., Gillespie, P.G., Vazquez, A.E., Yamoah, E.N. 2003. Developmental assembly of transduction apparatus in chick basilar papilla. J Neurosci 23, 10815-26.

Siemens, J., Kazmierczak, P., Reynolds, A., Sticker, M., Littlewood-Evans, A., Muller, U. 2002. The Usher syndrome proteins cadherin 23 and harmonin form a complex by means of PDZ-domain interactions. Proceedings of the National Academy of Sciences of the United States of America 99, 14946-14951.

Siemens, J., Lillo, C., Dumont, R.A., Reynolds, A., Williams, D.S., Gillespie, P.G., Muller, U. 2004. Cadherin 23 is a component of the tip link in hair-cell stereocilia. Nature 428, 950-5.

Sivaraman, T., Kumar, T.K., Jayaraman, G., Yu, C. 1997. The mechanism of 2,2,2-trichloroacetic acid-induced protein precipitation. J Protein Chem 16, 291-7.

Slepecky, N.B., Ulfendahl, M. 1992. Actin-binding and microtubule-associated proteins in the organ of Corti. Hear Res 57, 201-15.

Sobkowicz, H.M., Slapnick, S.M., August, B.K. 1995. The kinocilium of auditory hair cells and evidence for its morphogenetic role during the regeneration of stereocilia and cuticular plates. J Neurocytol 24, 633-53.

Stauffer, E.A., Scarborough, J.D., Hirono, M., Miller, E.D., Shah, K., Mercer, J.A., Holt, J.R., Gillespie, P.G. 2005. Fast adaptation in vestibular hair cells requires myosin-1c activity. Neuron 47, 541-53.

Stauffer, T.P., Ahn, S., Meyer, T. 1998. Receptor-induced transient reduction in plasma membrane PtdIns(4,5)P2 concentration monitored in living cells. Curr Biol 8, 343-6.

Thalmann, I., Hughes, I., Tong, B.D., Ornitz, D.M., Thalmann, R. 2006. Microscale analysis of proteins in inner ear tissues and fluids with emphasis on endolymphatic sac, otoconia, and organ of Corti. Electrophoresis 27, 1598-608.

Thorne, P.R., Ameratunga, S.N., Stewart, J., Reid, N., Williams, W., Purdy, S.C., Dodd, G., Wallaart, J. 2008. Epidemiology of noise-induced hearing loss in New Zealand. N Z Med J 121, 33-44.

Tilney, L.G., Tilney, M.S. 1984. Observations on how actin filaments become organized in cells. J Cell Biol 99, 76s-82s.

Tilney, L.G., Tilney, M.S., Cotanche, D.A. 1988. Actin filaments, stereocilia, and hair cells of the bird cochlea. V. How the staircase pattern of stereociliary lengths is generated. J Cell Biol 106, 355-65.

Tilney, L.G., Tilney, M.S., DeRosier, D.J. 1992. Actin filaments, stereocilia, and hair cells: how cells count and measure. Annu Rev Cell Biol 8, 257-74.

Tilney, L.G., Egelman, E.H., DeRosier, D.J., Saunder, J.C. 1983. Actin filaments, stereocilia, and hair cells of the bird cochlea. II. Packing of actin filaments in the stereocilia and in the cuticular plate and what happens to the organization when the stereocilia are bent. J Cell Biol 96, 822-34.

Tilney, L.G., Tilney, M.S., Saunders, J.S., DeRosier, D.J. 1986. Actin filaments, stereocilia, and hair cells of the bird cochlea. III. The development and differentiation of hair cells and stereocilia. Dev Biol 116, 100-18.

Tilney, M.S., Tilney, L.G., Stephens, R.E., Merte, C., Drenckhahn, D., Cotanche, D.A., Bretscher, A. 1989. Preliminary biochemical characterization of the stereocilia and cuticular plate of hair cells of the chick cochlea. J Cell Biol 109, 1711-23.

Vartiainen, M., Ojala, P.J., Auvinen, P., Peranen, J., Lappalainen, P. 2000. Mouse A6/twinfilin is an actin monomer-binding protein that localizes to the regions of rapid actin dynamics. Mol Cell Biol 20, 1772-83.

Vartiainen, M.K., Sarkkinen, E.M., Matilainen, T., Salminen, M., Lappalainen, P. 2003. Mammals have two twinfilin isoforms whose subcellular localizations and tissue distributions are differentially regulated. J Biol Chem 278, 34347-55.

Verpy, E., Weil, D., Leibovici, M., Goodyear, R.J., Hamard, G., Houdon, C., Lefevre, G.M., Hardelin, J.P., Richardson, G.P., Avan, P., Petit, C. 2008. Stereocilin-deficient mice reveal the origin of cochlear waveform distortions. Nature 456, 255-8.

Walsh, T., Walsh, V., Vreugde, S., Hertzano, R., Shahin, H., Haika, S., Lee, M.K., Kanaan, M., King, M.C., Avraham, K.B. 2002. From flies' eyes to our ears: mutations in a human class III myosin cause progressive nonsyndromic hearing loss DFNB30. Proc Natl Acad Sci U S A 99, 7518-23.

Washburn, M.P., Wolters, D., Yates, J.R. 2001. Large-scale analysis of the yeast proteome by multidimensional protein identification technology. Nature Biotechnology 19, 242-247.

Wolters, D.A., Washburn, M.P., Yates, J.R. 2001. An automated multidimensional protein identification technology for shotgun proteomics. Analytical Chemistry 73, 5683-5690.

Wu, C.C., MacCoss, M.J., Howell, K.E., Yates, J.R., 3rd. 2003. A method for the comprehensive proteomic analysis of membrane proteins. Nat Biotechnol 21, 532-8.

Xu, Z., Peng, A.W., Oshima, K., Heller, S. 2008. MAGI-1, a candidate stereociliary scaffolding protein, associates with the tip-link component cadherin 23. J Neurosci 28, 11269-76.

Yamada, S., Uchimura, E., Ueda, T., Nomura, T., Fujita, S., Matsumoto, K., Funeriu, D.P., Miyake, M., Miyake, J. 2007. Identification of twinfilin-2 as a factor involved in neurite outgrowth by RNAi-based screen. Biochem Biophys Res Commun 363, 926-30.

Zellner, M., Winkler, W., Hayden, H., Diestinger, M., Eliasen, M., Gesslbauer, B., Miller, I., Chang, M., Kungl, A., Roth, E., Oehler, R. 2005. Quantitative validation of different protein precipitation methods in proteome analysis of blood platelets. Electrophoresis 26, 2481-9.

Zheng, L., Sekerkova, G., Vranich, K., Tilney, L.G., Mugnaini, E., Bartles, J.R. 2000. The deaf jerker mouse has a mutation in the gene encoding the espin actin-bundling proteins of hair cell stereocilia and lacks espins. Cell 102, 377-85.